The Relativistic String in the Caltech-II Model of Hadronization and Electron-Positron Annihilation

Thesis by

Duncan Andrew Morris

In Partial Fulfillment of the Requirements

for the Degree of

Doctor of Philosophy

California Institute of Technology

Pasadena, California

1987

(submitted May 4, 1987)

Acknowledgements

I would like to thank my advisor, G.C. Fox, for his support and guidance during my stay at Caltech. I especially thank T.D. Gottschalk for providing an opportunity for me to participate in what I believe to be a unique branch of physics. I have benefited greatly from his insight and experience. I hope that I have gained not only part of his knowledge, but also his friendship.

I appreciate and acknowledge my contacts with B. Andersson and T. Sjöstrand. Their perspectives on the LUND model, as well as the Caltech model, were quite helpful.

I cannot forget my housemates, officemates and other friends. They are responsible for my "other half" and have played a big part in my cultural education.

I am grateful to Caltech and the Natural Science and Engineering Research Council of Canada for providing financial support.

Finally, I thank my parents for their patience and respect for my studies. I owe them more than I can say. I dedicate this thesis to them.

Abstract

This study uses the full equations of motion of the massless relativistic string as a phenomenological model of color flux tubes in the process of hadronization in electron-positron annihilation. Perturbatively generated sets of partons are mapped onto color singlet strings, which fragment according to a generalization of the covariant decay law for point relativistic particles. String evolution is terminated when string masses are a few GeV above particle production threshold. Low-mass strings are decayed into primary hadrons using a parameterization of low-mass data. The complete model, which factorizes event evolution into three stages including perturbative QCD, string fragmentation and parameterized low-mass decays, is implemented as a Monte Carlo program known as the Caltech-II model of hadronization. An exact formalism is presented for the fragmentation function of heavy quarks within the string model.

The main results are, in their order of appearance: (1) The kinematics of the evolution and decay of arbitrarily complex massless relativistic strings is most conveniently expressed in terms of momentum currents. (2) The Caltech-II model, which uses the momentum current formalism to describe relativistic strings, provides a good description of electron-positron annihilation data over a wide range of center-of-mass energies. (3) Introducing transverse momentum at the sites of string breaks is conceptually necessary and may be required to further improve agreement between the Caltech-II model and data. (4) Fragmentation functions are predictions, not assumptions, of the string model in Caltech-II. The fragmentation function of heavy quarks in the Caltech-II string model is shown to exhibit the behavior expected from model-independent arguments. The discovery of the top quark or additional generations of heavy quarks will be a testing ground for future studies of hadronization.

Contents

List of Figures

List of Tables

Chapter 1

Preamble

1.1 Introduction

Classify, quantify, postulate, predict. This is the traditional route physicists have followed to gain an understanding of physical phenomena. Today we are at a different stage of understanding for each of the fundamental forces of nature. While the electroweak theory has been spectacularly successful both qualitatively and quantitatively, quantum gravity is still in the "postulate" phase. Interestingly enough, we can't succinctly categorize our understanding of the remaining force, the strong force. Though the field theory of the strong force, Quantum Chromodynamics (QCD), is, *in principle*, well defined, it has many unexplored corners.

It is customary to summarize our "first principles" knowledge of the strong force by writing down the $SU(3)_{\text{color}}$ gauge invariant QCD Lagrangian for massive quarks

$$L_{\text{QCD}} = -\frac{1}{4}\sum_{i=1}^{8} G^i_{\mu\nu} G^{i\,\mu\nu} + \sum_{\text{flavors}} \bar{q}(i\gamma^\mu(\partial_\mu - igA_\mu) - m)q. \qquad (1.1)$$

In this equation g is the strong coupling constant and the field tensor $G_{\mu\nu}$ is defined in terms of the potential A_μ by

$$G_{\mu\nu} = \partial_\mu A_\nu - \partial_\nu A_\mu - ig[A_\mu, A_\nu], \qquad (1.2)$$

where A_μ has the color space decomposition

$$A_\mu = \sum_{i=1}^{8} A^i_\mu \frac{\lambda^i}{2}. \qquad (1.3)$$

The commutator term in eq. (1.2) introduces self-couplings for the gauge fields because the commutation relations for $SU(3)$

$$\left[\frac{\lambda_i}{2}, \frac{\lambda_j}{2}\right] = if^{ijk}\frac{\lambda_k}{2} \tag{1.4}$$

involve nonzero structure constants f^{ijk}.

Two important qualitative features of QCD are

1. QCD is a non-Abelian field theory so that the gauge (gluon) fields A_μ^i couple to themselves.

2. The fundamental fields (quarks and gluons or collectively, partons) in $L_{\rm QCD}$ do not appear to exist in isolation — only composite color singlets have so far been observed in nature.

The weakening of the strong force at large momentum transfers, so-called asymptotic freedom, is closely related to the non-Abelian nature of QCD [1,2]. Asymptotic freedom permits us, at large momentum transfers, to use perturbation theory to calculate quantities on the parton level. However, when it comes to experimental physics, this is not enough. The problem is that the language of perturbative QCD, that is, the language of quarks and gluons, is foreign to the experimentalist's detector which has, to date, heard only the dialect of hadrons (protons, neutrons, kaons etc.) What perturbation theory will not tell us, and what we ultimately need to know, is how partons condense into hadrons. Unfortunately, we do not yet have reliable techniques for solving QCD in the nonstatic, nonperturbative regimes that are undoubtedly relevant to hadron formation.

While there are many ongoing efforts to understand the nonperturbative aspects of QCD, such as lattice gauge theory simulations, solitons, etc., they each have a relatively limited applicability. At high center of mass energy, processes like

$$e^+e^- \rightarrow \text{partons} \rightarrow \text{hadrons}, \tag{1.5}$$

require an understanding of a wide range of both perturbative and nonperturbative phenomena. Progress has been slow in linking perturbative and nonperturbative QCD; not only is the theory difficult to work with and the questions hard to answer, but also we are not really sure what the relevant questions are! The only unfaltering guidance we have comes from experimental data.

Just because we do not know how to "solve" all of QCD exactly does not mean that we should be deterred from testing what we do know. More specifically, QCD perturbation theory provides a means of getting from the initial e^+e^- in eq. (1.5) to a set of partons. What is lacking is a reliable way of turning these partons in hadrons — we need to understand the hadronization process.

In this thesis we present a sensible approach to hadronization, which incorporates many of our theoretical and phenomenological prejudices. The end result is a quantitative model of hadronization (Caltech-II [3]) capable of reproducing the observed features of hadronization in e^+e^- annihilation over the entire range of center of mass energies for which data are currently available ($3\,\mathrm{GeV} \leq E_{\mathrm{CM}} \leq 45\,\mathrm{GeV}$.)

Why do we need a phenomenological model of hadronization? Depending on one's philosophical biases, there are many answers to this question. On the practical side, we need *something* to help us connect the hadrons observed in detectors to the partons that roam the range of perturbative QCD. Hadronization models are important not only for interpreting existing data, but also for designing new experiments — they can tell us when experimental signatures are feasible as well as help in the design of detectors. On a more fundamental level, we need a model of hadronization that can tell us something about the mechanisms at work in hadron production. Caltech-II strives to answer the question at the beginning of this paragraph both ways by successfully reproducing experimental data *and* by doing so within the constraints of a physically plausible framework.

How far can we go? Ideally, we would like to be able to describe 100% of
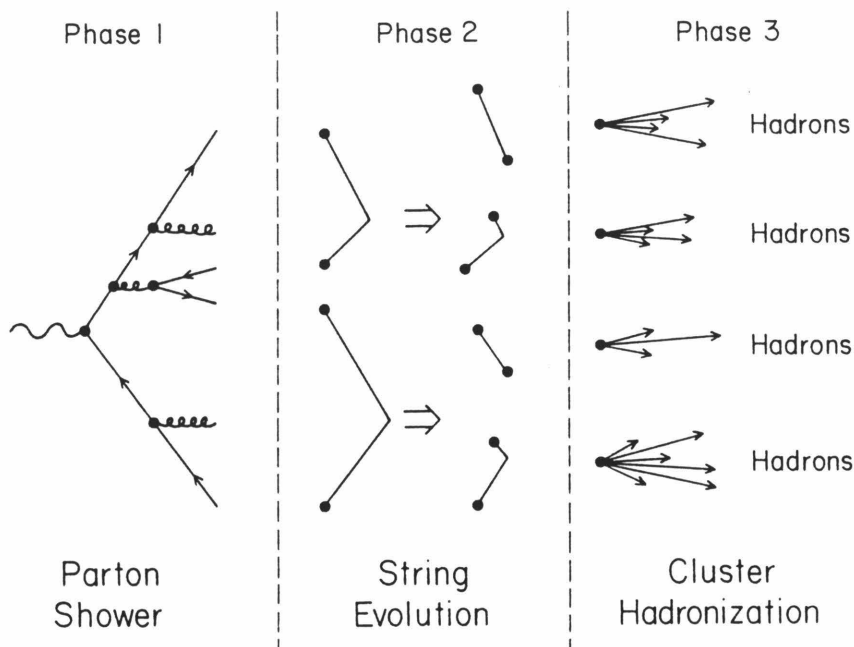
Figure 1.1 Factorization of event evolution in Caltech-II.

hadronization effects so that we could, for example, accurately determine the strong coupling constant α_s. No existing model of hadronization can justifiably be trusted to this level — there is too much we still do not know. For example, the physics of hadronization on mass scales of a few GeV is still an unsolved problem. Until such problems are tackled in a sensible way, we must find a way to work around them without introducing spurious complications.

The structure of the Caltech-II model is summarized schematically in fig. 1.1. The model factorizes the event evolution of eq. (1.5) into three distinct phases:

1. The formation of a parton system using the leading log approximation to perturbative QCD, modified to account for gluon coherence effects.

2. The mapping of partons onto relativistic strings (a phenomenological model for confining QCD flux tubes) that evolve and decay according to a simple, covariant ansatz until the strings are within 1-2 GeV of particle production threshold.

3. The decay of low-mass strings (clusters) using a parameterization of low-mass data.

Of course, parceling out of the physics burden between three distinct phases is nothing more than a reflection of our ignorance of the "exact" solutions to QCD. This is quite evident if we consider the rationale for the partitioning: phase 1 has a relatively strong theoretical motivation since it is based on L_{QCD}; phase 2 has more of a phenomenological motivation, derived from general confinement criteria and the success of lattice studies; phase 3 deals with physics issues which are, currently, too difficult to handle in any fundamental way.

Recognizing *where* the difficulties arise in hadronization allows us to avoid them in a systematic way. By assuming the decay of low-mass clusters is a local, universal phenomena, Caltech-II factors off that part of the physics which is best described by a fixed parameterization and instead concentrates on the physics issues for which there *is* some fundamental motivation.

The Caltech-II model is an improvement of the Caltech-I model [4,5] in that it incorporates the full equations of motion for the relativistic string [6]. It uses the gross dynamics of the relativistic string as an approximation to QCD flux tubes. In this thesis we focus on the role of strings in Caltech-II. We point out i) the defects of the Caltech-I model that motivate the full string model, ii) how the space-time picture of string evolution can be decomposed to suit a computer implementation, iii) how strings are modeled in Caltech-II, iv) how the resulting model compares with data, v) how the model differs with other string models in its predictions for heavy quark fragmentation and vi) how the model may be elaborated.

Chapter 2 provides a brief introduction to hadronization models and discusses the intentions of the string model in Caltech-II. In that chapter it is stressed that we are using the relativistic string as a very coarse model of QCD flux tubes, *not* as a "fundamental" model of hadronic physics (for which purposes the theory was

originally proposed almost twenty years ago). We use the relativistic string to describe only the gross, "stringy," properties of flux tubes.

Chapter 3 discusses the general problems encountered when implementing the relativistic string in Caltech-II. Because Caltech-II chooses a simple covariant ansatz for the fragmentation of strings, it must be capable of determining the evolution of strings through many generations. In that chapter we devise a technique for obtaining string motions by superposing momentum currents that circulate on the world sheet of the string. We demonstrate a correspondence between fragmenting strings and a topological fragmentation of the domain on which momentum currents circulate. These developments are crucial to an efficient implementation of strings in Caltech-II.

Chapter 4 addresses the specifics of string evolution in Caltech-II. We explain how the Artru-Mennessier ansatz for the decay of arbitrarily complex strings is interpreted in the formalism of Chapter 3. We discuss the details of the string model such as the transition to the parameterized decay of low-mass clusters, the treatment of heavy quarks and flavor selection at string breaks.

Chapter 5 compares the full Caltech-II model with available e^+e^- data over the energy range $3\,\mathrm{GeV} \leq E_{\mathrm{CM}} \leq 45\,\mathrm{GeV}$. We show how the behavior of the model is governed by five energy-independent parameters. We point out places where the model deviates from the data and suggest specific improvements.

Chapter 6 develops an analytical approach to heavy quark fragmentation in the string model. Not only can this approach be used as an independent check of the implementation of strings in the full Caltech-II model, but it is much more efficient in predicting the behavior of systems containing very heavy quarks. We demonstrate how the heavy quark fragmentation functions predicted by the analytic approach (and hence also Caltech-II) agree with the general asymptotic arguments of Bjorken [7] and Suzuki [8].

Chapter 2

Pictures of Hadronization: Old and New

2.1 Introduction

One of the biggest hurdles in the hadronization game is the first one: getting oriented. The field has matured rapidly since its inception approximately ten years ago, with growth spurts correlated with the availability of new data. To fully appreciate the central results of thesis, it is best to have a bird's-eye-view of the field; with this perspective, the overall physics picture in Caltech-II is seen to be both appealing and sensible. The dual goals of this chapter are to give the neophyte a walking tour of hadronization models and to lay out the basic ingredients of the Caltech-II model. As we shall see, Caltech-II is the latest logical step towards a model of hadronization, which embodies most of our theoretical and phenomenological prejudices. Yet before we describe the details of the model, we pay homage to its predecessors and contemporaries: the quickest way to get where we're going is to know where we've already been. To avoid complicating our introduction to the various models, we shall assume a familiarity with the perturbative aspects of QCD (see appendix A) and instead let the hadronization models pick up where perturbative QCD leaves off.

In sect. 2.2 we discuss the Field-Feynman model, the first serious attempt at a

model of hadronization. This section is important since it introduces the concept of a fragmentation function. Throughout this thesis we suggest that models that assume fragmentation functions as their starting points, such as the Field-Feynman and LUND pictures, are more *parameterizations* than full-fledged models; they use their many parameters to reproduce features of the data without isolating the dynamical mechanisms that give rise to those features.

Sect. 2.3 points out the glaring neglect of confinement in the Field-Feynman model. The independent evolution of partons in the Field-Feynman model makes no intrinsic allowance for the color degrees of freedom: a problem that is remedied, to various extents, by cluster and string models.

Sect. 2.4 discusses cluster models in detail and outlines how they relegate the intricacies of hadronization to the parameterized decay of low-mass clusters (see appendix B). Cluster models use the color flow provided by LLA QCD, so-called preconfinement [9], to form color singlets at an early stage in event evolution. Unfortunately, cluster models (like Caltech-I [5] and the Webber model [10]) are sensitive to soft or collinear gluon radiation. This problem leads to discontinuities in particle multiplicities and is one of the motivations for using the relativistic string in Caltech-II [3].

Sect. 2.5 shows how the sensitivity of cluster models to soft or collinear gluon radiation may be eliminated by employing the relativistic string as a semiclassical model of flux tubes, which are thought to give rise to QCD confinement. We briefly review the history of the relativistic string as well as give some simple examples of string motion. In this section we point out the fundamentally different approaches to string fragmentation in the Caltech-II and LUND [11] models.

Sect. 2.6 allows us to catch our breath and put sects. 2.2-2.5 into perspective. We summarize the progression of hadronization models and reemphasize the different uses of relativistic strings in the Caltech-II and LUND models.
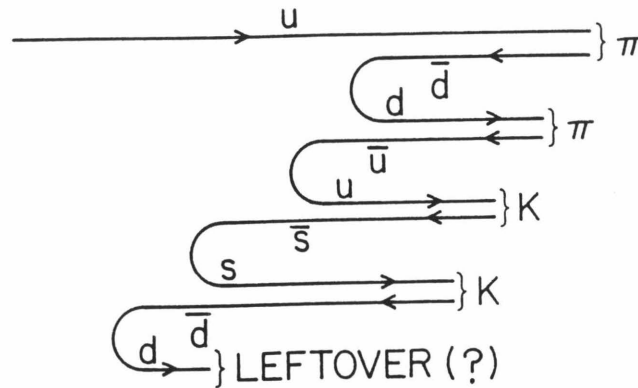
Figure 2.1 Independent evolution of quarks in the Field-Feynman model produces physical particles at each node of a decay chain.

Sect. 2.7 recapitulates and provides a brief summary of the Caltech-II model before we launch into the details of the string model in chapters 3 and 4.

2.2 The Field-Feynman Model

In 1978 Field and Feynman [12] proposed a simple parameterization of jet properties, which idealized hadronization as an iterative process in which highly virtual partons undergo the transition

$$q \rightarrow (q\bar{q}') + q'. \tag{2.1}$$

The physical picture implied by eq. (2.1) is that of a virtual quark q inciting the vacuum to produce a quark-antiquark pair $q'\bar{q}'$ so that q and $\bar{q}'$ combine to form a meson $(q\bar{q}')$, while the virtual q' becomes the initial state for the next transition. This decay chain, illustrated in fig. 2.1, is iterated until the residual quark gets close to its mass shell (O(1) GeV), at which point it is combined with other debris to avoid the appearance of free quarks. One of the key features of the Field-Feynman model is that given a perturbatively generated multiparton state, say $\gamma^* \rightarrow q\bar{q}$, it

evolves each quark *independently*. For this reason the Field-Feynman model is also known as the independent jet model or independent fragmentation model.

The fragmentation chain in the Field-Feynman model may be viewed as a succession of two body decays in which a physical particle is peeled off at each node. Because jets, by their very nature, define a preferred axis about which there is limited transverse momentum, it is convenient to work in $1 + 1$ dimensions where it takes only one variable, conventionally called z, to specify the kinematics of the decay in eq. (2.1) (assuming we know the masses of the meson and the initial virtual quark). With the intent of reproducing the experimentally observed approximate scaling features of jets, Field and Feynman proposed the existence of a scale invariant distribution $f(z)$, which could be applied to each node of the decay chain.

A convenient choice of fragmentation variable is the Lorentz invariant (at least in $1 + 1$ dimensions) scaled rapidity difference

$$z = e^{y - y_{\max}}, \tag{2.2}$$

where

$$y = \frac{1}{2} \ln \left[\frac{E + p}{E - p} \right], \tag{2.3}$$

is the rapidity of the emitted meson with energy E and momentum p. In eq. (2.2), $y_{\max}$ is the maximum meson rapidity (a function of the initial virtual quark mass $\sqrt{s_q}$, the meson mass $\sqrt{s_{\text{meson}}}$ and the minimum mass of the virtual quark recoil system $\sqrt{s_{\text{recoil}}}$). By exponentiating the boost invariant quantity $y - y_{\max}$, z is restricted to the interval $[e^{-2y_{\max}^*}, 1]$ where, in the CM frame of the parent,

$$e^{-y_{\max}^*} = \frac{2\sqrt{\frac{s_{\text{meson}}}{s}}}{1 + \frac{s_{\text{meson}}}{s_q} - \frac{s_{\text{recoil}}}{s_q} + \lambda^{1/2}\left(1, \frac{s_{\text{meson}}}{s_q}, \frac{s_{\text{recoil}}}{s_q}\right)}. \tag{2.4}$$

As usual, $\lambda(a, b, c) = a^2 + b^2 + c^2 - 2ab - 2ac - 2bc$.

There is, fortunately, a rather simple interpretation of z. If we go to a frame in which the initial virtual quark of eq. (2.1) has infinite momentum, then z is

the fraction of the energy (or momentum) carried off by the meson. This intuitive interpretation gives meaning to the experimentally measured quantities

$$x_E = \frac{E}{E_{\text{max}}}, \qquad x_p = \frac{|p|}{p_{max}}, \qquad (2.5)$$

which are identical to z in the limit of sources that have infinite momentum.

The predictions of the Field-Feynman model depend on the specific form chosen for the quark fragmentation function $f(z)$. Strictly speaking, we should consider a plethora of functions $f_q^M(z)$ corresponding to the particular quark flavor q and emitted meson M, but we shall neglect such complications in the interest of clarity. It should be obvious that, because of the iterative nature of the Field-Feynman ansatz, $f(z)$ is generally not the experimentally measured distribution of the meson energy fraction. Assuming a world with only one quark flavor and one type of meson, the Field-Feynman model requires the experimentally measurable z distribution of mesons emitted from a quark jet, $D(z)$, to be given by the integral equation

$$D(z) = f(z) + \int_z^1 \frac{d\eta}{\eta} D(z/\eta) f(1 - \eta). \qquad (2.6)$$

In this equation z is the fraction of the *original* quark energy even though the meson may not contain the quark that initiated the jet. The additive $f(z)$ term accounts for the possibility that an observed meson contains the original quark that initiated the jet, while the integral term sums the probabilities that the meson originated from subsequent nodes in the fragmentation chain. Field and Feynman considered the functional form

$$f(z) = 1 - a + 3a(1 - z)^2 \qquad (2.7)$$

with $a = .88$. Subsequent groups have investigated alternative parameterizations [13].

The simple $1 + 1$ dimensional Field-Feynman model may be extended to $3 + 1$

dimensions by assuming a Gaussian distribution

$$\exp\left(-\frac{p_\perp^2}{2\sigma^2}\right) dp_\perp^2 \qquad (2.8)$$

for the transverse momentum of each quark pulled from the vacuum. Phenomenological considerations require $\sigma \sim 300\,\mathrm{MeV}$. The model can also be elaborated by incorporating different quark flavors and meson types as well as allow baryon production by pulling diquark pairs from the vacuum [14]. Gluons can be treated by forcing a splitting $g \to q\bar{q}$ according to the Alterelli-Parisi equations [15] as was done by Ali et $al.$ [16] or by postulating, as Hoyer et $al.$ do [17], a separate gluon fragmentation function $f_g(z)$ with the basic transition $g \to g' + \mathrm{Meson}$.

The conceptual simplicity of the Field-Feynman model is achieved at the cost of violating local conservation laws and Lorentz covariance. The leftover quark at the end of a fragmentation chain carries flavor, color, energy and momentum that must be dealt with, in some ad hoc manner, so as to at least preserve global conservation laws. Although various techniques exist for patching up these flagrant violations, it has been demonstrated that many results are sensitive to the details of the scheme employed [18,19,20].

Aside from these obvious drawbacks there are other objections to treating partons independently. Perhaps most striking is the neglect of QCD! No account is taken of the color force other than to dispose of the free quark at the end of each fragmentation chain. A related problem is a discontinuity in the particle multiplicity when two partons are collinear. Experimentally, the multiplicity of a jet of energy E varies roughly as $\ln E$. Because QCD cannot distinguish between a quark of energy $2E$ and a collinear quark and gluon, each with energy E, the multiplicity in either case should vary as $\ln 2E$. On the contrary, a literal application of the Field-Feynman model would evolve each member of a collinear pair $independently$ and hence predict a multiplicity varying as $2\ln E$. The operative point is that the

Field-Feynman model is very sensitive to the initial parton configurations.

Regardless of its shortcomings, the Field-Feynman model was an important first step. As the original authors noted, the Field-Feynman picture is not so much a model or theory as it is a *parameterization* of the then known properties of quark jets. Owing to its simplicity, the Field-Feynman model is still used in most hadron-hadron collision Monte Carlos [21,22,23,24,25], where the focus is not yet on hadronization proper but rather on testing perturbative QCD and the electroweak theory. Unfortunately, testing these theories without an accurate knowledge of hadronization effects will, in almost all cases, be difficult and frustrating. Our motive for presenting the Field-Feynman model is not to advocate its use but rather to provide a reference point for the comparison of more plausible models of hadronization.

2.3   Color Comes To Town

The essential neglect of QCD in the Field-Feynman model correspondingly limits its applicability. Any reasonable treatment of QCD beyond the perturbative regime should respect color quantum numbers since the effective increase of the strong coupling α_s means that color degrees of freedom become more important, not less important as implied in the Field-Feynman model. Since only color singlets have been observed in nature so far, it is plausible that the screening of color charges occurs early on in the process of hadronization [26]. This theoretical bias has been incorporated, in varying degrees, in cluster models [27,5,10] and string models [11,3] by partitioning perturbatively generated partons into color singlets.

Consider the tree diagram in fig. 2.2, which depicts the results of a LLA QCD shower. An important conclusion from LLA QCD analyses is that color flow is planar: color lines (dashed) never cross (see ref. [26] and appendix A). Generalizations of planar color flow beyond LLA QCD have been discussed in ref. [28]. String models map the color singlets onto relativistic strings S_1 and S_2, which subsequently evolve

Figure 2.2 Color flow (dashed lines) allows formation of colorless objects by mapping partons onto strings S_1, S_2, or by dividing the color charge on gluons between adjacent clusters Cl_1, Cl_2, Cl_3.

and fragment according to some, as yet unspecified, dynamical string model. In contrast, cluster models force the "final state" gluons, which contain two color charges, to undergo the effective splitting $g \to q\bar{q}$ to form smaller singlets, Cl_1, Cl_2 and Cl_3, called clusters. Clusters, as such, are then decayed into hadrons using some variant of a phase space model. In the next sections we examine the content of string and cluster models and point out their role in the (r)evolution of hadronization models.

2.4 Cluster Models

Cluster models are the simplest hadronization schemes to use the color information provided by perturbative QCD. They make no assumptions about underlying fragmentation functions (unlike the Field-Feynman picture and, as we shall see, the LUND model) and hence avoid specifying a mechanism for the direct production of hadrons. Cluster models advocate that, if LLA QCD can be used to get from the initial $\gamma^* \to q\bar{q}$ vertex to massive colorless objects a few GeV above particle

production threshold, then the subsequent condensation of low-mass clusters into hadrons is a local, universal phenomenon that can be factored out of the overall event evolution [5]. In essence, the gross properties of hadronization are generated by LLA QCD, while many of the details, such as limited transverse momentum, are attributed to low energy phenomena. This philosophy makes it possible to factor the cluster model event evolution into three distinct stages:

1. Perturbative generation of partons with unique color flow;

2. Subdivision of color singlets into low-mass colorless clusters;

3. Independent decay of low-mass clusters according to a universal ansatz.

By relegating much of the physics to steps 2 and 3, the cluster model does not have to make any assumptions about fragmentation functions or transverse momentum distributions. Fragmentation functions are *predictions* of cluster models rather than assumptions; transverse momentum is generated by the isotropic decay of low-mass clusters. Step 3 is the only phase of the cluster model not presently calculable by QCD and is assumed to be essentially independent of the process by which low-mass clusters are created. Though the decay of low-mass clusters is an important component, cluster models make no radical physics claims about this phase – for most purposes a well-tuned black box would suffice. Conceptually, in fact, a "black box" tuned to low-mass data is precisely what factorization requires! While the decays of low-mass systems are implicit in all hadronization models, cluster models avoid "contaminating" the perturbative physics with the complications of low energy phenomena.

The original cluster model, due to Field and Wolfram [27], proposed that low-mass cluster hadronization was dominated by the two-body phase space decay

$$\text{Cluster} \rightarrow \text{Hadron} + \text{Hadron}. \tag{2.9}$$

Noting that this scheme was adequate only for clusters with mass $\lesssim 1.5$ GeV, Gottschalk [5] extended the decay spectrum of eq. (2.9) to include the subcluster production

$$\text{Cluster} \rightarrow \text{Cluster} + \text{Hadron}. \tag{2.10}$$

This generalization was achieved by assuming a form for the mass spectrum of the daughter cluster and parameterizing low energy data such as $p\bar{p}$ annihilation at rest (see appendix B). The results were incorporated in Caltech-I [5], an improved version of the Field-Wolfram model.

At the beginning of 1987 the only cluster model actively being pursued is BIG-WIG (Branching Iterative Generator With Interfering Gluons), written by Webber [10], which has essentially the same form as the original Field-Wolfram model. Webber's major improvement over the Field-Wolfram model is the incorporation of gluon coherence effects (see appendix A) in the LLA QCD phase. While string models are gaining prominence, BIGWIG attempts to account for the so-called string effect, to be discussed in sect. 5.4, using the perturbative QCD effects suggested by gluon coherence.

The fundamental conceptual drawback of cluster models is their treatment of gluons in step 2 , when color singlets are formed [29,30]. While taking the "independent" out of independent fragmentation, cluster models make use only of nearest neighbor color effects. Like the Field-Feynman model, cluster models force splittings of the form $g \rightarrow q\bar{q}$, which requires an assumption for the sharing of momentum. Regardless of the sharing scheme adopted, there is potential for disaster when soft gluons are generated, as is demonstrated by a simple example.

Consider the $q\bar{q}g$ system of fig. 2.3 where the four-momenta of the quark, antiquark and gluon are, respectively, p_q, $p_{\bar{q}}$, and p_g. If two clusters are formed by artificially splitting the gluon into a $q'\bar{q}'$ pair (dashed lines), then the cluster masses
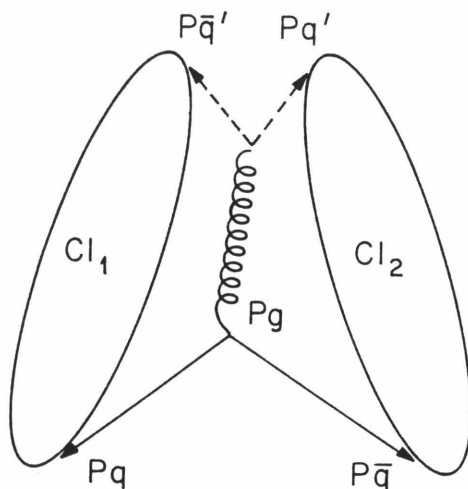
Figure 2.3 Gluon of momentum p_g is artificially split into a quark-antiquark pair (dashed lines) to form two clusters.

are

$$M_1^2 = \left[p_q + p_{\bar{q}'} \right]^2 = 2 E_q E_{\bar{q}'} (1 - \cos \theta_{q\bar{q}'}) \qquad (2.11)$$

$$M_2^2 = \left[p_{\bar{q}} + p_{q'} \right]^2 = 2 E_{\bar{q}} E_{q'} (1 - \cos \theta_{\bar{q}q'}), \qquad (2.12)$$

where we have assumed massless partons, and the notation for energies and angles should be apparent. If the gluon were not present, there would be only one cluster, of mass squared $(p_q + p_{\bar{q}})^2$, which would decay into on-shell particles. Invoking the infrared stability of QCD, there should be no observable difference between a $q\bar{q}$ system and a $q\bar{q}g$ system in which $E_g \to 0$. Yet according to eqs. (2.11-2.12), not only are there two clusters in this limit, but both their masses vanish and hence particle production is impossible! This state of affairs is clearly unacceptable. In practice this disaster is skirted by giving the gluon a mass or by cutting off the perturbative QCD showers early (before very soft gluons are generated). However, since perturbative QCD likes to give soft gluons, cutoffs of this nature end up having a disproportionately large influence on the physics predictions. Either "patch" compromises the original intent of cluster models so that a more consistent treatment

of color effects is warranted.

2.5   String Models

The use of strings in hadronization completely avoids the problems incurred by cluster models' naive treatment of color. Strings are inherently insensitive to soft and collinear gluon radiation and provide a dynamical mechanism for confinement. Before demonstrating how the gluon problem is eliminated, we shall review the origins of strings and consider the treatment of simple $q\bar{q}$ systems in various implementations of the string model.

Strings were originally proposed by Nambu [31], Nielson [32] and Susskind [33] with the intent of giving dual models of strong interactions a field theoretic basis. It was originally hoped that strings might provide *the* field theory of the strong interaction. Unfortunately, a consistent quantization of the theory requires the dimensionality of space-time to be other than four. With the popularization of Yang-Mills QCD in the early 1970s, "fundamental" string theory fell out of grace until it was realized that "superstrings" might be the key to describing physics at the Planck scale of 10^{-33} cm and thus might be a contender for a unified theory [34]. The question remains: What do we make of the salient string-like features on hadronic length scales of 10^{-13} cm, which string theory intended to describe in the first place?

Theoretical conjecture [35,36] and now lattice calculations [37,38] lend credence to the view that hadronic strings are the results of collective phenomena in non-perturbative QCD. A popular view is that the QCD vacuum behaves as a type-II superconductor in which the color flux lines between color charges separated by more than about $\sim .1$ fm are confined to thin filaments with diameter O(.1) fm. These filaments, or strings, give rise to a linear interquark potential, and provide a plausible mechanism for confinement. This state of affairs contrasts that in QED,

QED FIELD LINES
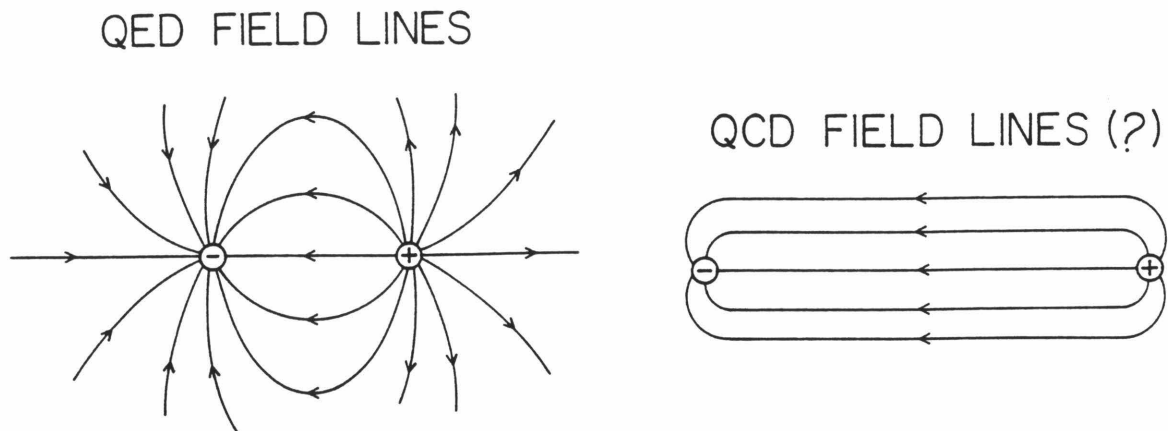
QCD FIELD LINES (?)

Figure 2.4 The spreading of field lines in QED contrasts the proposed containment of field lines in QCD.

where field lines spread out in the vacuum and the familiar $1/r$ potential dominates for large separation of electric charge (see fig. 2.4). As quarks are separated, the potential energy stored in the connecting string increases linearly. Eventually, there is a nonzero transition probability to states containing an additional $q\bar{q}$ pair, at which point a pair is "pulled" from the vacuum and two separate strings result (see fig. 2.5).

The previous two paragraphs illustrate the interesting role of strings in hadronic physics. While there is strong motivation for string-like phenomena on hadronic length scales, most of the original artillery developed for analyzing strings anticipated them to be elementary objects – not some complex manifestation of QCD. Yet we are not deterred. It is clear that what we want is not "correct" string theory (in the sense of, e.g., superstrings) but rather a language in which we can describe hadronic strings without having to specify their inner workings. Admittedly, there is an interest in deriving string-like phenomena directly from the QCD Lagrangian [39], but we should not have to wait for all of the details to be worked out before we know what the basic dynamical consequences of strings are.
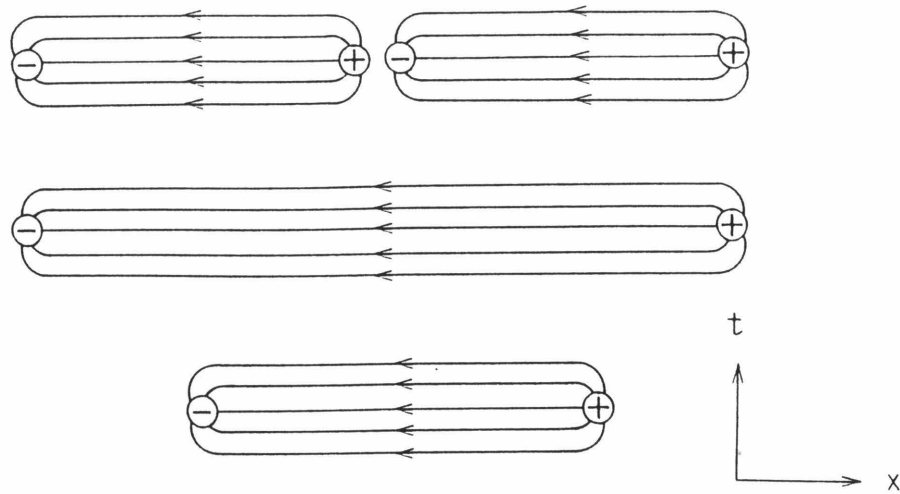
Figure 2.5 Creation of $q\bar{q}$ pairs leads to the creation of substrings.

At this point we must make clear the distinction between "pure" theory and phenomenology. A fitting analogy is the response of a theorist and a phenomenologist when asked to model small amplitude lattice vibrations in a monatomic crystal. While the theorist may try to derive the crystal structure and crystal potentials using just the properties of a bare atom, the phenomenologist would make use of the knowledge that crystals exist, that there are equilibrium points about which atoms vibrate and that the crystal potential at a given lattice site may be approximated by a quadratic potential — resulting in a simple harmonic oscillator model. The phenomenologist would then go to experimental data to determine the value of the "spring constant" implicit in his model. The moral is that we don't have to know everything to know something. Applying this philosophy to hadronic strings, we want only the gross properties of strings — not the details. All we shall initially require of our hadronic strings are that they provide a linear confining potential and be consistent with special relativity.

The first string model of hadronization was proposed by Artru and Mennessier [40] and Artru [41] in which they considered the breakup of $q\bar{q}$ systems. In $1 + 1$
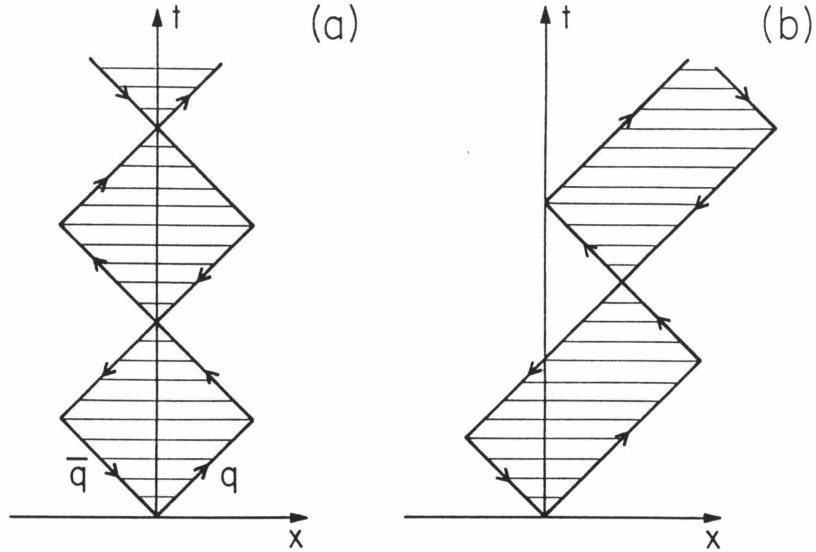
Figure 2.6 (a) Space-time motion of $q\bar{q}$ system of massless quarks in CM frame. (b) Same system viewed from a frame boosted along $-x$ axis.

dimensions the equation of motion of an endpoint quark in the CM frame of a $q\bar{q}$ system is

$$\frac{dp}{dt} = -\text{sign}(p)\kappa, \tag{2.13}$$

where κ is the tension of a string at rest, which gives rise to the linear potential, p is the quark momentum, and the function

$$\text{sign}(p) = \begin{cases} -1 & p < 0 \\ +1 & p > 0 \end{cases}, \tag{2.14}$$

ensures that the potential is confining. Eq. (2.13) is covariant but not manifestly so. Comparisons of this simple model with Regge trajectories yield a string tension $\kappa = .2\,\text{GeV}^2$. The space-time picture of the motion of a $q\bar{q}$ system of massless quarks, affectionately known as a yo-yo, as viewed from its CM frame, is shown in fig. 2.6a. Fig. 2.6b shows the same system as viewed from a frame boosted along the $-x$ axis. Since the world sheet of the string is a geometrical object with properties independent of any reference frame, it is not surprising that the invariant area A (the two-dimensional analogue of proper time) swept out during one complete cycle

t

C_1 C_2 C_3 C_4

3

1   2

$\bar{q}_0$ q_0
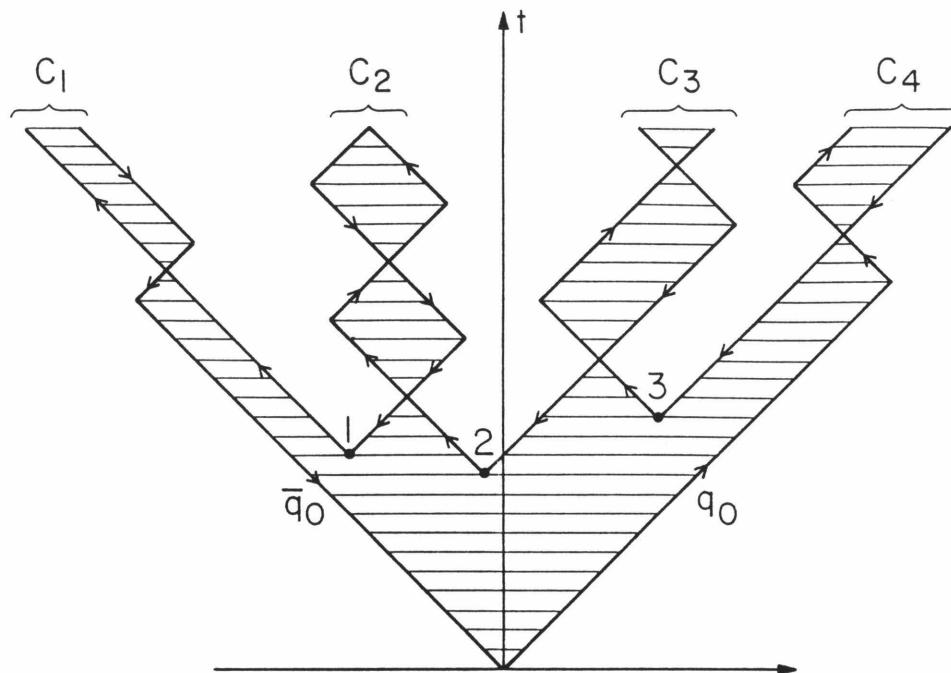
Figure 2.7 A string system of massless quarks fragments into less massive systems by pulling massless quark pairs from the vacuum.

of yo-yo motion is a function of κ and the invariant mass W of the system, the only invariants available. For a yo-yo it is easy to show that

$$A = \frac{M^2}{\kappa^2}. \tag{2.15}$$

The implication is that the areas of the rectangles in figs. 2.6a,b are equal.

Fig. 2.7 schematically depicts how a $q\bar{q}$ system breaks up into a number of less massive systems by pulling quark pairs from the vacuum. Note how the color field vanishes in the immediate future of the space-time points where massless pairs are created. However, if we want more than a schematic view, we have to specify the space-time distribution of string breaks. The only true guideline we have in this area is that we must not allow string breaks to produce substrings with masses below that of a pion. Below, we discuss two alternative prescriptions for breaking strings: one proposed by Artru and Mennessier [40], which predicts a continuous mass spectrum of substrings and one proposed by the LUND group [11], with a substring mass spectrum identical to the discrete mass spectrum of hadrons. Caltech-II adopts the

Artru-Mennessier ansatz and follows it with the parameterized decay of low-mass clusters (appendix B) while the LUND picture is reminiscent of the Field-Feynman model in that substrings (which they identify with hadrons) are "peeled" off at each node of a decay chain.

The Artru-Mennessier prescription for string breaking is the simplest covariant ansatz possible. It assigns a uniform string-breaking probability $\mathbf{P}_0$ per unit invariant area of the string world sheet

$$dP_{\text{break}} = \mathbf{P}_0 dA. \tag{2.16}$$

This is simply a generalization of the familiar radioactive decay law in which the probability of a point particle decaying during an interval dt of its proper time is given by a decay constant. We shall henceforth refer to eq. (2.16) as the area law or area decay law. The worrisome implication of the area law is that, if applied literally, a massive $q\bar{q}$ system ultimately fragments into an infinite number of zero mass strings, since no account is taken of the physical particle mass spectrum. In practice, this is avoided by terminating string evolution once string masses fall below a certain cutoff and then applying some variant of a phase space model. This is precisely the approach taken in the Caltech-II model, where low-mass strings are identified with low-mass clusters and are decayed using a parameterization of low energy data.

The LUND model [11] for string fragmentation is based on the iterative chain

$$\text{String} \rightarrow \text{String} + \text{Hadron}, \tag{2.17}$$

except at the end of the chain, in which case a string decays into two hadrons. The requirement that the produced hadrons be on-shell puts restrictions on the allowed space-time distribution of string breaks. To illustrate this point, consider a toy model in $1 + 1$ dimensions in which there exists only one flavor of massless quark
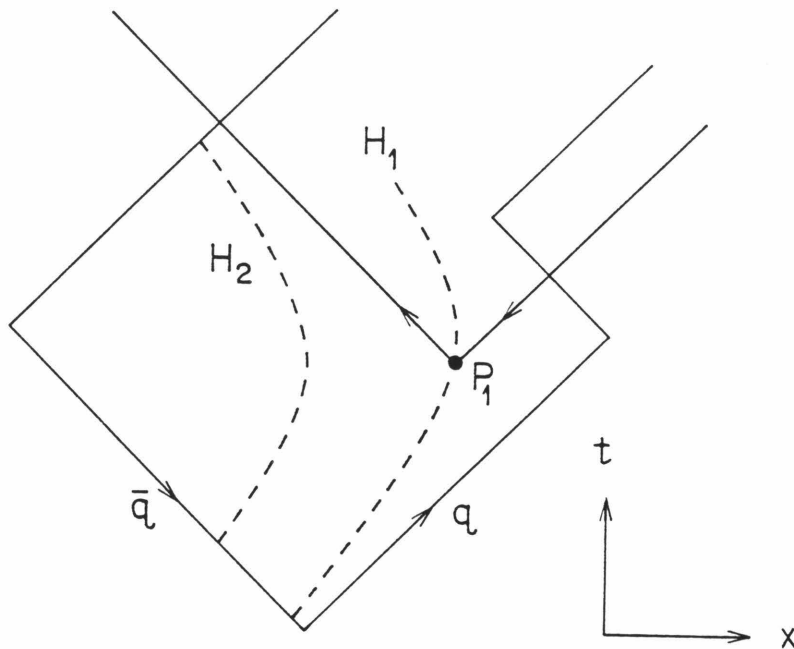
Figure 2.8 Mass shell constraints in the LUND model require string breaks to occur along hyperbolas. Positions along a given hyperbola are parameterized by the variable z.

and only one species of stable hadron, of mass M. Suppose we start peeling hadrons off the q end of a string as in fig. 2.8. Because of the relationship between the mass of a string and the invariant area in one half-cycle, the break closest to the q end must occur somewhere along the hyperbola H_1. If it happens that the break occurs at point P_1, then the next break must occur somewhere along hyperbola H_2, and so on for subsequent iterations. Given this set of constraints, and parameterizing the break position along each hyperbola by the variable z, LUND seeks a string fragmentation function $f(z)$, which determines the space-time distribution of the string breaks. Further requiring that the iterative application of $f(z)$ yield the same physics, on average, regardless of which end of the string hadrons are peeled off, it can be shown [42] that the fragmentation function is restricted to be of the form

$$f(z) = N\frac{1}{z}(1 - z)^a e^{-bM^2/z}, \tag{2.18}$$

where a and b are adjustable parameters and N is a normalization constant. Gener-

alizing to many flavors requires, in principle, a corresponding increase in parameters but in practice $a = 1$ and $b = .7\,\text{GeV}^{-2}$ are used for all flavors. By starting from a fragmentation function, the LUND procedure parallels the Field-Feynman model except that the basic object undergoing fragmentation is a string system rather than a single parton. Nevertheless, this is an improvement, since confinement effects are taken account of explicitly.

As stated above, string models offer an attractive picture of gluons. When generalizing the string model beyond $q\bar{q}$ systems, we invoke a dynamical principle, namely, the principle of least action, to yield string motions. As will be discussed more fully in Sect. 3.2, the string action is taken to be

$$S = -\kappa \int\limits_{\tau_1}^{\tau_2} d\tau \int\limits_{0}^{\pi} d\sigma \sqrt{(\dot{x} \cdot x')^2 - x'^2 \dot{x}^2}, \qquad (2.19)$$

where

$$\dot{x}^\mu = \frac{\partial x^\mu}{\partial \tau}, \qquad x'^\mu = \frac{\partial x^\mu}{\partial \sigma}, \qquad (2.20)$$

and we employ a metric such that $g^{00} = -g^{ii} = 1; g^{ij} = 0, i \neq j$. Our notation is such that $\dot{x} \cdot x' = \dot{x}^\mu x'_\mu$. The world sheet coordinates σ and τ are respectively spacelike and timelike. Though eq. (2.19) is the same action as is used for bosonic strings in "fundamental string theory," we are using it with much less lofty expectations. We are using it simply because we want a relativistic theory, and eq. (2.19) is the two-dimensional analogue of the action for a point relativistic particle: we look for extrema in the invariant area of a world sheet rather that for extrema in the invariant length of a world line. Not only does this Lagrangian lead to a linear confining potential as in eq. (2.13), but it also accommodates an interpretation of gluons as energy- and momentum-carrying kinks on the string.

The string motion for one half-cycle of a symmetrical $q\bar{q}g$ system is shown in fig. 2.9. During the first phase of motion the three partons diverge from each other, all the while losing energy and momentum that is stored in the interconnecting

Full String
Motion

G → qq̄
Ansatz

(a)

y + t

x

(b)
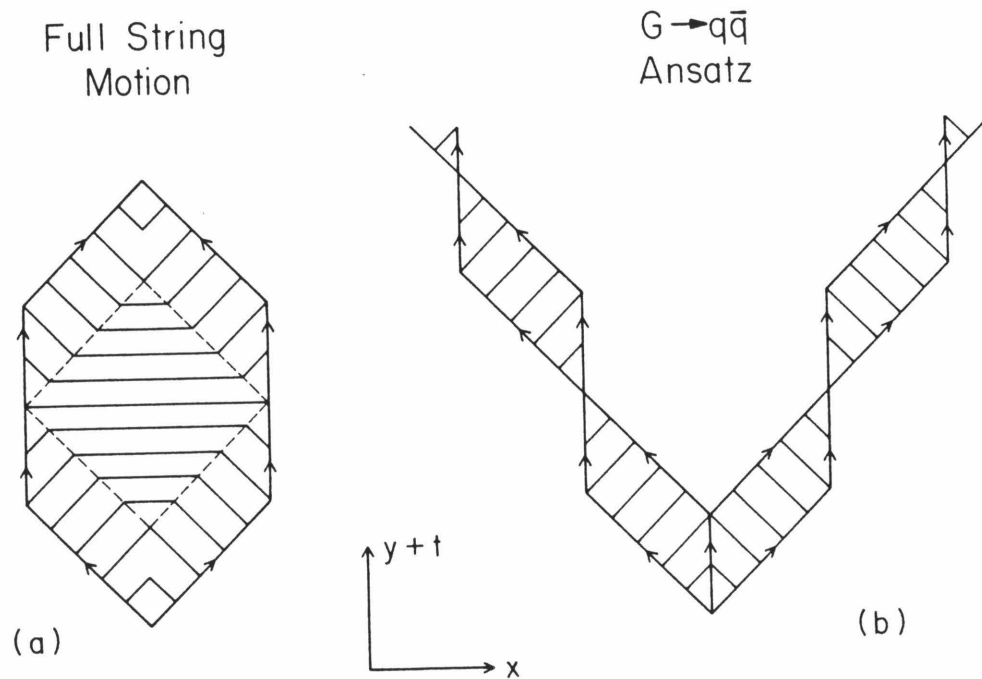
Figure 2.9 (a)One half-cycle of string motion for symmetrical $q\bar{q}g$ system. (b) Corresponding string motions if original gluon is forced to split into quark-antiquark pair.

string. The gluon loses energy and momentum at twice the rate of the endpoint quarks, since gluons carry twice as much color charge. When the gluon loses all of its energy, two new oppositely moving kinks appear. Unlike the original gluon kink, these new kinks carry no energy or momentum: a point that is not obvious unless one examines the solutions to the equations of motion. These momentumless kinks bounce off the ends of the strings and eventually recombine in the middle of the string where energy and momentum again start to accrete. This process continues in a periodic fashion.

If we reconsider the infrared gluon problem encountered by cluster models, we can appreciate its resolution by the string picture. Fig. (2.9b) shows the space-time development of a $q\bar{q}$ system, where the initial gluon is artificially split into a quark-antiquark pair with an equal division of energy and momentum. The space-time history of the two resulting yo-yos is certainly different from the full string motion in fig. 2.9a. If we let the gluon energy go to zero, it is easy to see that the full string motion in fig. 2.9a reduces uniformly to that of a yo-yo, while the ansatz of fig. 2.9b predicts two massless yo-yos separating at the speed of light. The insensitivity of string models to soft gluons is manifest.

2.6 Review

The discussion in the previous sections was intended as an overview of different approaches to hadronization. Here we wish to emphasize and summarize the most important of these differences. We have presented the Field-Feynman model as a zeroth order model, that parameterizes hadronization through a *quark* fragmentation function that neglects QCD. We summarily dismissed that scheme since it is an unrealistic hadronization picture.

Taking color into account, we arrived at cluster models based on perturbative QCD and simple phase space arguments, in which fragmentation functions are *pre-*

dictions, not assumptions. Finally, we showed string models to be the most sophisticated of the QCD-motivated hadronization pictures. But within a string framework there remain vestiges of both the Field-Feynman model and cluster models. The LUND scheme parallels the Field-Feynman model by assuming a "string fragmentation function," while the Caltech-II picture embraces the cluster model philosophy by adopting the Artru-Mennessier ansatz for string breaks, followed by a phase space parameterization. These differences can be rephrased in terms of answering the question: "At what stage of hadronization do hadrons appear?" LUND contends that hadrons appear very early in event evolution by employing the iterative chain

$$\text{String} \rightarrow \text{String} + \text{Hadron}, \tag{2.21}$$

in which string fragments are immediately identified with hadrons. On the other hand, models such as Caltech-II take the conservative view that hadrons are the results of the decay of low-mass clusters that are produced in a framework relatively unconstrained by hadron mass shell requirements.

There are already hints that nature is actually a combination of the LUND and Caltech-II pictures. Caltech-II must sometimes invoke the mechanism of eq. (2.21) to reproduce the observed population of high z particles (sect. 5.3.4), while there is evidence that the LUND fragmentation function of eq. (2.18) is at variance with general expectations for quarks heavier than bottom (sect. 6.9).

We have compiled a pictorial summary of the models in fig. 2.10, assuming each one is given the same perturbatively generated $q\bar{q}g$ set of partons. In all the models, hadrons are represented by solid circles. Note how the Field-Feynman and cluster models must effectively split the gluon into a quark-antiquark pair (dotted lines) before they continue hadronizing the system. Whereas the Field-Feynman model evolves each quark separately, without regard to color screening, the cluster model immediately forms colorless clusters (circles), which then decay into hadrons.
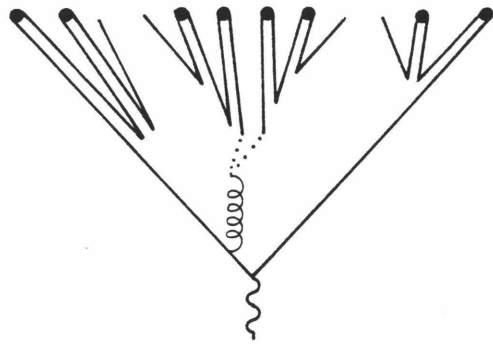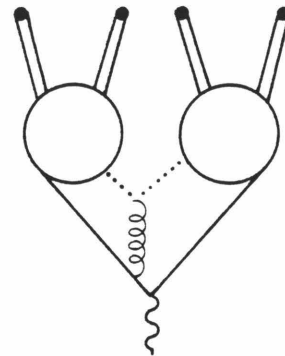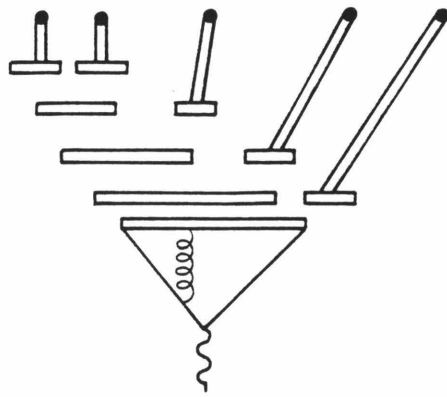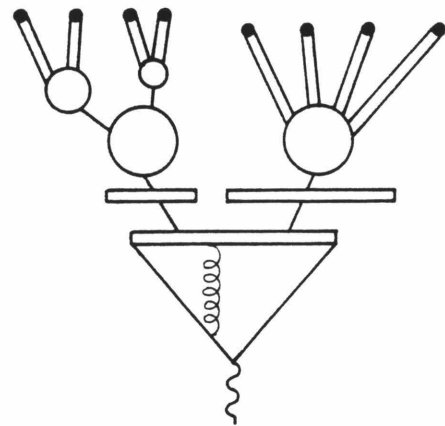
Figure 2.10 Schematic illustration of hadronization in the Field-Feynman, Cluster (Webber), Caltech-II and LUND models. Graphical notation is described in the text.
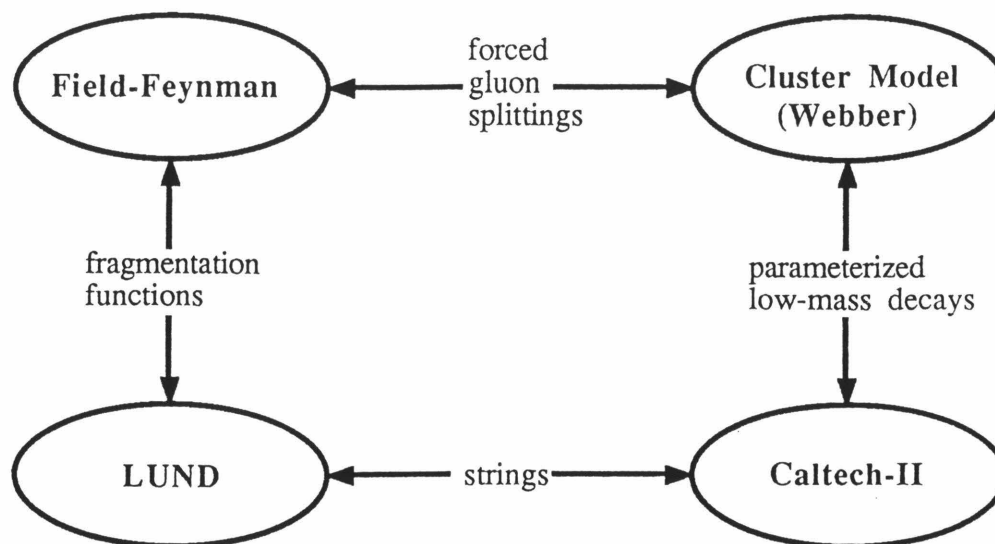
Figure 2.11 Summary of the features common to pairs of models. This diagram expresses in words what fig. 2.10 illustrates schematically.

Both the LUND and Caltech-II models refrain from artificially splitting the gluon by mapping the partons onto strings (horizontal bars). These string models differ in that LUND forces string fragmentation to yield at least one hadron each time a string breaks, making a direct connection between string fragments and a physical particles. On the other hand, Caltech-II uses string fragmentation to produce low-mass substrings, which are then identified with clusters. The clusters may break into subclusters or decay directly into hadrons using a parameterization of low-mass data.

Fig. 2.11 summarizes the essential features shared between pairs of the various models. We have intentionally omitted differences in the implementations of perturbative QCD.

2.7 Summary

In this chapter we have presented a brief history and critique of hadronization pictures to show how Caltech-II incorporates our theoretical and phenomenological biases into a sensible and appealing model of hadronization. Though we have only

scratched the surface of the various models, this chapter has been rather drawn out — our goal will be accomplished if the reader has a cursory knowledge of the differences between the Field-Feynman, Cluster, Caltech-II and LUND models.

At this point it is helpful to restate the structure of the Caltech-II model. The model makes hadronization tractable by factorizing event evolution into the three stages

$$\text{LLA QCD} \otimes \begin{array}{c} \text{Relativistic String} \\ +\text{Area Decay Law} \end{array} \otimes \begin{array}{c} \text{Low} - \text{Mass} \\ \text{Parameterization.} \end{array} \qquad (2.22)$$

Each stage in eq. (2.22) has either theoretical or phenomenological motivations. The first phase, the generation of multiparton systems according to leading log QCD, has the most apparent ties to the Lagrangian framework of QCD. The string phase, in which LLA partons are mapped onto relativistic strings and decayed into a collection of colorless clusters, is an elementary dynamical embodiment of the phenomenon of color confinement — the best that can be done with our current understanding of nonperturbative QCD. The third and final phase, the parameterized decay of low-mass clusters into hadrons, is mandated by the known complexity of hadronization at small mass scales. In the context of a larger hadronization model, there is nothing to be gained by proposing a dynamical model for cluster decay; there are many missing pieces to the hadronization puzzle, so that progress will be made faster (and more accurately) if we simply use what is empirically known from low-mass data.

Although this thesis is devoted primarily to the string phase in eq. (2.22), it important to remember that the structure of the string phase will be determined largely by the phases surrounding it. The string phase receives its input from the LLA QCD phase, using the final state partons to define the world sheets of the associated strings. Though we use the full equations of motion for the relativistic string, we trust the semiclassical string model to give only the gross characteristics of fragmentation and instead relegate the details of hadronization to the decay of low-mass clusters.

In the next two chapters we go into the string model in more detail. Though the role of strings in Caltech-II is a conceptually simple one, implementing the model in the form of a Monte Carlo program is straightforward only if we first develop a familiarity with the basics of string kinematics. Chapter 3 outlines the general concepts that make it easy to work with relativistic strings, while chapter 4 discusses the specifics of implementing strings in Caltech-II.

Chapter 3

Relativistic String Kinematics

3.1 Introduction

Caltech-II is the only hadronization model capable of treating arbitrary relativistic strings with an area decay law. Though Artru and Mennessier [40] were the first to propose an area decay law for strings, they considered only the evolution of $q\bar{q}$ systems. As outlined in Chapter 2, a proper treatment of QCD must make allowances for gluons and be infrared stable. In this and the next chapter, we demonstrate how the area decay law can be made compatible with the motion of arbitrarily complicated relativistic strings. There is a natural division between the material of this chapter and the following one. In this chapter we develop a framework for the kinematics of relativistic strings, while the next chapter covers the specifics of how this framework is applied to Caltech-II.

Since our goal is to incorporate the string model into a Monte Carlo program, we need a completely unambiguous interpretation of string motion. While "pencil pushing" calculations manipulate abstract quantities in their most general form, we are instead interested in numerical specifics. With these constraints in mind, we have developed a novel interpretation of strings in terms of momentum currents [6], making the simulation of relativistic string motion and fragmentation a rather trivial exercise.

Before developing our formalism, it is worthwhile to point out why this hasn't been done sooner. Although the LUND model [11] is also based on relativistic strings, its ansatz for string breaks uses fragmentation functions, as discussed in Chapter 2. LUND sets up the world sheet of the string associated with perturbative partons, only to use it to define the boundaries of the domain of their fragmentation function. Because of the iterative nature of the LUND fragmentation chain,

$$\text{String} \rightarrow \text{String} + \text{Hadron}, \tag{3.1}$$

the world sheet of the daughter "recoil" string is nothing but that portion of the parent's world sheet that hasn't already been identified with hadrons. LUND avoids dealing with the complications of string kinematics by immediately identifying the "new" piece of the world sheet (which is *not* simply a leftover piece of parent's world sheet) with a physical hadron.

As we shall see in the next chapter, the area decay law for string fragmentation can be expressed in a decay chain format similar to LUND, where decay products are successively peeled off one end of a string. The crucial difference is that Caltech-II, unlike LUND, allows string decays of the form

$$\text{String} \rightarrow \text{String} + \text{String}, \tag{3.2}$$

where neither of the decay products is required to be on the mass shell of a physical particle. Whereas the world sheet of one of the daughter strings may be identified with an "unused" portion of the parent's world sheet (like LUND), the detailed shape of the other daughter's world sheet (the object peeled off) requires additional work. Since Caltech-II may want to fragment this other daughter using the area decay law, we must be able to calculate the detailed shape of its world sheet. The remainder of this chapter discusses how we can economically determine the world sheet of *any* string produced during string fragmentation from a knowledge of the original parton four-momenta.

Our approach will be to deduce the string equations of motion starting from a plausible string Lagrangian. We then propose an interpretation of the solution to the equations of motion in terms of quarks and gluons and show how an arbitrary initial parton configuration is mapped onto an associated string. Up to this point the formalism is useful to either the Caltech-II or LUND models, since no mention is made of mass shell constraints. However, we point out the technical difficulties with the naive approach to string evolution through many generations as is required by Caltech-II if an area decay law is adopted. Fortunately, by recasting the formalism in terms of momentum currents, we are able to make the propagation of string configuration information through many generations transparent and easy to implement.

3.2 String Equations of Motion

In sect. 2.5 we presented the simple solution to a phenomenological model of two massless quarks connected by a linear potential characterized by a string tension κ. The intuitive picture we had in mind was that of a color flux tube stretched between the color triplet charges of the quarks. Extending this picture to gluons, which belong to a color octet, we might anticipate one of the two string configurations for a $q\bar{q}g$ system pictured in fig. 3.1. In (a) a gluon is connected to a piece of "color octet string" that meets two "color triplet" strings at a junction, while in (b) a gluon is connected to two pieces of "color triplet" string. Case (a) has been discussed by Montvay [43] and in general requires a separate string tension for the octet string. We will consider the case in (b). Since the gluon is attached to two pieces of string, the gluon loses energy twice as fast as quarks. This is to be compared with the QCD results for the case of N_c colors in which the ratio between forces on gluons and quarks is $2/(1 - 1/N_c^2)$, which is 2 for $N_c \rightarrow \infty$ and 9/4 for $N_c = 3$.

In $(1 + 1)$ dimensions it is a straightforward exercise to extend the differential
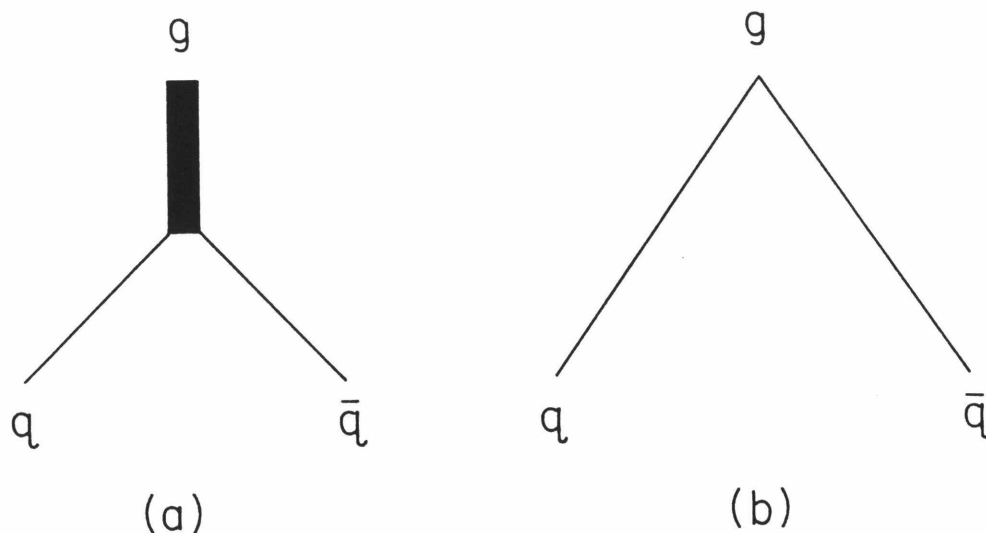
Figure 3.1 Two types of flux tube connections in a $q\bar{q}g$ system.

equation eq. (2.13) to account for gluons. Yet in that format one must explicitly account for the discontinuities in dp/dt that occur when partons, connected by a common string, intersect. This complication is manageable for $q\bar{q}$ systems but becomes unwieldy for arbitrary systems of partons. Furthermore, we ultimately want to work in $(3 + 1)$ dimensions where partons are not necessarily collinear. If we dealt only with $q\bar{q}$ systems, we could always boost to the rest frame of the string and thus use the $(1 + 1)$ dimensional theory. In general, however, there are many nonparallel pieces of string within a color singlet so that there is no global string rest frame. In that event we have either to set up local string rest frames or choose one global frame and accordingly modify the effective string tension, which is a function of the string's transverse velocity. Neither alternative is aesthetically pleasing nor particularly easy to implement, since each requires keeping track of bits and pieces of strings. Fortunately, a more coherent treatment is possible by applying a dynamical principle — the principle of least action.

The action for a point relativistic particle of mass m is

$$S = -m \int_{\tau_1}^{\tau_2} d\tau, \tag{3.3}$$

where τ is the particle's proper time. Lorentz invariance is manifest since the action is proportional to the invariant length of the world line of the particle. Generalizing this concept to objects with one-dimensional spatial extent, we can write down the Nambu-Goto [31] action for the string

$$S = -\kappa \int_{\Omega} dA, \tag{3.4}$$

where dA is an element of Lorentz invariant area, the integral is performed over a region Ω of the string's world sheet and κ is a proportionality constant we can later identify with the string tension in a frame in which the string is at rest. An expression for dA follows immediately from the metric tensor, which we take as $g^{00} = -g^{ii} = 1; g^{ij} = 0, i \neq j$, so that the action takes the form

$$S = -\kappa \int_{\tau_1}^{\tau_2} d\tau \int_0^{\pi} d\sigma \sqrt{(\dot{x} \cdot x')^2 - x'^2 \dot{x}^2}, \tag{3.5}$$

with

$$\dot{x}_{\mu} = \frac{\partial x_{\mu}}{\partial \tau}, \qquad x'_{\mu} = \frac{\partial x_{\mu}}{\partial \sigma}, \tag{3.6}$$

where σ and τ are, respectively, *arbitrary* spacelike and timelike coordinates on the world sheet subject to the convention that $\sigma = 0$ and $\sigma = \pi$ are identified with the ends of open strings. The string we are describing is often referred to as the massless relativistic string; however, the qualifier "massless" is somewhat misleading since a segment of string of length l in segment's rest frame has a mass of κl. It is more appropriate to think of "massless" as referring to the explicit absence of massive endpoint quarks in our formulation. The theory described by eq. (3.5) may be viewed as a field theory in two dimensions (σ, τ) of a four-vector valued field. The results of analyzing this problem using the techniques of classical field theory

appear in many detailed review articles [44,45,46,47], but we'll reproduce some key results for the sake of completeness.

Defining the string Lagrangian as

$$L = -\kappa\sqrt{(\dot{x} \cdot x')^2 - \dot{x}^2 x'^2},$$ (3.7)

we vary the world sheet and look at the change in the action

$$\delta S = \int d\sigma \frac{\partial L}{\partial \dot{x}_\mu} \delta x_\mu \bigg|_{\tau=\tau_1}^{\tau=\tau_2} + \int d\tau \frac{\partial L}{\partial x'_\mu} \delta x_\mu \bigg|_{\sigma=0}^{\sigma=\pi} - \int_{\tau_1}^{\tau_2} d\tau \int_0^\pi d\sigma \left[\frac{\partial}{\partial\tau} \frac{\partial L}{\partial \dot{x}_\mu} + \frac{\partial}{\partial\sigma} \frac{\partial L}{\partial x'_\mu} \right] \delta x_\mu.$$ (3.8)

If we fix the "initial" and "final" configurations of the string on the spacelike curves $\tau = \tau_1$ and $\tau = \tau_2$, then an extremum in the action, $\delta S = 0$, requires the integrand in the first term of eq. (3.8) to vanish while the vanishing of the integrand in the third term yields the Euler-Lagrange equations

$$\frac{\partial}{\partial\tau} \frac{\partial L}{\partial \dot{x}_\mu} + \frac{\partial}{\partial\sigma} \frac{\partial L}{\partial x'_\mu} = 0.$$ (3.9)

For closed strings the integrand of the second term in eq. (3.8) vanishes identically since $\sigma = 0$ and $\sigma = \pi$ are the same physical positions, but open strings must require

$$\frac{\partial L}{\partial x'_\mu} = 0 \qquad \sigma = 0, \pi.$$ (3.10)

Writing out the equations of motion explicitly, eq. (3.9) turns into the unsightly behemoth

$$\frac{\partial}{\partial\tau} \left[\frac{(\dot{x} \cdot x')x'_\mu - (x')^2 \dot{x}_\mu}{\sqrt{(\dot{x} \cdot x')^2 - \dot{x}^2 x'^2}} \right] + \frac{\partial}{\partial\sigma} \left[\frac{(\dot{x} \cdot x')\dot{x}_\mu - (\dot{x})^2 x'_\mu}{\sqrt{(\dot{x} \cdot x')^2 - \dot{x}^2 x'^2}} \right] = 0.$$ (3.11)

The arbitrariness of the parameters σ and τ is usually referred to as the reparameterization invariance of the world sheet – a reflection of the fact that the world sheet is a geometrical object with properties (e.g., invariant area) independent of any coordinate system. We can use this arbitrariness in σ and τ to simplify eq. (3.11). We can partially fix σ and τ by going into the local tangent plane of the string and

erecting orthogonal axes with the timelike τ axis aligned with the time axis of a global Lorentz frame. With these directions specified, we can also require the σ and τ basis vectors to have the same normalization. The only degree of freedom left is in specifying the constant of proportionality between, say, τ and the time. The orthogonality requirement and relative normalization condition are summarized as

$$\dot{x} \cdot x' = 0, \qquad \dot{x}^2 + x'^2 = 0, \tag{3.12}$$

where the plus sign in the normalization condition reflects the fact that one axis is spacelike, while the other is timelike. In the parlance of string theory, this is a particular choice of gauge called the orthonormal gauge (a slight misnomer because only the *relative* normalization is fixed). This choice of gauge reduces the equation of motion to a wave equation

$$\frac{\partial^2 x_\mu}{\partial \tau^2} - \frac{\partial^2 x_\mu}{\partial \sigma^2} = 0, \tag{3.13}$$

where the boundary conditions for an open string are

$$x'_\mu(\sigma=0, \tau) = 0, \qquad x'_\mu(\sigma=\pi, \tau) = 0, \tag{3.14}$$

and the continuity conditions for a closed string are

$$x'_\mu(\sigma=0, \tau) = x'_\mu(\sigma=\pi, \tau), \qquad \dot{x}^\mu(\sigma=0, \tau) = \dot{x}^\mu(\sigma=\pi, \tau). \tag{3.15}$$

Using the usual techniques for extracting conserved currents from the Lagrangian, it is easy to show that components of the momentum current on the surface of the world sheet are

$$P_\tau^\mu = -\frac{\partial L}{\partial \dot{x}^\mu}, \tag{3.16}$$

and

$$P_\sigma^\mu = \frac{\partial L}{\partial x'^\mu}, \tag{3.17}$$

which in our gauge become

$$P_\tau^\mu(\sigma, \tau) = \kappa \dot{x}^\mu(\sigma, \tau), \tag{3.18}$$

and

$$P_\sigma^\mu(\sigma,\tau) = -\kappa x'^\mu(\sigma,\tau). \tag{3.19}$$

It is thus easy to see that the boundary condition eq. (3.14) is simply the statement that no momentum flows out of the ends of an open string. If one works with closed strings, the periodic boundary conditions in eq. (3.15) correspond to the uninterrupted flow of momentum around a loop. Since closed strings require only a slightly different treatment from open strings, we relegate their treatment to appendix C and hereafter focus our attention on open strings.

We can develop our intuition for the string motion if we familiarize ourselves with the (σ,τ) coordinate system. Suppose we define τ to be the time x^0 in the global Lorentz frame from which we view the string, scaled by κ, so that $\tau = \kappa x^0$ has the dimensions of energy. In this case

$$P_\tau^\mu = \frac{\partial x^\mu}{\partial x^0}, \tag{3.20}$$

so that the cumulative energy measured from one end of the string at a fixed time is

$$P^0(\sigma) = \int_0^\sigma P_\tau^0 \, d\xi = \sigma. \tag{3.21}$$

We conclude that σ is the cumulative energy stored in the string. This brings us to an interesting point. Substituting the boundary condition of eq. (3.14) into the gauge condition of eq. (3.12) implies that ends of the string move at the speed of light. This is consistent with the view of identifying the string endpoints with massless quarks: the vanishing of x'_μ at the ends of the string corresponds to point concentrations of energy and momentum according to eq. (3.21). The extension of this interpretation to gluons will become clear when we work out a simple example of a $q\bar{q}g$ system. A particularly attractive feature of this formalism is that of homogeneity. Quarks and gluons are, within this framework, energy- and momentum-carrying "kinks" or

point discontinuities on the string. This view contrasts our previous view of quarks and gluons as separate entities connected by a distinct string medium.

The canonical solution to the wave equation may be written in the familiar form

$$x^\mu(\sigma,\tau) = \frac{1}{2}\left[f^\mu(\sigma+\tau) + f^\mu(\sigma-\tau) + \int_{\sigma-\tau}^{\sigma+\tau} g^\mu(\xi)\,d\xi\right], \tag{3.22}$$

where

$$f^\mu(\sigma) = x^\mu(\sigma,\tau{=}0), \qquad g^\mu(\sigma) = \dot{x}^\mu(\sigma,\tau{=}0), \qquad 0 \le \sigma \le \pi. \tag{3.23}$$

Outside the interval $\sigma = [0,\pi]$, $f(\sigma)$ and $g(\sigma)$ are the even periodic extensions about $\sigma = 0$ and $\sigma = \pi$ as a consequence of the boundary conditions. Our identification of the σ and τ coordinates affords us an interpretation of wave disturbances moving in opposite directions along the string.

We now have all the necessary ingredients for describing string motions. What remains to be done is to make a correspondence between a set of partons and initial conditions of the associated string. As an example, suppose we are given a $q\bar{q}g$ color singlet, where all partons are massless and emerge from a common space-time point. Their respective four-momenta p_q, p_g, $p_{\bar{q}}$ have components of the form (p^0, p^1, p^2, p^3). For purposes of illustration we shall take $\kappa = 1$ in eq. (3.21), so that σ is identically the cumulative energy measured from one end of the string and so runs from 0 to $E_q + E_g + E_{\bar{q}}$ instead of 0 to π. With this convention we can start at, say, the quark end of the string and use the color ordering to uniquely associate a parton with an energy interval

$$q \mapsto \quad \sigma_0 \le \sigma \le \sigma_1,$$

$$g \mapsto \quad \sigma_1 < \sigma \le \sigma_2, \tag{3.24}$$

$$\bar{q} \mapsto \quad \sigma_2 < \sigma \le \sigma_3,$$

$$\tag{3.25}$$

where

$$\begin{pmatrix} \sigma_0 \\ \sigma_1 \\ \sigma_2 \\ \sigma_3 \end{pmatrix} = \begin{pmatrix} 0 \\ E_q \\ E_q + E_g \\ E_q + E_g + E_{\bar{q}} \end{pmatrix}. \tag{3.26}$$

Since the string initially has zero spatial extent, $f(\sigma, \tau) = 0$. Furthermore, because the partons are massless and we have chosen $\tau = x^0$, the "velocity" components of $g(\sigma)$ are obtained by dividing the four-momentum vectors by their respective energy so that we have

$$g^\mu(\sigma) = \begin{cases} p_q^\mu/E_q & \sigma_0 \leq \sigma \leq \sigma_1; \\ p_g^\mu/E_g & \sigma_1 < \sigma \leq \sigma_2; \\ p_{\bar{q}}^\mu/E_{\bar{q}} & \sigma_2 < \sigma \leq \sigma_3. \end{cases} \tag{3.27}$$

The generalization of $g^\mu(\sigma)$ to the case of multiple gluons is straightforward. It might be pointed out that if LLA QCD is not used, color ordering for multiple gluons becomes a nontrivial issue, since different orderings will in general lead to different string motions [28].

In principle, we have a complete solution to problem of string motion for an arbitrary set of partons. Using initial parton momenta, we have shown how to generate the initial conditions for the wave equation so that one has only to insert values into eq. (3.22). If it should happen that the string breaks at the point $(\bar{\sigma}, \bar{\tau})$ and creates two new strings (as opposed to a recoil system and an on-shell particle à la LUND), we could generate the initial conditions for each daughter by evaluating $x^\mu(\sigma, \tau = \bar{\tau})$ and $\dot{x}^\mu(\sigma, \tau = \bar{\tau})$ for the parent; after defining the suitable extensions for the initial conditions of the daughters, we may iterate the whole process to generate a cascade of string breaks.

Practically speaking, a naive implementation of this algorithm leads to an "information explosion." To understand this phenomenon consider an initial system of a quark, antiquark and $n - 2$ gluons. From the discussion above, the function $g^\mu(\sigma)$ will be piecewise constant on n intervals. As the system evolves in time, the superposition of left- and right-moving waves will, in general, make $\dot{x}^\mu(\sigma, \tau)$ a piecewise constant function on $2n - 1$ intervals. Introducing a break in the string forces us

to keep track of $2n$ intervals so that iterating this process through m generations entails knowledge of $2^m n$ intervals. An associated problem, albeit a technical one, is that this scheme involves many intermediate calculations. Determining the initial conditions for the "next" generation involves forming some superposition of the "current" initial conditions, which are themselves a result of previous calculations.

The above algorithm is a scenario in which we are forced to double our workload each time a string breaks. In the next few sections we demonstrate how a frugal decomposition of the wave equation requires us to keep track of only $2(n - 2 + 2^m)$ intervals. Better yet, we never have to generate new initial conditions from successive combinations of old ones. The significance of this result is apparent when one considers the prospect of fragmenting systems with large numbers of partons ($n \gtrsim 5$), which are not uncommon in shower models of perturbative QCD [48,49] .

3.3 Waves Expressed In Momentum Currents

The apparent doubling of information each time a string fragments is easily traced back to the conspiracy of superposition. In this section we reexpress the solution to the wave equation to illuminate the fact that superposition may be effected by a time dependent linear operator acting on the initial state of the string. The initial state is expressed in terms of momentum currents so that a physical interpretation of the solutions in terms of momentum flow becomes possible.

Because of its even extension about $\sigma = 0$ and $\sigma = \pi$, the initial condition $g^\mu(\sigma)$ enjoys the properties $g(\sigma)^\mu = g^\mu(-\sigma)$ and $g^\mu(\pi-\sigma) = g^\mu(\pi+\sigma)$. Identical properties are shared by the initial condition $f^\mu(\sigma)$. The topology of the σ domain best suited to these circumstances is S^1, that of a circle. $f^\mu(\sigma)$ and $g^\mu(\sigma)$ are equivalent to functions defined on a unit circle such that $f^\mu(\sigma) = f^\mu(-\sigma)$ and $g^\mu(\sigma) = g^\mu(-\sigma)$, as demonstrated in fig. 3.2. From now on we shall regard $f^\mu(\sigma)$ and $g^\mu(\sigma)$ as suitably extended and defined on the compact domain $\sigma \in [0, 2\pi)$. Acknowledging
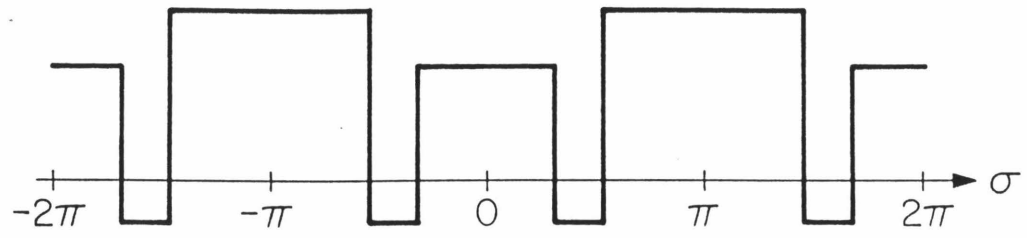
(a)
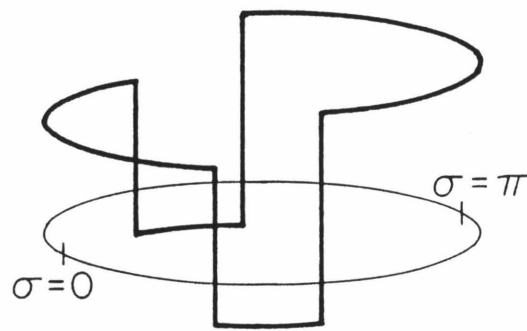
(b)

Figure 3.2 A function symmetric about 0 and π (a) is equivalent to a function defined on a circle (b).

the contrived nature of the topology, we refer to the intervals $[0, \pi]$ and $(\pi, 2\pi)$ as being physical and unphysical, respectively.

We can make our lives easier if we note that the integral term in the solution to the wave equation is responsible for the uniform space-time translation of the center of mass of the string. This uninteresting feature may be eliminated by working exclusively with $x'^{\mu}(\sigma, \tau)$ and $\dot{x}^{\mu}(\sigma, \tau)$. As previously noted in eq. (3.18), these quantities are proportional to the components of the conserved four-momentum current on the world sheet of the string.

The appearance of the combinations $\sigma \pm \tau$ in the canonical solution eq. (3.22) is routinely interpreted as waves moving in opposite directions along the string. We may exploit this feature by defining local light cone frames at each point of the world sheet by the reparameterization $\xi^{\pm} = \frac{1}{\sqrt{2}}(\tau \pm \sigma)$. In these coordinates the components of the momentum current are

$$P_{\pm}^{\mu}(\sigma, \tau = 0) = \frac{\kappa}{\sqrt{2}} [g^{\mu}(\sigma) \mp f'^{\mu}(\sigma)]. \tag{3.28}$$

We may then express $\dot{x}^{\mu}(\sigma, \tau)$ and $x'^{\mu}(\sigma, \tau)$ as superpositions of currents

$$\dot{x}(\sigma, \tau) = \frac{1}{\kappa\sqrt{2}} [P_{-}(\sigma + \tau, \tau = 0) + P_{+}(\sigma - \tau, \tau = 0)], \tag{3.29}$$

$$x'(\sigma, \tau) = \frac{1}{\kappa\sqrt{2}} [P_{-}(\sigma + \tau, \tau = 0) - P_{+}(\sigma - \tau, \tau = 0)]. \tag{3.30}$$

A consequence of the boundary conditions is that $P_{+}^{\mu}(\sigma, \tau = 0)$ and $P_{-}^{\mu}(\sigma, \tau = 0)$ are dependent. In fact, $\dot{x}^{\mu}(\sigma, \tau)$ and $x'^{\mu}(\sigma, \tau)$ are derived by operating on $P_{+}^{\mu}(\sigma, \tau = 0)$ with combinations of linear operators that are independent of the initial conditions. We can formalize this statement by defining a time translation operator $\hat{T}(\tau)$ and a reflection operator $\hat{R}$ by their actions on an arbitrary function $h^{\mu}(\sigma)$ defined on the unit circle:

$$\hat{T}(\tau)h^{\mu}(\sigma) = h^{\mu}(\sigma - \tau), \tag{3.31}$$

$$\hat{R}h^{\mu}(\sigma) = h^{\mu}(-\sigma). \tag{3.32}$$

$\hat{T}(\tau)$ rotates the contours of a function by τ units in the positive sense and $\hat{R}$ reflects the function in the plane defined by the diameter through $\sigma = 0$ and $\sigma = \pi$. In this language the relations

$$P_\pm^\mu(\sigma, \tau) = \hat{T}(\pm\tau) P_\pm^\mu(\sigma, \tau = 0), \tag{3.33}$$

$$P_-^\mu(\sigma, \tau = 0) = \hat{R} P_+^\mu(\sigma, \tau = 0) \tag{3.34}$$

permit us to rewrite $\dot{x}^\mu$ and x'^μ as

$$\dot{x}^\mu(\sigma, \tau) = \frac{1}{\kappa\sqrt{2}} \left[\hat{T}(-\tau)\hat{R} + \hat{T}(\tau) \right] P_+^\mu(\sigma, \tau = 0) \tag{3.35}$$

$$x'^\mu(\sigma, \tau) = \frac{1}{\kappa\sqrt{2}} \left[\hat{T}(-\tau)\hat{R} - \hat{T}(\tau) \right] P_+^\mu(\sigma, \tau = 0). \tag{3.36}$$

These equations are the formal statements, that one may factor the solutions to the equations of motion so that $\dot{x}^\mu(\sigma, \tau)$ and $x'^\mu(\sigma, \tau)$ depend explicitly on only one independent function. In sect. 3.5 we shall make implicit use of eq. (3.35) since it clearly demonstrates the superposition of circulating momentum currents.

So as not to lose sight of our objective, a brief word on how strings break is in order. As we have already pointed out, the area decay law assumes a uniform probability $\mathbf{P}_0$ for a break-per-unit invariant area of the world sheet

$$dP_{\text{break}} = \mathbf{P}_0 \, dA = \mathbf{P}_0 \sqrt{(\dot{x} \cdot x')^2 - x'^2 \dot{x}^2} \, d\tau \, d\sigma. \tag{3.37}$$

Much of our analysis tacitly hinges upon the fact that the expression for dA, as given in eq. (3.37), is a function of only the *derivatives* $\dot{x}^\mu$ and x'^μ. For this reason we are contented with the solutions of eq. (3.35) and eq. (3.36). Monte Carlo implementations worry only about the momentum space picture of hadronization. In the Caltech-II model, when low-mass strings are identified with clusters, the spatial distribution of string momentum is disregarded.

3.4 The Directrix vs. Momentum Currents

As a matter of completeness, it should be mentioned that the motion of complex string systems has been described by other authors using a construct known as the directrix [41,50]. Consider the motion of the $\sigma = 0$ end of an open string, given that the string emerges from a point at $\tau = 0$. The directrix is the world line of the $\sigma = 0$ endpoint as given by eq. (3.22)

$$A^\mu(\tau) \equiv x^\mu(\sigma\!=\!0, \tau) = \int_0^\tau g^\mu(\xi)\, d\xi. \tag{3.38}$$

The algorithm for forming the directrix is simply a geometrical interpretation of the above equation: given a ordering for the partons that define the string, lay down the initial three-momentum vectors of the partons "tail to tip" until one exhausts all the vectors. Then repeat the process for the vectors in the reverse order as in fig. 3.3. Up to a scale factor, the piecewise linear curve produced will be the world line of the endpoint $\sigma = 0$.

The sufficiency criterion of the directrix is seen by noting that any point on the world sheet may be expressed as

$$x^\mu(\sigma, \tau) = \frac{A^\mu(\tau\!+\!\sigma) + A^\mu(\tau\!-\!\sigma)}{2}. \tag{3.39}$$

More complex algorithms for the directrix could be formulated for cases in which $f^\mu(\sigma) \neq 0$, but the momentum current formalism is much more amenable to manipulation for the general case and is especially transparent for visualizing the distribution of momentum when a string decays. Nevertheless, it should be apparent that the directrix and $P_+(\sigma, \tau)$ contain the same information and are thus formally equivalent.
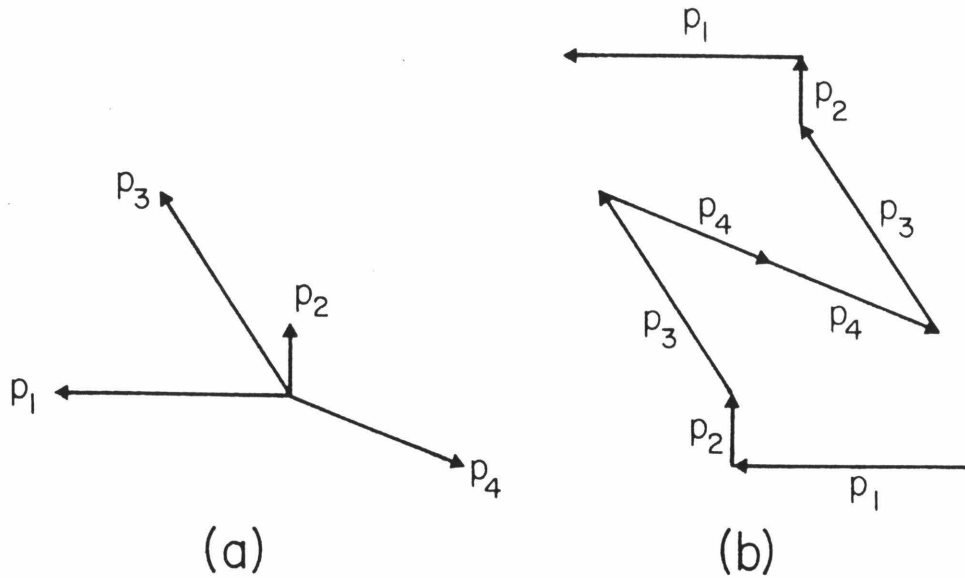
Figure 3.3 The ordered set of parton momentum vectors in (a) is assembled to form the directrix in (b).

3.5 String Breaks and Topological Fragmentation

As promised, we shall apply our momentum current formalism of sect. 3.3 to the problem of fragmenting strings. Consider what happens to the momentum at the ends of a string. Since only the interval $\sigma \in [0, \pi]$ is physical, it would appear that $P_+^\mu(\sigma, \tau)$ corresponds to a momentum source at $\sigma = 0$ and a momentum sink at $\sigma = \pi$. Though this is true, $P_-^\mu(\sigma, \tau)$ has characteristics complementary to those of $P_+^\mu(\sigma, \tau)$ such that local energy-momentum conservation is preserved. From eq. (3.35) it is apparent that whenever momentum disappears at $\sigma = \pi$ to the unphysical interval $\sigma \in [\pi, 2\pi]$ via $P_+^\mu(\sigma, \tau)$, a compensating amount enters the interval $\sigma \in [0, \pi]$ by courtesy of $P_-^\mu(\sigma, \tau)$. The utility of this formalism is that the reflection of momentum from an endpoint is inherent; considering $P_+^\mu(\sigma, \tau)$ and $P_-^\mu(\sigma, \tau)$ individually, we note that they circulate uninhibited by the presence of the string boundaries so that the endpoints $\sigma = 0, \pi$ serve only to define the transition
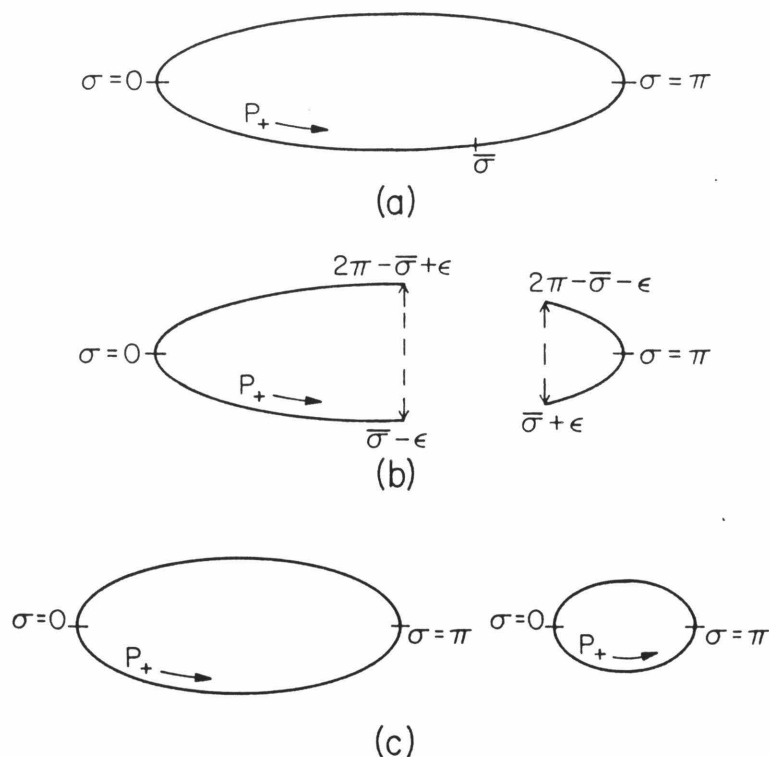
Figure 3.4 (a) P_+ circulates on a domain. (b) A break occurs at $\bar{\sigma}$ and corresponding points on the physical and unphysical sides are associated. (c) Two new domains are formed by pasting.

between the physical and unphysical intervals of the domain.

This interpretation of momentum flow has a direct application to the problem of a string fragmenting into two daughters. The relevant question is: "What is the equivalent of $P_+^\mu(\sigma, \tau = 0)$ for each of the daughters?" Suppose the parent fragments at $(\sigma = \bar{\sigma}, \tau = \bar{\tau})$. At this instant the momentum current along the positive branch of the light cone is $P_+^\mu(\sigma - \bar{\tau}, \tau = 0)$. From the above discussion it follows that for the first daughter we identify the point $\sigma = \bar{\sigma} - \epsilon$ on the physical region with the point $\sigma = 2\pi - \bar{\sigma} + \epsilon$ on the unphysical region and take the limit $\epsilon^+ \to 0$ (see fig. 3.4). Similarly for the second daughter, we identify $\sigma = \bar{\sigma} + \epsilon$ and $\sigma = 2\pi - \bar{\sigma} - \epsilon$. The reason this algorithm works is that a break in the string creates two new string ends. Since we already know how the momentum currents behave at endpoints, it is a trivial matter to form the momentum currents for the daughters. The function

$P_+^\mu(\sigma - \bar{\sigma}, \tau = 0)$, now defined on a disconnected domain, is used as the initial condition for the daughters and subsequently may be evolved using eqs. (3.35-3.36). The evolution of a string through many generations of cuts is equivalent to literally partitioning the domain of the original $P_+^\mu(\sigma, \tau = 0)$ function among all of the final state strings.

To see how fast the information increases in a fragmentation process, consider an initial string with n partons. The initial circular domain will have $2n - 2$ intervals on it. The factor of 2 arises from the even extension of the initial conditions to the interval $(\pi, 2\pi)$ and the -2 compensates for double-counting the intervals that straddle $\sigma = 0, \pi$. The fragmentation of the string and the associated cutting of the domain force us to keep track of two new intervals. If the fragmentation process continues geometrically, then after m generations we must follow a total of $2(n - 2 + 2^m)$ intervals. Not only have we tamed the naive prospect of having to deal with $n2^m$ intervals, but more significantly, we see that the piecewise constant momentum currents of the daughters take on values drawn only from the original n values that comprise the momentum current of the original string: no intermediate calculations are required!

3.6 Summary

In this chapter we have shown how the full equations of motion for the relativistic string may be interpreted in terms of momentum currents on the world sheet of a string. This interpretation allows an accurate, efficient implemention of the string model in Caltech-II.

Chapter 4

String Dynamics in Caltech-II

4.1 Introduction

Having discussed the kinematics of the relativistic string in chapter 3, we now turn to the question of dynamics. Even though the relativistic string embodies many of our theoretical prejudices concerning partons and confinement, it is a semiclassical model and as such has no clear connection with final state particles. We must supplement the kinematics with a mechanism by which strings ultimately lead to on-mass-shell particles.

The obvious approach would be to "do it properly from the beginning" by quantizing the relativistic string. This is more easily said than done. Since the quantum hadronic string (unlike the superstring) is a composite object, it is not easily expressed in terms of quarks and gluons, let alone stable particles. Little work has been done on the dynamics of the quantum string – mainly static flux tubes have been investigated [38]. Though string potentials have been used to predict the spectroscopy of bound systems of heavy quarks [51] and exclusive decay modes of mesons [52], the dynamical degrees of freedom of the string have been largely ignored. Until more is known about quantum string dynamics and even then, unless the theory is computationally tractable, we will explore the consequences of the semiclassical model.

While it is clear that we have to augment the semiclassical relativistic string with additional rules to make allowances for quantum effects, we must avoid the temptation of overelaborating the model. The number and nature of "patches" is a function of the detail we wish to extract from the string. As a rough guideline, each modification introduces a new parameter or degree of freedom. Caltech-II minimizes the number of refinements to the basic string model by relegating the details of hadronization to a parameterization of the decay of low-mass strings. By not asking too detailed questions, we can successfully separate the gross dynamics of the relativistic string from the processes that lead directly to particle production.

This chapter outlines the modifications made to the basic string model in Caltech-II. In essence, we shall present the details of string fragmentation. So as not to be overwhelming, we will introduce complications one at a time. Starting with the kinematics of the relativistic string and its associated massless quarks, we will

1. introduce the area decay law for strings and explain how causality constrains its implementation;

2. devise a simple picture for evaluating the invariant area of arbitrarily complicated world sheets;

3. make the semiclassical string respect the physical particle mass spectrum by terminating string evolution below a certain mass scale and then use a paramterization of low energy hadronization data;

4. specify how to handle quark masses and flavor abundances.

4.2   Invariant Area Sampling

As has been pointed out in chapter 3, Caltech-II employs an area decay law that assumes a constant probability for a string break to occur in an element of invariant

area

$$dP_{\text{break}} = \mathbf{P}_0 \, dA, \tag{4.1}$$

where our choice of gauge in eq. (3.12) with $\tau = \kappa x^0$ permits us to express dA as

$$dA = \frac{1}{\kappa^2}(1 - v_\perp^2) \, d\sigma \, d\tau, \tag{4.2}$$

where $v_\perp$ is the transverse velocity of the string. Since σ is an energy coordinate whose scale is given by the initial parton energies and since τ also has the dimensions of energy, all the physical constants may be lumped together by defining

$$\rho_c = \frac{\mathbf{P}_0}{\kappa^2}. \tag{4.3}$$

At first, this result might seem surprising, but a closer look reveals that we are not getting something free. Indeed, by combining κ^2 with $\mathbf{P}_0$, we lose access to the scale parameter that gives the physical size of the strings. Fortunately, we don't need this information since we already know that hadronic strings are small on the scale of laboratory detectors. As pointed out before, present hadronization models (including Caltech-II) are essentially momentum space pictures — all particles emerge from a point. If so desired, one can add, by hand, information on the position of decay vertices of unstable particles that travel macroscopic distances, but this phenomenological detail is essentially irrelevant to the physics we are attempting to describe.

We can now concentrate on putting the area decay law to work. Noting that eq. (4.1) is the kernel for a Poisson process, we can reexpress it in terms of the differential probability that the *first* break occurs after an invariant A is sampled:

$$dP_{\text{break}}(A) = \mathbf{P}_0 e^{-\mathbf{P}_0 A} \, dA. \tag{4.4}$$

The obvious question,"What are the boundaries defining the invariant area A?", is a fundamental one, which warrants close attention if causality is to be obeyed.
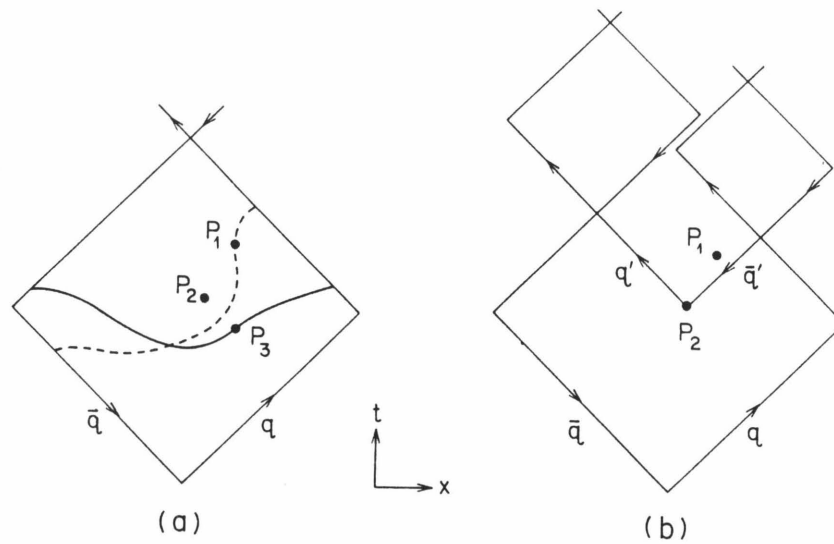
Figure 4.1 (a) Solid and dashed curves bound the same invariant area but only the solid curve is consistent with causality. (b) A break at P_2 results in P_1's not being on the world sheet.

To preserve causality, area must be swept out so that A increases as the boundary is expanded towards the absolute future. The world lines of the quarks must form the boundary in the absolute past of any point in the region contributing to A. This idea is best illustrated with the aid of fig. 4.1, which depicts the world sheet of a simple $q\bar{q}$ system. Suppose a curve bounds an area A chosen according to the distribution in eq. (4.4). In a $q\bar{q}$ system, a break will occur with equal probability anywhere along the boundary provided that the boundary is consistent with causality.

The dashed curve in fig. 4.1a is inadmissible since there are points on it (e.g., P_1) that lie in the absolute future of world sheet points not contained within the boundary (e.g., P_2). If a point is not interior to the region defining A, there is a possibility that the string might break at that point. For example, if a break were to occur at P_2, the screening of the created color charge would change the form of the world sheet to that depicted in fig. 4.1b, so that there is no flux tube at P_1. All world sheet points in the absolute past of a point on an admissible boundary must already lie within the boundary in order to have a self-consistent Lorentz invariant
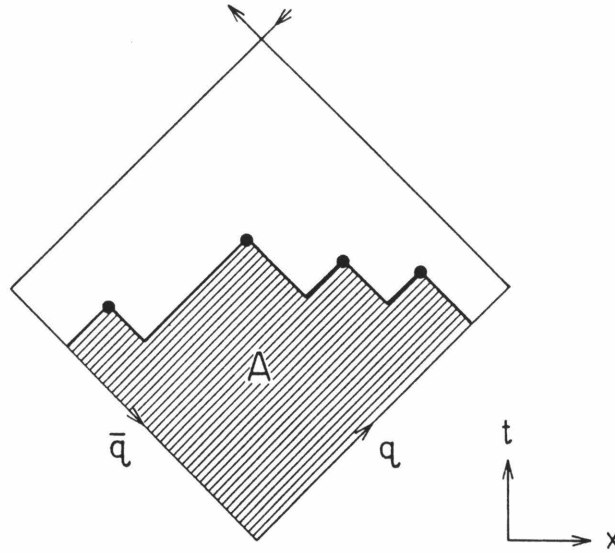
Figure 4.2 Prototype admissible boundary curve for the area decay law. Area A is the union of the area bounded by the backwards light cones and the edges of the world sheet.

theory. This is nothing but a fancy way of saying that we can break the string only where it exists. The solid line in fig. 4.1a is an admissible boundary.

We can quantify our causality condition quite easily. Fig. 4.2 shows a prototype admissible curve. It is constructed by taking a number of points and letting the area A be the union of the areas bounded by their backwards light cones and the edges of the world sheet. From this simple example we can extract the two essential features of an admissible curve $t(x)$:

- $t(x)$ must be single valued ($t(x)$ has a unique inverse)
- $t(x)$ must not be timelike ($|dt/dx| \leq 1$).

$$(4.5)$$

Other points to be considered when generating string breaks are the incorporation of local color screening and the avoidance of double-counting invariant area. These principles can be illustrated by extending our above example. Suppose a break occurs at P_3 in fig. 4.1a. If no further breaks were to occur, the world sheet of the system would look like fig. 4.3a. The boundaries of this new world sheet are the ones we must use in the area decay law to determine the position of subsequent
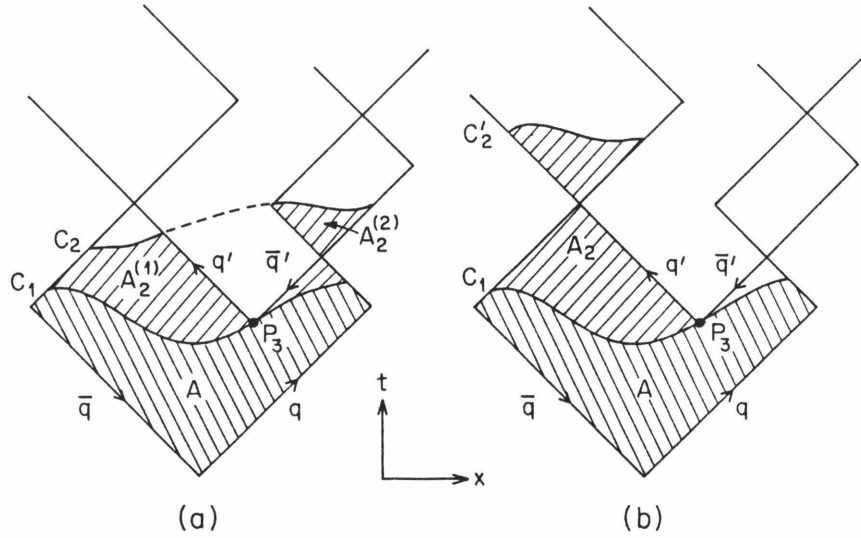
Figure 4.3 (a) Both daughter strings contribute to the invariant area A_2 bounded by C_1 and C_2. (b) Only one daughter contributes the invariant area A_2 bounded by C_1 and C_2'.

breaks.

Suppose the area decay law says that an additional area A_2 is swept out before the next break. Any admissible curve obeying the guidelines outlined above would provide a suitable boundary, provided we start sweeping out area from where we left off and not do count any of the area contributing to A. In general, such a boundary would enclose invariant area associated with each of the daughter strings as indicated by curve C_2 in fig. 4.3a. However, as a simplifying assumption, Caltech-II evolves each daughter color singlet independently, so that we can ignore situations where decay products interact with each other — Caltech-II considers boundary curves like C_2', in fig. 4.3b, which associate all of the area A_2 with one daughter.

4.3 Calculation of Invariant Area

Though the area decay law tells us *when* enough invariant area A has been swept out and the causality criterion tells us *where* A can be swept out, neither

tells us *how A* is to be calculated. To avoid distending our imaginations in an effort to visualize the convoluted world sheet topology of multiparton strings, we shall show in this section that working in (σ, τ) space greatly facilitates the calculation of invariant area. It would be difficult to overstate the importance of this somewhat technical point, since this point and the momentum redirection formalism discussed in sect. 3.5 are the two key ingredients in the string evolution phase of Caltech-II.

In our gauge, an area element may be expressed in terms of momentum currents by

$$dA = \dot{x}^2 \, d\sigma d\tau = P_+(\sigma, \tau) \cdot P_-(\sigma, \tau) \, \frac{d\sigma d\tau}{\kappa^2}. \tag{4.6}$$

Since the factor of $1/\kappa^2$ is absorbed into the definition of ρ_c, our task is to evaluate the contraction of the momentum currents.

Throughout this section it will be useful to have a specific example in mind. For this purpose consider a $q\bar{q}g$ system in its CM frame, where the original parton energies are

$$
\begin{aligned}
E_q &= 4\,\text{GeV} \\
E_g &= 3\,\text{GeV} \\
E_{\bar{q}} &= 5\,\text{GeV},
\end{aligned}
\tag{4.7}
$$

so that the total string energy is $E_{\text{string}} = E_q + E_g + E_{\bar{q}}$. Fig. 4.4 illustrates the mapping of this system to the circular σ domain at $\tau = 0$. As discussed in sect. 3.3, the partitioning of the circle is a way of visualizing the even extension of the initial conditions about $\sigma = 0$ and $\sigma = E_{\text{String}}$. The circle may be divided into four intervals (as opposed to six) because the even extensions of the intervals touching $\sigma = 0$ and $\sigma = E_{\text{string}}$ produce adjacent copies of themselves. This results in intervals of "length" $2E_q$ and $2E_{\bar{q}}$ straddling the points $\sigma = 0$ and $\sigma = E_{\text{string}}$, respectively. In contrast, the central gluon is associated with *two* intervals, each of length E_g. In any case, each interval is uniquely associated with one of the original partons
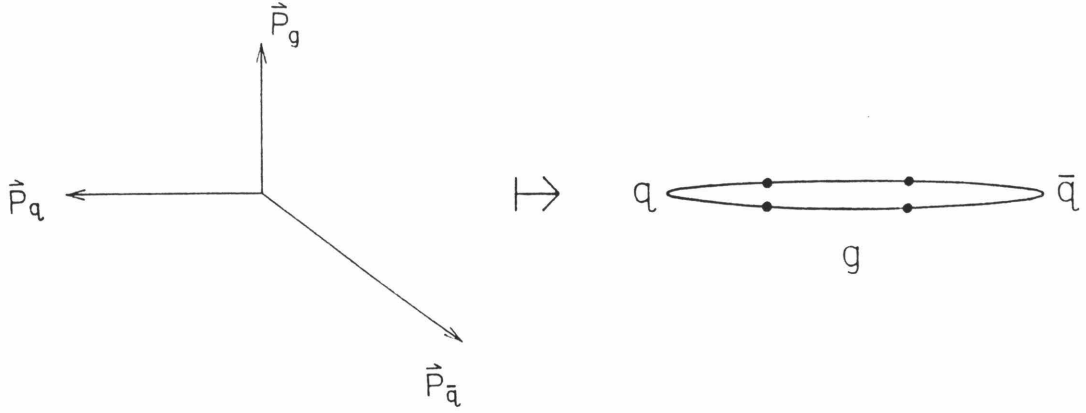
Figure 4.4 A $q\bar{q}g$ system with energies $E_g = 3\,\text{GeV}$, $E_{\bar{q}} = 5\,\text{GeV}$ and $E_q = 4\,\text{GeV}$ is mapped onto a circular σ domain.

(though there are generally more intervals than partons).

We begin our development by recalling how $P_+(\sigma, \tau = 0)$ in eq. (3.28) is defined on the circular σ domain. As time progresses, $P_+(\sigma, \tau)$ is obtained by rotating $P_+(\sigma, \tau = 0)$ according to eq. (3.34) and then projecting out the portion defined on the physical interval of the domain. We can form an intuitive "space-time" picture of this evolution if we map the world sheet parameterization onto a cylinder where the circular σ domain is identified with the compact dimension of the cylinder and τ is identified with the long dimension. In our example the evolution of $P_+(\sigma, \tau = 0)$ can then be visualized as the partitioning of the "world cylinder" into 4 winding bands, each associated with a parton, as illustrated in fig. 4.5a.

Since only the interval $\sigma \in [0, E_{\text{string}}]$ is physical, we project the corresponding half of the cylinder onto a rectangular strip as indicated by the solid lines in fig. 4.5b. The flow of P_+ partitions the strip into diagonal bands, each of which is uniquely associated with one of the original partons. Using eq. (3.34) to relate $P_-(\sigma, \tau)$ and $P_+(\sigma, \tau)$, it is evident that the trace of the interval boundaries of $P_-(\sigma, \tau)$ are obtained by projecting the *unphysical* portion of the world cylinder of $P_+(\sigma, \tau)$ onto the physical portion of the rectangular strip as indicated by the dashed lines in
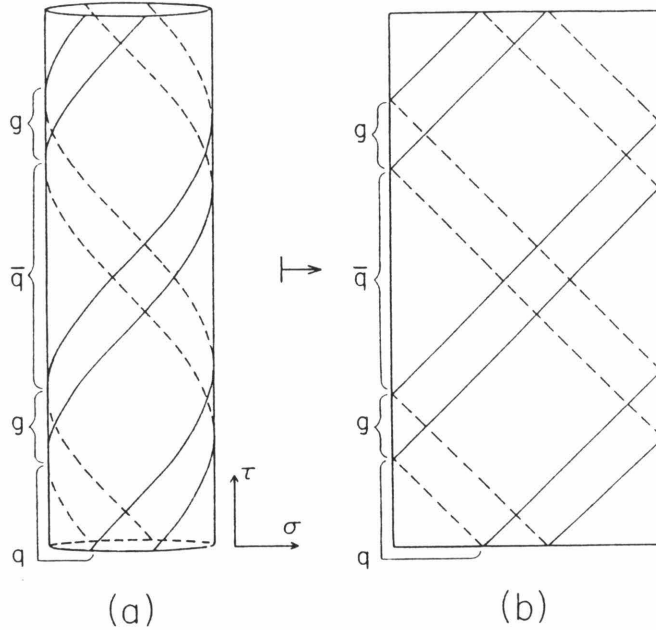
Figure 4.5 (a) Helical bands of P^μ_+ on the world cylinder. (b) Physical region of world cylinder mapped to a strip.

fig. 4.5b. The end result on the rectangular strip is a network of intersecting bands corresponding to the superposition of bands of $P_+(\sigma,\tau)$ and $P_-(\sigma,\tau)$.

The evaluation of invariant area is now straightforward. The world sheet is effectively divided into many regions over which $P_+(\sigma,\tau) \cdot P_-(\sigma,\tau)$ is constant. The identification of each band of P_+ with a particular parton permits us to label each region of superposition with a pair of parton indices as indicated in fig. 4.6. The first index corresponds to the parton associated with the P_+ current in the region, while the second index corresponds to the parton associated with the P_- current in the region. In the general case, suppose we go to the region of superposition of currents corresponding to partons i and j. Since the parent string formed from the original partons initially has no spatial extent, the interval with indices (i, j) has

$$P_+(\sigma,\tau) \cdot P_-(\sigma,\tau) = P^{(i)}_+ \cdot P^{(j)}_+ = \frac{1}{2}(1 - \cos\theta_{ij}), \qquad (4.8)$$

where $P^{(i)}_+$ is the positive light-cone momentum current density associated with parton i and θ_{ij} is the *original* angle between the three-momenta of partons i and
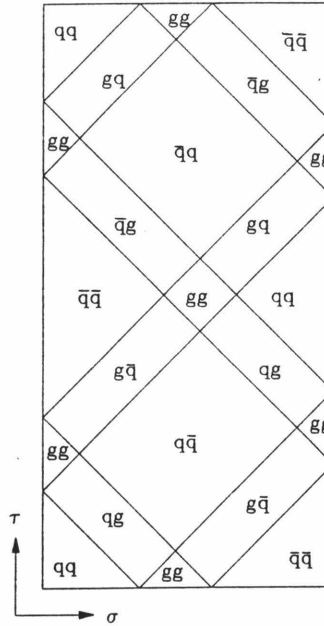
Figure 4.6 Each region of superposition on the (σ, τ) plane is uniquely labeled by a pair of parton indices.

j. An immediate consequence is that there is no contribution to the invariant area at the intersection of bands corresponding to the same parton. Such regions of the world sheet correspond to the energy grains associated with quarks and gluons.

Fig. 4.7 shows the correspondence between regions on the (σ, τ) plane and the instantaneous configuration of a $q\bar{q}g$ system. The shaded areas in fig. 4.7a correspond to the superposition of oppositely moving currents originating from the same parton — which, according to eq. (4.8), give no contribution to the invariant area. The borders at $\sigma = 0$ and $\sigma = E_{\mathrm{string}}$ are always shaded, corresponding to the lightlike point concentrations of energy and momentum at the ends of the string. The central shaded region at $\tau = 0$ corresponds to the gluon kink. From this diagram it is easy to see that the gluon loses energy twice as fast as the endpoint quarks.

Fig. 4.7b shows the instantaneous string configuration corresponding to each of the times marked off on the τ axis in fig. 4.7a. Each configuration is a function of the spacelike components of the original parton momenta (as can be seen from the di-
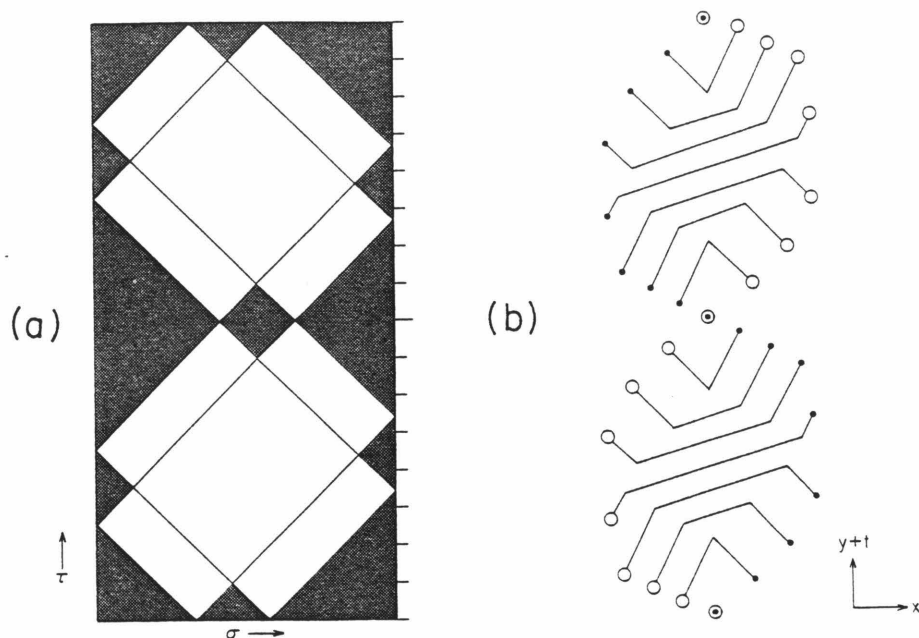
Figure 4.7 (a) Shaded regions in (σ, τ) space give no contribution to invariant area. (b) String configurations corresponding to times indicated on τ axis. The quark end is represented by an open circle, the antiquark end by a solid circle.

rectrix formalism of sect. 3.4 and hence cannot be obtained from the (σ, τ) diagram, which contains only the timelike (energy) information. In this sense figs. 4.7a,b are complementary. For example, the (σ, τ) diagram allows us to distinguish between momentumless kinks and *bone fide* gluon kinks on the string. The second string configuration in fig. 4.7b corresponds to the moment at which the gluon kink has lost all of its energy. Immediately afterwards, the kink breaks up into two oppositely moving kinks. The fact that these two new kinks are momentumless is only obvious after inspecting the (σ, τ) diagram.

Now that we have a convenient way to calculate contributions to the invariant area, we must translate admissible boundaries on the world sheet to admissible boundaries in (σ, τ) space. The causality criteria restricting the form of the area boundaries on the world sheet have direct analogues in (σ, τ) space. In fact, *exactly* the same constraints apply to a boundary $\tau(\sigma)$ as to $t(x)$ in eq. (4.5) if we make
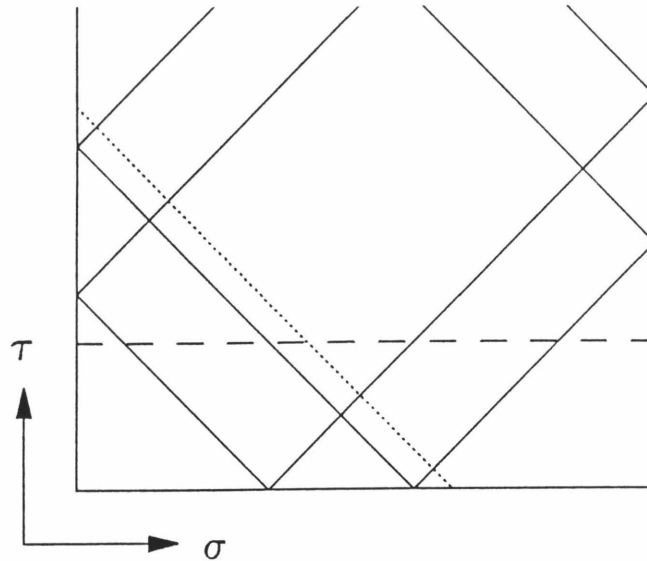
Figure 4.8 Lightlike (dotted) and spacelike (dashed) boundaries define the same invariant area. These particular choices of boundaries facilitate the calculation of the cumulative invariant area used in the area decay law.

the replacements $x \rightarrow \sigma$ and $t \rightarrow \tau$. Though a particular choice of boundary is not manifestly covariant, the consistent application of a choice ultimately leads to the same physics in the distant absolute future. With this in mind, we choose the boundary that makes calculations the easiest.

An obvious choice for a moveable boundary is to use a lightlike line as indicated by the dotted line in fig. 4.8. The fixed boundaries are the lines $\tau = 0$, $\sigma = 0$ and $\sigma = E_{\text{string}}$. Since none of the triangular regions contribute to the invariant area (see fig. 4.7a), the bounded invariant area is a piecewise *linear* function of the moveable boundary position. Another possibility is to use a moveable boundary parallel to the σ axis indicated by the dashed line in fig. 4.8. With this choice the bounded area is a piecewise quadratic function of the boundary position. One choice is as good as the next — even a mixture is permissible as long no double counting occurs and causality is obeyed.

Before pointing out the deficiencies of the area decay law, we end this section with an interesting aside. Using the tools developed above, we can prove a fundamental result regarding the invariant area $A_{1\ \text{cycle}}$ swept out during one complete cycle of string motion. In sect. 2.5 we pointed out that dimensional considerations suggest that $A_{1\ \text{cycle}}$ be a function of W^2, the invariant mass squared of the string — the only available Lorentz invariant. It is a simple matter to determine this function exactly. We will continue to use our $q\bar{q}g$ system, but the generalization to other systems should be apparent.

Consider once more fig. 4.5, which shows one complete cycle of motion in (σ, τ) space. The periodicity of the motion allows us to identify the top and bottom of the figure (i.e., $\tau = 0$ and $\tau = 2E_{\text{string}}$). If we recall how the semi-infinite (σ, τ) strip was obtained from the world cylinder, it should be obvious that each band of P_+ (and hence each band of P_-) winds around the world cylinder exactly once during one cycle of string motion. This is significant since it means that the invariant area of one cycle on both sides of the world cylinder is exactly twice the area $A_{1\ \text{cycle}}$ on just the physical side. During one cycle on the world cylinder (including both the physical and unphysical sides), each band of P_+ intersects each band of P_- exactly twice. Thus, we can sum all the contributions to the invariant area by summing over all the possible intersections of bands of P_+ and P_-.

We can make our demonstration simpler if we artificially divide the σ intervals corresponding to the endpoint quarks into two equal parts. This results in there being exactly twice as many σ intervals on the circular domain as there are associated partons. The sum over band intersections on the whole world cylinder can then be written as

$$2A_{1\ \text{cycle}} = \frac{8}{\kappa^2} \sum_{i,j=q,\bar{q},g} P_+^{(i)} \cdot P_-^{(j)} \frac{E_i}{\sqrt{2}} \frac{E_j}{\sqrt{2}}, \qquad (4.9)$$

where the sums are over all partons, and $P_\pm^{(i)}$ and E_i are, respectively, the momentum current densities corresponding to the parton i and the original energy of parton

i. The factor of $8 = 2 \times 4$ accounts for a combination of symmetries. A factor of 2 reflects the topological necessity of each band of P_+ band intersecting each band of P_- twice during one cycle. The remaining factor of four is a result of our construction in which there are twice as many bands of P_+ (and P_-) as there are partons. This factor of four allows us to express a double sum over bands as a double sum over partons. The factors of $\sqrt{2}$ arise from the fact that the rectangular regions of intersection are inclined at 45° to the σ axis. Because our string has no initial spatial extent, we have $P_\pm^i E_i = p_i / \sqrt{2}$ (no sum implied), where p_i is the initial four momentum of parton i. This allows us to rewrite eq. (4.9) as

$$
\begin{aligned}
A_{1\ \text{cycle}}^{(\text{open})} &= \frac{1}{\kappa^2} \sum_{i,j=q\bar{q}g} p_i \cdot p_j \\
&= \frac{1}{\kappa^2} \left(p_q + p_{\bar{q}} + p_g \right)^2 \\
&= \frac{p_{\text{string}}^2}{\kappa^2} \\
&= \frac{W^2}{\kappa^2}
\end{aligned}
\tag{4.10}
$$

The above argument may be generalized for arbitrary open strings, including those that do not arise directly from perturbative partons, with the same result. The analogous result for closed strings is

$$
A_{1\ \text{cycle}}^{(\text{closed})} = \frac{W^2}{2\kappa^2}.
\tag{4.11}
$$

These results are the simplest ones consistent with the naive dimensional argument, yet an explicit analysis was required to get the multiplicative factors correct. It may have been noted from fig. 4.7 that there is a symmetry between the first half and second half of one complete cycle. This symmetry can be summarized by the equation

$$
A_{1/2\ \text{Cycle}}^{(\text{open})} = \frac{W^2}{2\kappa^2}.
\tag{4.12}
$$

These analytical results concerning areas swept out in complete cycles make finding

the location of a break easier. In a momentum space picture, the relevant quantity is not the invariant area A but rather $A \bmod A_{1 \text{ cycle}}$.

4.4 The Transition From Strings to Clusters

Since the area decay law contains no provision for stopping string fragmentation, it ultimately results in an infinite number of zero mass strings — as a semiclassical model it knows nothing of the physical particle mass spectrum. The question at hand is "Can we retain the desirable features of the semiclassical area decay law and still end up with physical particles?" The answer is a qualified yes. The identification of a string with a stable particle imposes severe constraints on the world sheet location of viable string breaks and is contrary to the spirit of the area decay law. By limiting the frequency with which we identify strings with particles, most of the string fragmentation is still controlled by the basic area decay law.

We have little reason to believe *a priori* that we should be able to identify a string in our semiclassical model with an on-mass-shell particle. To avoid this dilemma, Caltech-II *parameterizes* the decays of low-mass strings into hadrons, since that is the least well understood stage of hadronization. Once the mass of a string falls below a cutoff mass, the string fragmentation picture is abandoned in favor of the parameterization of low-mass data described in appendix B. Since the parameterization is a function only of mass and flavor, we call a low-mass string to be decayed this way a "cluster." Though it is just a matter of terminology, we will refer to an object as a string if it decays via the string model and call it a cluster if it decays via the low-mass parameterization. In this section we will discuss the motivation and implementation of the transition from strings to clusters.

Because of our reluctance to identify strings directly with hadrons, we must not, at the very least, let a string mass fall below the strong interaction, two-particle

production threshold W_{2pth} corresponding to the valence flavor of the string. By valence flavor, we mean the flavor of the string's endpoint quarks or diquarks. For example, the mass of a $u\bar{u}$ string must never be less than $W_{\text{2pth}}(u\bar{u}) = 2m_{\pi^0}$. Even this constraint is still relatively loose since it condones the use of a string model down to a regime where the physics is highly nonperturbative. It makes sense to trust a semiclassical string model of fragmentation only in the region of high quantum numbers (i.e., the semiclassical limit).

A string is not a well-defined object in a system just above threshold. With very little energy available to the string degrees of freedom, the string length may be comparable to its transverse dimensions. This is precisely the nonperturbative region we wish to avoid modeling. A parameterization of the hadronization of low-mass objects provides a convenient solution to this problem and implicitly tests the hypothesis of being able to factor the hadronization process into the stages

$$\text{LLA QCD} \otimes \begin{array}{c} \text{Relativistic String} \\ \text{+Area Decay Law} \end{array} \otimes \begin{array}{c} \text{Low} - \text{Mass} \\ \text{Parameterization.} \end{array} \tag{4.13}$$

To make the transition from strings to clusters, we introduce a parameter W_{max}, which is roughly the maximum amount of invariant mass *above the two-particle threshold* that an object can have in order to be identified as a cluster; otherwise, the object is identified as a string. In order to provide a smooth transition between strings and clusters, we adopt a continuous distribution for $P_{\text{string}}(W)$, the probability that an object of invariant mass W is treated as a string

$$P_{\text{string}}(W) = \begin{cases} 0 & W < W_{\text{2pth}} + W_{\text{max}}, \\ 1 - e^{-\frac{1}{2}\rho_c(W - W_{\text{2pth}} - W_{\text{max}})^2} & \text{otherwise} \end{cases} \tag{4.14}$$

which is plotted in fig. 4.9.

In principle, W_{max} could be a function of flavor but it is found empirically that a universal value of $W_{\text{max}} = 2.2\,\text{GeV}$ is sufficient (see sect. 5.3). The need for the cutoff W_{max} is consistent with the expectations of the quantized string. Artru [53],
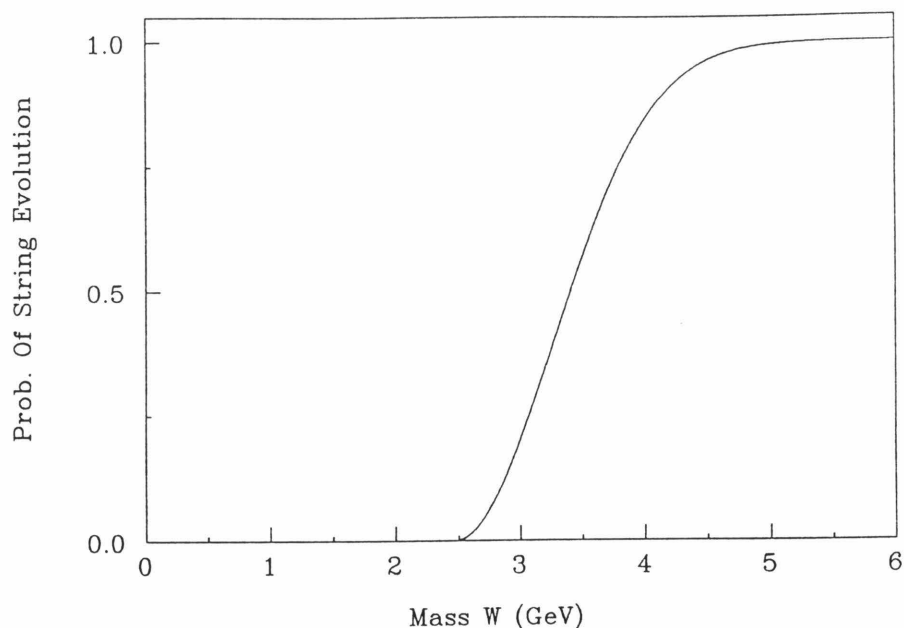
Figure 4.9 Probability that a $u\bar{u}$ object of mass W is identified as a string where $W_{\text{max}} = 2.2\,\text{GeV}$, $\rho_c = 1.6\,\text{GeV}^{-2}$ and $W_{\text{2pth}} = .270\,\text{GeV}$.

Andersson and Hoffmann [54], and Artru and Bowler [55] have recently revived interest in the general features of the quantized string. It is worth reproducing some of the key points of these authors' work that is relevent to Caltech-II.

Whereas the area decay law gives the *probability* $e^{-\mathbf{P}_0 A}$ of a string sweeping out invariant area A, a quantum treatment should deal with amplitudes. With this in mind, one would expect the amplitude for string propagation to be proportional to

$$e^{-i\kappa A}e^{-\mathbf{P}_0 A/2}, \tag{4.15}$$

where the first factor is the path integral amplitude $e^{i\,\text{Action}}$ and the second factor is the square root of the area decay law probability. When this amplitude is summed over histories, the propagator for a string of mass W has a sequence of poles at

$$W^2 = \frac{2\pi\kappa l}{\left[1 + i\frac{\mathbf{P}_0}{2\kappa}\right]}, \tag{4.16}$$

where l is an integer and, in the limit $\mathbf{P}_0 \to 0$, the poles give the Veneziano mass

spectrum $W_l^2 = 2\pi\kappa l$. Expanding the propagator about a given W_l gives

$$\frac{i\kappa}{W^2 - W_l^2 + i\frac{\mathbf{P}_0 W^2}{2\kappa}}, \tag{4.17}$$

which implies each resonance has a full width $\Gamma = \frac{\mathbf{P}_0 W}{2\kappa}$. The overlapping of these resonances in the region $\mathbf{P}_0 W^2/2\kappa^2 > 1$ suggests a continuum. With $\mathbf{P}_0/2\kappa^2 = .5\,\mathrm{GeV}^{-2}$, the region starts about $W \sim 2\,\mathrm{GeV}$, which should be compared to the spacing in the Veneziano mass spectrum. Though only a guideline, this simple picture lends support to Caltech-II, which allows the creation of strings with a continuous mass spectrum above a cutoff W_{max}.

4.5 String Evolution with Massive Quarks

Up to this point we have restricted our discussion to the case of massless partons, since they arise quite naturally as point concentrations of energy and momentum on the relativistic string. There have been many attempts at developing a formalism to accommodate nonzero masses for endpoint quarks [56,57]. One approach is to supplement the relativistic action for the string with the relativistic action of two massive endpoint quarks. The resulting equations of motion partition the system into three distinct phases (Q,$\bar{Q}$, string) with mutual boundary conditions controlling the exchange of energy and momentum between the phases. These modifications give rise to nonlinearities that void the simple treatment afforded by massless partons, except for the simplest of cases. A partial solution to this problem is to include quark masses by evolving an associated massless string to which additional unphysical string segments have been added to account for the boundary conditions of massive quarks.

Consider first a simple $1 + 1$ dimensional $Q\bar{Q}$ yo-yo of total CM energy W and $M_Q \neq 0$. The naive string equation in eq. (2.13) can be solved for the quark

String Motion With Massive Quarks
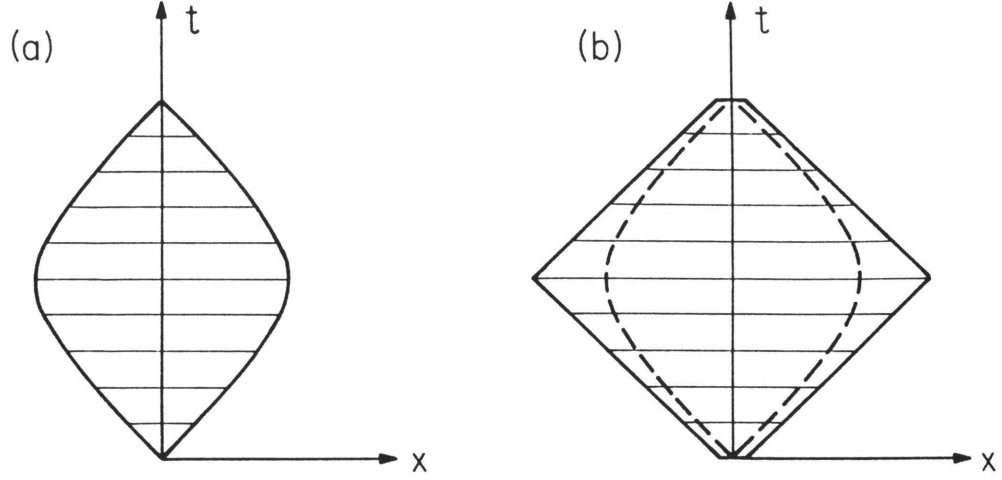
Figure 4.10 String evolution for (a) a simple $Q\bar{Q}$ system with $M_Q \neq 0$, and (b) the associated massless $q\bar{q}$ system.

trajectories during the first half-cycle of motion

$$x_{Q,\bar{Q}}(t) = \pm \frac{1}{\kappa} \left[\frac{W}{2} - \sqrt{M_Q^2 + (P_0 - \kappa t)^2} \right] \quad \text{for } 0 \leq t \leq t_{1/2}, \qquad (4.18)$$

where

$$t_{1/2} = \frac{2P_0}{\kappa} \qquad (4.19)$$

is the time it takes to complete one half-cycle, and

$$P_0 = \frac{\sqrt{W^2 - 4M_Q^2}}{2} \qquad (4.20)$$

is the magnitude of the initial heavy quark three-momentum. Fig. 4.10a shows the evolution of this system for times $0 \leq t \leq t_{1/2}$ in the overall CM frame. The horizontal lines are the string configurations at fixed times.

We map the $Q\bar{Q}$ system onto an associated massless $q\bar{q}$ state as follows. The $q\bar{q}$ system be taken to have $W(q\bar{q}) = W(Q\bar{Q})$ and

$$\vec{p}_0(q) = \vec{p}_0(Q) = P_0 \hat{x}, \qquad (4.21)$$

$$\vec{p}_0(\bar{q}) = \vec{p}_0(\bar{Q}) = -P_0 \hat{x}. \qquad (4.22)$$

Energy conservation then requires that the initial string length of the massless quark system be nonzero

$$\Delta x_0 \equiv 2\Delta x' = \frac{W - 2P_0}{\kappa}. \tag{4.23}$$

The motion of this associated massless quark system for times $0 \le t \le t_{1/2}$ is shown in fig. 4.10b.

The dashed curves in fig. 4.10b are curves $x'_{Q,\bar{Q}}(t)$ defined by

$$\left[p_q(t) + \kappa \left| x_q(t) - x'_Q(t) \right| \right]^2 - p_q^2(t) = M_Q^2 \tag{4.24}$$

$$\left[p_{\bar{q}}(t) + \kappa \left| x_{\bar{q}}(t) - x'_{\bar{Q}}(t) \right| \right]^2 - p_{\bar{q}}^2(t) = M_Q^2, \tag{4.25}$$

where $x_{q,\bar{q}}(t)$ are given by eq. (4.18) with $M_Q = 0$. The association of massless parton string states with massive quark systems is done by identifying the massive quark endpoints in fig. 4.10a with the extended "endpoint plus string segment" regions of fig. 4.10b,

$$\text{"}Q(t)\text{"} \to \text{"}q(t) + \Delta x(t)\text{"}, \tag{4.26}$$

where the length $\Delta x \sim |x_q(t) - x'_Q(t)|$ is determined by mass shell constraints as in eqs. (4.24,4.25).

The incorporation of string breaking according to the area decay law is trivial. Potential string break points for the massless quark system in fig. 4.10b are generated according to the simple area decay law, assuming all points on the world sheet are accessible. However, if the provisional break position lies within the string segment associated with quark masses according to eq. (4.26), the break is summarily rejected. A new prospective break point is then generated by continuing to sample invariant area for the simple decay law, making sure that no region is counted twice. It is straightforward to show that uniform breaking with rejection in the string region of fig. 4.10b is equivalent to uniform breaking in the string region of fig. 4.10a, since it is just a routine application of the Monte Carlo acceptance-rejection method [58].

Extensions of this algorithm to multiparton strings in $3 + 1$ dimensions are straightforward, though nonunique. In more than $1 + 1$ dimensions, there is an ambiguity in the orientation and velocity of the additional string segments. (There is already an unrelated 2-fold orientation uncertainty in the $1 + 1$ dimensional example of fig. 4.10.) One can impose additional constraints involving combinations of other parton momenta, but such an ansatz is not unique and in general gives rise to different physical situations. In Caltech-II the three-momentum of the massless quark associated with a massive quark is

$$\vec{p}(q) \equiv \vec{p}(Q), \tag{4.27}$$

and the length of the extra string segment at time $t = 0$ is again given by

$$\Delta x_0 = \frac{E_0(Q) - |\vec{p}_0(Q)|}{\kappa}. \tag{4.28}$$

The additional string segment is assumed to lie along the initial momentum direction. We have investigated other initial orientations for this string segment and find that the overall physics results are insensitive to the choice made.

The possibility of nonzero quark masses raises an interesting point concerning pair creation and string fragmentation. In order to conserve energy and momentum, a finite length of flux tube must condense into heavy quarks if the probability of pulling heavy quarks from the vacuum so dictates. In our semiclassical model, this means that finite portions of the world sheet effectively "disappear" or are attributed to the simulation of the mass of heavy quarks. This problem would persist even if we had exact solutions to the nonlinear equations governing massive quark systems. Nevertheless, we give all massive quarks the same treatment since we can't expect to simulate the quantum process of particle production that appears to be nonlocal in our semiclassical model.

4.6   Flavor Selection

The only remaining detail of string fragmentation is the specification of flavors at break points. The valence flavors of the initial strings are determined in the perturbative QCD stage of hadronization and are assumed to be given. If the original strings fragment, the flavors of the daughter strings are determined by the flavors at the ends of the parent string and the flavor of the pair pulled from the vacuum. Caltech-II allows both quark pairs and diquark pairs to be pulled from the vacuum. These correspond to the baryon number conserving processes

$$\underbrace{S[q_a, \bar{q}_b]}_{\text{``Meson''}} \rightarrow \underbrace{S[q_a, \bar{q}_c]}_{\text{``Meson''}} + \underbrace{S[q_c, \bar{q}_b]}_{\text{``Meson''}}, \tag{4.29}$$

$$\underbrace{S[q_a, \bar{q}_b]}_{\text{``Meson''}} \rightarrow \underbrace{S[q_a, q_c q_d]}_{\text{``Baryon''}} + \underbrace{S[\overline{q_c q_d}, \bar{q}_b]}_{\text{``Antibaryon''}}, \tag{4.30}$$

$$\underbrace{S[q_a, q_b q_c]}_{\text{``Baryon''}} \rightarrow \underbrace{S[q_a, \bar{q}_d]}_{\text{``Meson''}} + \underbrace{S[q_d, q_b q_c]}_{\text{``Baryon''}}. \tag{4.31}$$

Once a potential break is chosen on the world sheet, the invariant masses W_1 and W_2 of the candidate daughters are specified. The nominal relative probabilities for various flavor assignments are then taken to be

$$P[f] = P_0^f \theta(W_1 - W_{1\,(th)}) \theta(W_2 - W_{2\,(th)}), \tag{4.32}$$

where

$$f \in \{u, d, s, \ldots, uu, ud, us, \ldots\}, \tag{4.33}$$

P_0^f are constant parameters, and $W_{i\,(th)} = W_{2\text{pth}} + W_{\min}$ in the theta functions of eq. (4.32) represent minimal threshold constraints. The parameter $W_{\min}$ is used for flexibility by supplementing the minimum *kinematic* threshold constraints with a constant offset. A typical value for $W_{\min}$ is 100-200 MeV. In the event that one of the daughters falls below the corresponding threshold mass, it checked to see

whether it is possible to perturb the break point and identify the daughter with an on-shell particle as discussed in sect. 4.7. If this can be done, the relative probability for producing the corresponding flavor is taken to be P_0^f. The flavor production parameters P_0^f are provisionally taken to be identical to the corresponding flavor parameters in the low-mass hadronization part of the model (see appendix B). In addition to the economy of parameters, this assumption helps avoid discontinuities in flavor production rates during the transition from strings to clusters.

4.7 Hadrons Directly From Strings

As mentioned in the previous section, it is possible to generate hadrons directly from strings if, in special instances, we perturb the position of a string break so that one of the daughters is on the mass shell of a physical hadron.

In Caltech-II the string decay

$$\text{String} \rightarrow \text{String} + \text{Hadron} \tag{4.34}$$

is considered a viable decay mode only if one of the candidate daughter masses is below $W_{\text{2pth}} + W_{\text{min}}$ for the particular flavor pulled from the vacuum (assuming the original break position was chosen using the area decay law). If a mode of the form in eq. (4.34) is chosen, the orignal break position is adjusted to put one of the strings on-mass-shell.

We can show that this ansatz is reasonable by considering the change in mass of a daughter as a function of the breakpoint position. Consider the situation where a break occurring at $\sigma = \bar{\sigma}$ on an arbitrary string produces a daughter with four-momentum

$$p(\bar{\sigma}) = \int_0^{\bar{\sigma}} \dot{x} d\sigma. \tag{4.35}$$

The squared mass of this daughter is

$$W^2(\bar{\sigma}) = p(\bar{\sigma}) \cdot p(\bar{\sigma}), \tag{4.36}$$

so that taking the differential of both sides gives

$$W dW = \dot{x} \cdot p(\bar{\sigma}) d\bar{\sigma}. \tag{4.37}$$

In the frame in which the string element containing the original break is at rest,

$$\dot{x} \cdot p(\bar{\sigma}) = E, \tag{4.38}$$

where E is the energy of the daughter *in that frame*. Substituting eq. (4.38) into eq. (4.37), and recalling that $dl = \kappa d\bar{\sigma}$ is the relation between energy coordinates and physical lengths in the rest frame of a string segment, we have

$$dl = \frac{W}{E} \frac{dW}{\kappa} \leq \frac{dW}{\kappa}. \tag{4.39}$$

Thus, for a shift in mass of $\Delta W \sim 200\,\text{MeV}$,

$$|\Delta l| \sim 0.2\,fm \times \frac{W}{E}. \tag{4.40}$$

This result tells us that the physical shift in the position of the breakpoint is comparable to the width of QCD flux tubes indicated by lattice calculations [38]. Inasmuch as we use the relativistic string only for the gross properties of fragmentation, small perturbations such as those implied by eq. (4.40) are easily absorbed.

As we show in sect. 5.3, the mechanism of eq. (4.34) is rather *ad hoc* since the only observable it appears to affect is the production of very energetic hadrons in the upper tails of momentum distributions. We point out in sect. 5.4 that, in keeping with the philosophy of not letting string mechanisms control the details of hadronization, relatively few hadrons are produced through the mechanism of eq. (4.34).

Chapter 5

Caltech-II vs. Data

5.1   Introduction

As we have repeatedly stressed in the previous chapters, the overall physics
picture in Caltech-II is both appealing and sensible. Any realistic phenomenological
model of hadronization entails a large number of parameters — a simple reflection of
the fact that we do yet have exact solutions to QCD over all the energy scales relevant
to hadronization. However, just because we have a large number of parameters does
not mean that they are all at our disposal. Caltech-II's sensibility derives from the
observation that by factoring event evolution into the three stages

$$\text{LLA QCD} \otimes \begin{array}{c}\text{Relativistic String}\\+\text{Area Decay Law}\end{array} \otimes \begin{array}{c}\text{Low} - \text{Mass}\\\text{Parameterization}\end{array}, \tag{5.1}$$

the majority of parameters occur in the last stage and are *fixed* by available low en-
ergy data. With such parameters fixed, the model need only explain where *clusters*,
not hadrons, come from.

Herein lies the appeal of Caltech-II: with only five energy-independent (and, un-
fortunately, highly correlated) parameters, we can describe cluster formation at *any*
center of mass energy in e^+e^- annihilation. Subsequently, using the parameterized
decay of low-mass clusters, Caltech-II is able to provide a good description of data
over the entire energy range $3\,\text{GeV} \leq E_{\text{CM}} \leq 45\,\text{GeV}$. In this chapter we confront
Caltech-II with the available e^+e^- annihilation data to determine reasonable values

for its five parameters and to assess the model's strengths and weaknesses.

In sect. 5.2 we isolate five "basic" parameters and suggest nominal values for them within the context of the complete Caltech-II model. Sect. 5.3 discusses the effects of parameter variations on the predictions of the model with an emphasis on the string parameters ρ_c, W_{max}, and W_{min}. Inasmuch as all three stages of hadronization in eq. (5.1) are necessarily correlated, we will also discuss how the string parameters are related to the LLA QCD shower parameters t_0 and Λ_{QCD}.

Sect. 5.4 compares the results of Caltech-II (with fixed parameters) to data. We demonstrate how the model can reproduce details of distributions at fixed energies as well as the E_{CM} dependence of average values of observables. By virtue of incorporating the full string equations of motion, Caltech-II is shown to reproduce the so-called string effect [59,60,61,62,63,64] observed for three-jet events. The model also explains observed [65,66] angular correlations in $p\bar{p}$ production by allowing baryon creation during the string evolution phase.

Sect. 5.5 briefly discusses the known shortcomings of the full Caltech-II model and then concentrates on ways in which the string evolution phase can be elaborated. We describe how, aside from being theoretically consistent, the incorporation of transverse momentum at string breaks will result in a smoother transition between the string and cluster phases of the model.

In keeping with our desire to focus on the string aspects of Caltech-II, we relegate discussions of the shower and cluster stages of the model to appendices A,B.

5.2   Identification of Five Basic Parameters

Caltech-II's factorization of hadronization into the three stages of eq. (5.1) is effectively an attempt to conquer QCD by dividing it into the three regimes

$$
\begin{array}{ccccc}
\text{Perturbative} & & \text{Nonperturbative QM} & & \text{Nonperturbative QM} \\
\text{Quantum Mechanical} & \otimes & \text{(Semiclassical)} & \otimes & \text{(Nonclassical)}
\end{array} \quad . \quad (5.2)
$$

As discussed in chapter 2, there is both phenomenological and practical motivation for this division of event evolution. Though QCD is, in principle, a well-defined theory, it has resisted most conventional attempts to make predictions concerning nonperturbative dynamical phenomena. The relative successes of perturbative calculations and lattice gauge theory have already demonstrated two qualitatively different regimes of QCD roughly corresponding, respectively, to the first and second stages of eq. (5.1). On the other hand, comprehensive "QCD predictions" for the third stage of eq. (5.1) simply do not exist.

The attractive feature of factorization is that it gives us an opportunity to test those aspects of QCD which we believe we *do* know something about. Rather than speculate on the details of hadron formation in QCD, we instead assume that low-mass hadronization is a local, universal phenomenon that can be factored out of the event evolution in eq. (5.1) and replaced with a *parameterization* of the decays of low-mass systems. This "black box" approach to low-mass hadronization allows us to concentrate more fully on the first two stages in eq. (5.1), so that we might better assess their influence on the features of hadronization.

Aside from the *fixed* parameters describing the decays of low-mass clusters, the only free parameters in Caltech-II are Λ_{QCD}, which governs the scale in the first stage of eq. (5.1), ρ_c, which governs the string decays, and the three cutoff parameters t_0, W_{max}, and W_{min}. The cutoff t_0 for the perturbative shower evolution essentially governs the transition between the parton picture of the first phase and the string picture of the second phase, while W_{max} controls the transition from string picture to the low-mass parameterization. W_{min} is a junior partner to W_{max}, since it permits the occasional identification of a string with an on-mass-shell hadron as discussed in sect. 4.7.

It is found that the nominal parameter values

$$\rho_c \ = 1.6 \, \text{GeV}^{-2} \qquad (\pm 0.3 \, \text{GeV}^{-2}), \qquad (5.3)$$

$$W_{\mathrm{max}} \quad = 2.2\,\mathrm{GeV} \qquad (\pm 0.3\,\mathrm{GeV}), \qquad\qquad (5.4)$$

$$W_{\mathrm{min}} \quad = .25\,\mathrm{GeV} \qquad (\pm 0.1\,\mathrm{GeV}), \qquad\qquad (5.5)$$

$$\Lambda_{\mathrm{QCD}} \quad = 0.6\,\mathrm{GeV} \qquad (0.3 - 0.7\,\mathrm{GeV}), \qquad\qquad (5.6)$$

$$t_0 \quad = 1.0\,\mathrm{GeV^2} \qquad (1 - 2\,\mathrm{GeV^2}) \qquad\qquad (5.7)$$

provide a good description of e^+e^- annihilation data over the range $3\,\mathrm{GeV} \leq E_{\mathrm{CM}} \leq 45\,\mathrm{GeV}$. The parenthetical values give reasonable ranges or variations in the parameters that reflect the correlations induced by the factorization of event evolution. In the next section we discuss how we arrive at these values for the parameters.

5.3 Parameter Determination

Our approach to determining values for the five basic parameters will first involve isolating observables sensitive to variations in the parameters. With the benefit of hindsight and for purposes of illustration, we shall initially set the shower parameters Λ_{QCD} and t_0 to their nominal values to demonstrate how the string-breaking probability ρ_c and the string-to-cluster cutoff W_{max} influence event shape variables such as sphericity and transverse momentum. The remaining string parameter W_{min} is relatively superfluous, as it allows the occasional production of high z particles directly from the ends of a string. For this reason it can be fixed after all other parameters have been determined.

5.3.1 ρ_c

The left panel of fig. 5.1 compares the TASSO [67] 14 GeV sphericity distribution with the results of Caltech-II. The dashed curve uses the standard parameters of eqs. (5.3-5.7), while the solid curve corresponds to changing ρ_c to $.6\,\mathrm{GeV^{-2}}$. Sphericity is a convenient measure of the spherical nature of an event in momentum space [68]. The sphericity axis of an event is defined along the unit vector $\hat{n}$ that
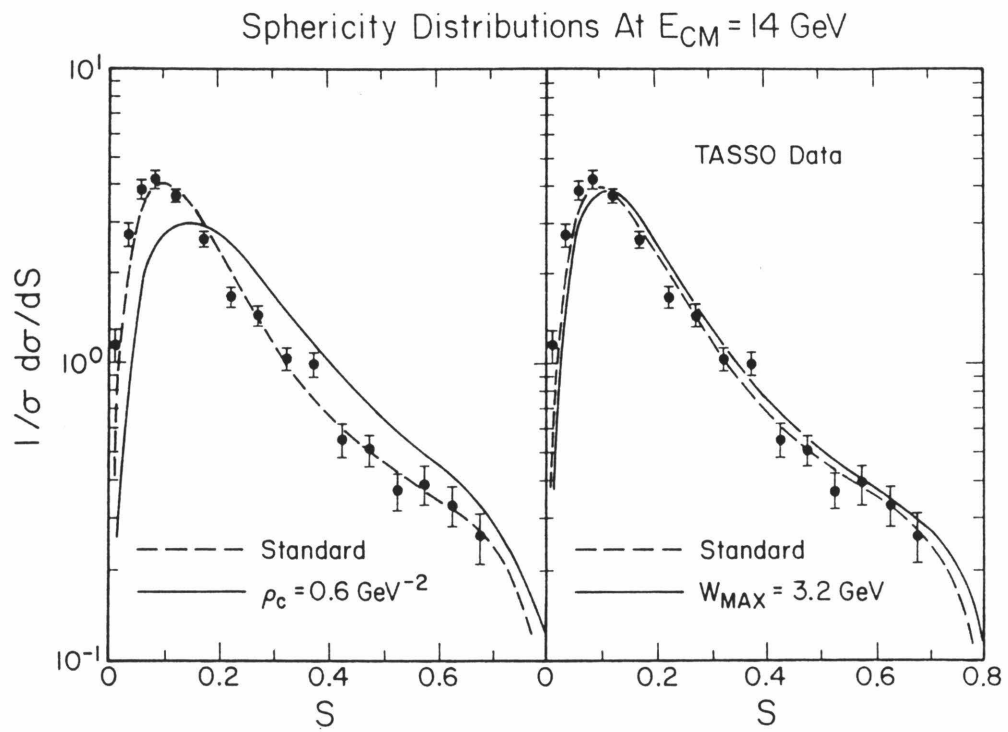
Figure 5.1 Sphericity distributions at $E_{CM} = 14\,\text{GeV}$ for various values of ρ_c and W_{max} (other parameters fixed at values in eqs. (5.5-5.7)). The data are from ref. [67].

maximizes

$$\sum_{i=1}^{N}(\hat{n}\cdot\vec{p_i})^2 + \lambda(\hat{n}^2 - 1). \tag{5.8}$$

In this equation the sum extends over N particles and λ is a Lagrange multiplier that ensures that $\hat{n}$ is normalized. Finding the extrema of eq. (5.8) is equivalent to solving the eigenvalue problem

$$M\hat{n} = \lambda\hat{n}, \tag{5.9}$$

where M is the momentum tensor

$$M^{\alpha\beta} = \sum_{i=1}^{N} p_i^{\alpha} p_i^{\beta} \qquad \alpha, \beta = x, y, z. \tag{5.10}$$

We can order the normalized eigenvalues Q_i of the momentum tensor, corresponding to the three orthonormal eigenvectors $\hat{n}_1$, $\hat{n}_2$, $\hat{n}_3$, so that

$$0 \le Q_1 \le Q_2 \le Q_3, \tag{5.11}$$

$$Q_1 + Q_2 + Q_3 = 1, \tag{5.12}$$

where

$$Q_j = \frac{\sum\limits_{i=1}^{N}(\hat{n}_j\cdot\vec{p_i})^2}{\sum\limits_{i=1}^{N}(\vec{p_i})^2}. \tag{5.13}$$

The sphericity of an event is defined as

$$S = \frac{3}{2}(1 - Q_3), \tag{5.14}$$

so that $0 \le S \le 1$ where $S = 0$ corresponds to a perfectly collimated 2-jet event in the CM frame and $S = 1$ corresponds to a spherical momentum distribution.

The increase in average sphericity with smaller ρ_c in fig. 5.1 may be qualitatively understood by considering the simple case of a $q\bar{q}$ system. The distribution of first generation breaks with respect to the proper time interval separating the breaks and the initial vertex is a Lorentz invariant quantity. Contours of constant invariant time are hyperbolae in (x, t) space as shown in fig. 5.2. According to the area decay law,
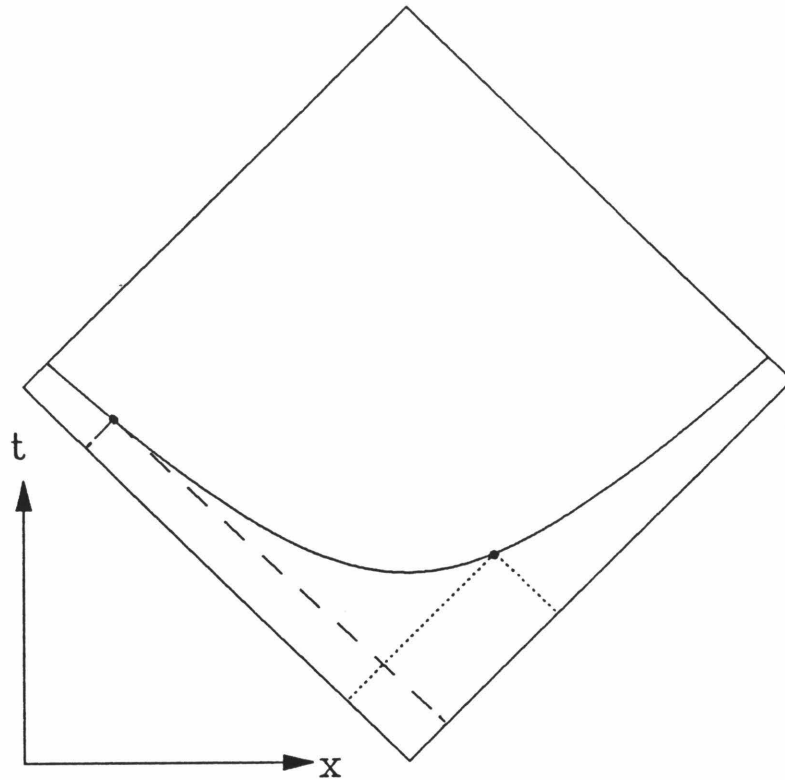
Figure 5.2 Points along the same contour of invariant time bound equal amounts of backwards light-cone area.

all points on a fixed hyperbola are equally probable break postions since all bound the same backwards light-cone area. The uniform distribution of breaks along a hyperbola corresponds to a uniform distribution in rapidity of the daughters. Since the probability of invariant area A being swept out before a break occurs is $e^{-\rho_c A}$, ρ_c can be viewed as a decay constant that implies an "area half-life" of $\rho_c^{-1} \ln 2$. Large ρ_c corresponds to hyperbolae closer to the world lines of the quarks and hence results in low-mass daughters, which populate a large range of rapidities. Accordingly, small ρ_c tends to break strings "later" and produces massive daughters within a limited rapidity interval. In the extreme case that daughters are produced at rest, jet-like phenomena disappear in favor of high sphericity configurations.

Table 5.1 Changes in average values of observables at $E_{CM} = 14\,\text{GeV}$ with variations of ρ_c and W_{max}. **Other parameters are fixed as in eqs. (5.5-5.7). Data are from ref. [67].**

$\rho_c\,(\text{Gev}^{-2})$	$W_{max}\,(\text{GeV})$	$\langle N_{ch} \rangle$	$\langle S \rangle$	$\langle p_T^2 \rangle (\text{GeV}^2)$
1.6	2.2	9.18	0.220	0.183
0.6	2.2	9.90	0.269	0.188
1.6	3.2	8.93	0.233	0.203
	data	9.08±0.05	0.213 ± 0.004	0.168 ± 0.002

5.3.2 W_{max}

The right panel of fig. 5.1 assesses the effect on the sphericity distribution when W_{max} is increased from the standard value of $2.2\,\text{GeV}$ to $3.2\,\text{GeV}$, leaving all other parameters at their standard values. Though the change is not as dramatic as when ρ_c was varied, the general trend is similar. Increasing W_{max} increases the use of paramaterized cluster decays. Since cluster decays are isotropic in the cluster rest frame, an increased dependency on the low-mass parameterization leads to more spherical events (i.e., events with more transverse momentum).

Though the above variations of ρ_c and W_{max} both lead to more spherical events, they have opposite effects on the average charge multiplicity, as can be seen from table 5.1. Decreasing ρ_c allows strings to evolve longer before breaking and so leads to more massive daughters. On the other hand, increasing W_{max} turns on the cluster decay sooner. Since the parameterized cluster decays of ref. [69] faithfully reproduce the empirical mass dependency

$$\langle N_{ch}(W) \rangle \sim 2 + \frac{W}{2\,\text{GeV}} \qquad 1\,\text{GeV} \leq W \leq 3\,\text{GeV}, \qquad (5.15)$$

the decay of a single large mass cluster gives fewer particles than if it first broke into two smaller mass clusters. Table 5.1 suggests that rather than look at $\langle S \rangle$ for the effects of W_{max}, it would be better to look at $\langle p_T^2 \rangle$, the average squared momentum transverse to the sphericity axis.
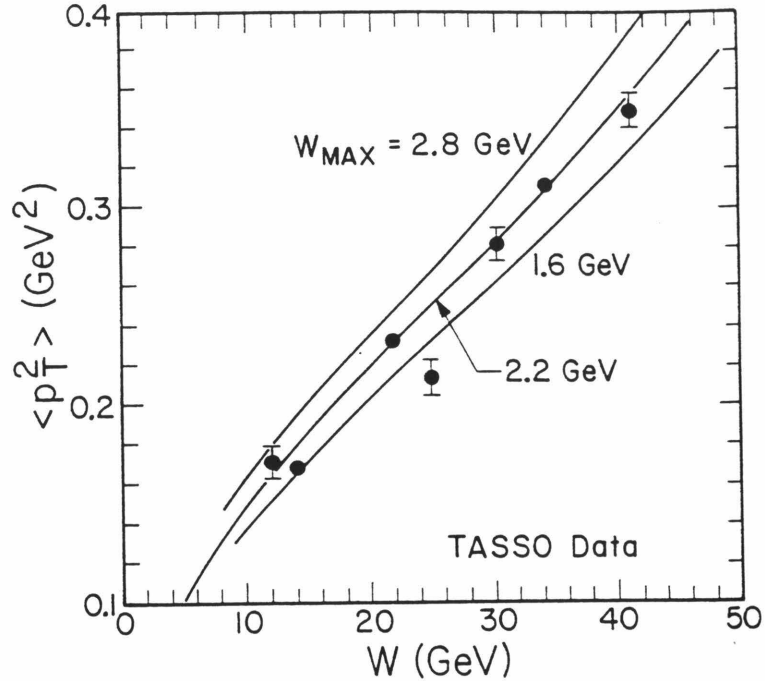
Figure 5.3 Sensitivity of $\langle p_T^2 \rangle$ to W_{max} as a function of E_{CM}. Data are from ref. [67].

The influence of W_{max} is clearly visible when we consider the E_{CM} dependence of $\langle p_T^2 \rangle$ as shown in fig. 5.3. Leaving all other parameters at their standard values, we note that the sensitivity of $\langle p_T^2 \rangle$ to W_{max} permits us to determine an optimal value of $W_{max} = 2.2\,\text{GeV}$.

That sphericity should be largely governed by ρ_c and that $\langle p_T^2 \rangle$ be controlled by W_{max} are not unexpected. Sphericity and $\langle p_T^2 \rangle$ are complementary in that they deal with different momentum components. Except for very high sphericity events, most of a primary hadron's longitudinal momentum can be traced back to the longtitudinal momentum of its parent cluster. As outlined above for the simple $q\bar{q}$ case, the longitudinal momenta of such clusters (i.e., strings that were too light to evolve using the string picture) are strongly influenced by ρ_c. On the other hand, $\langle p_T^2 \rangle$ is, by definition, invariant under boosts along the sphericity axis and should be sensitive to ρ_c only to the extent that the total longtitudinal momentum and total

transverse momentum are constrained by energy-momentum conservation.

5.3.3 t_0 and Λ_{QCD}

Now that. we know which observables are sensitive to ρ_c and W_{max}, we can briefly describe how the standard parameters of eqs. (5.3- 5.7) were determined. For different values of Λ_{QCD}, best values for ρ_c and W_{max} were determined by requiring agreement with sphericity distributions and $\langle p_T^2 \rangle$, respectively. Their opposite effect on $\langle N_{ch} \rangle$ also helps pin down values of ρ_c and W_{max}.

The perturbative cutoff t_0, which controls the amount of soft perturbative radiation, was set to the value $1 - 2\,\mathrm{GeV}^2$. Because of the continuous nature of the mapping of soft gluons onto the relativistic string, radiation below this mass scale is not found to influence subsequent event evolution. In this sense, the parameter t_0 is very uncontroversial.

The leading-log QCD scale Λ_{QCD} plays an interesting role in the model. The observables that appear to be most sensitive to Λ_{QCD} are the mean charge multiplicity and the various infrared safe jet measures such as thrust and the energy-energy correlation.

The standard energy-energy correlation function is defined as [70,71]

$$\frac{d\Sigma}{d\theta} = \frac{1}{\sigma_{tot}} \sum_{i,j} \int dx_i dx_j x_i x_j \left[\frac{d^3\sigma}{dx_i dx_j d\theta} \right], \qquad (5.16)$$

where the double sum extends over all observed particles and x_i is the fraction of the observed energy carried by the ith particle. The leftmost panel of fig. 5.4 compares Caltech-II (with standard parameters) to JADE data [72] for $d\Sigma/d\theta$, weighted by $\sin\theta_B$, where θ_B is the angle in the center of each bin. The middle panel of fig. 5.4 demonstrates how the central values $\theta \sim 90°$ are sensitive to changes in Λ_{QCD}. In the rightmost panel of fig. 5.4 we note how increasing ρ_c to give fatter events increases the central values of $d\Sigma/d\theta$.

Energy–Energy Correlations At $E_{CM} = 34\,GeV$
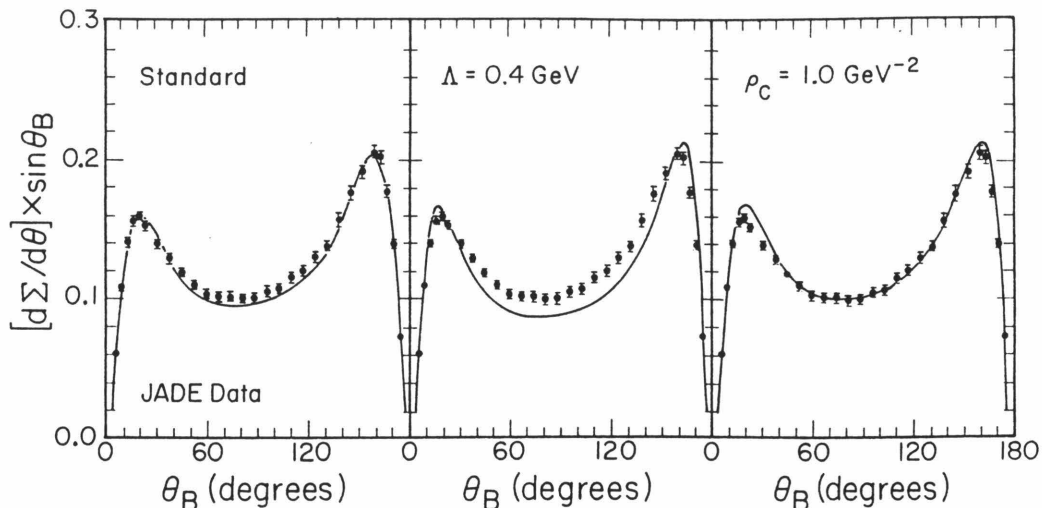
Figure 5.4 Energy-energy correlation functions. Parameters not specified explictly are given the standard values of eqs. (5.3-5.7). Data are from ref. [72].

Thrust is defined [73] as

$$T = \max_{\hat{n}_T} \left[\frac{\sum\limits_{i=1}^{N} \theta(\hat{n}_T \cdot \vec{p}_i)|\vec{p}_i \cdot \hat{n}_T|}{\sum\limits_{i=1}^{N} |p_i|} \right], \qquad (5.17)$$

where the unit vector $\hat{n}_T$ is called the thrust axis. Like sphericity, thrust is a measure of the two-jet nature of event topology. Unlike sphericity, thrust is an infrared-safe variable — it is invariant if a single particle is replaced with a collinear pair with the same total momentum, and it is unchanged by the addition of zero momentum particles. Thrust varies between $1/2 \leq T \leq 1$ with $T = 1$ corresponding to a perfectly collimated two-jet system.

The leftmost panel in fig. 5.5 shows how Caltech-II, with the standard parameters of eqs. (5.3-5.7), overestimates the number of high and low thrust events. Keeping all parameters fixed, except for decreasing Λ_{QCD}, as in the center panel of fig. 5.5, we see that the number of low thrust events can be decreased at the expense of increasing the number of high thrust events. In order to decrease the number of high thrust events, we are forced to decrease ρ_c, which, as shown in the rightmost panel of fig. 5.5, increases the number of low thrust events (if all other parameters

Thrust Distributions At $E_{CM} = 34$ GeV
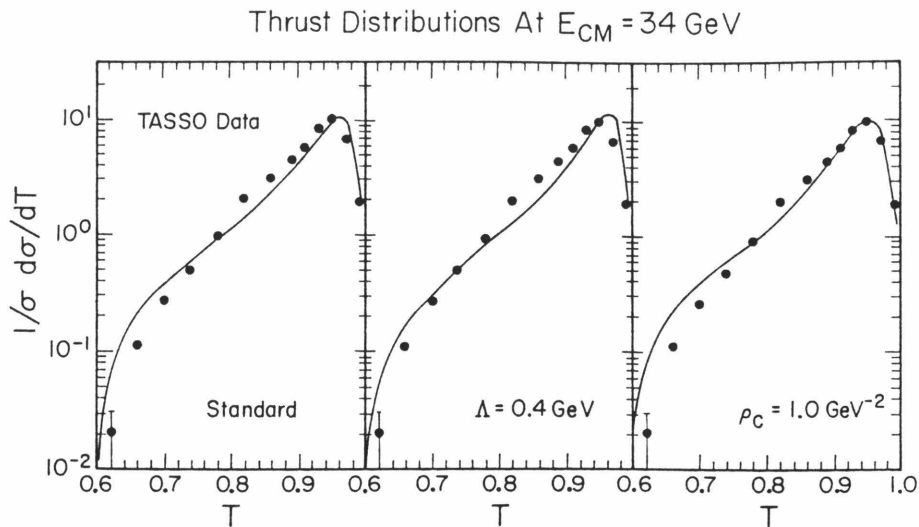
Figure 5.5 Sensitivity of thrust to variations in the LLA QCD scale Λ_{QCD} and the string parameter ρ_c. Data are from ref. [67]

are left at their standard values). It is possible to decrease ρ_c and Λ_{QCD} *together* to obtain the "fat jet" parameters of fig. 5.6, which lead to a better thrust distribution but overbroaden the left peak of the energy-energy correlation.

In choosing our standard set of parameters, we decided to fix Λ_{QCD} by requiring agreement with the central values of the energy-energy correlation function. This is the origin of our somewhat large value for Λ_{QCD} in eq. (5.6). The neglected $O(\alpha_s^2)$ corrections to the central values of $d\Sigma/d\theta$ are known [74,75,76,67,77] to be small, but positive; our high value of Λ_{QCD} is simply mimicking these corrections in an artificial way: the shower model results are sensitive to Λ_{QCD} for the classes of events where nonleading $O(\alpha_s^2)$ corrections are operative. We choose the energy-energy correlation instead of thrust to determine Λ_{QCD} because, as shown in ref. [78], the $O(\alpha_s^2)$ corrections to $d\sigma/dT$ are large and, in the region $T \rightarrow 1$, sensitive to the cutoff scheme used in dressed jet calculations.

5.3.4 $W_{\min}$

The parameter $W_{\min} = .25$ GeV is determined by requiring agreement with the high $z_p = 2|p|/Q$ data for inclusive charged particles as shown in fig. 5.7. Increasing

Event Shapes At $E_{CM} = 34$ GeV
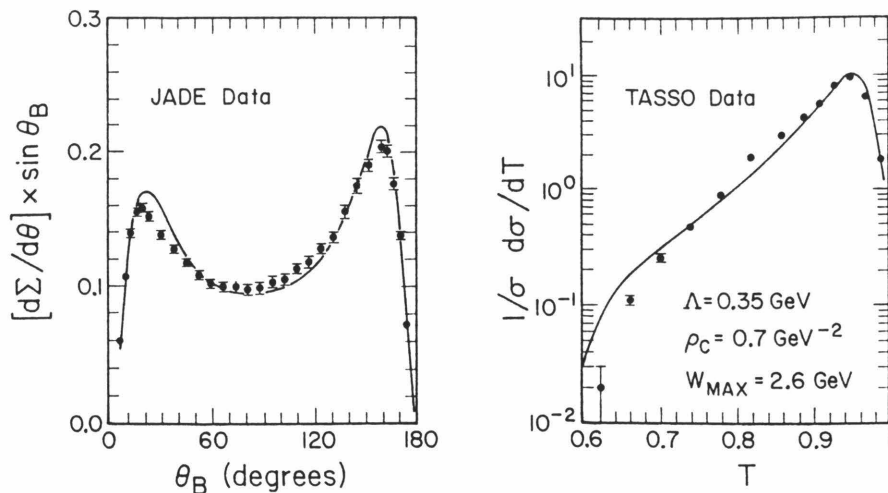
Figure 5.6 An alternate of set "fat jet" parameters improves the agreement with TASSO thrust data [67] but implies a broadening of the left peak in the energy-enery correlation. JADE data are from ref. [72].

W_{min} increases the probability that a string break near the end of the world sheet will produce an on-mass-shell particle. To see why this affects only the high z region of fig. 5.7, let us go back once more to our simple $q\bar{q}$ example. Consider a hyperbola on the world sheet formed by points bounding the same backwards light-cone area as in fig. 5.2. As we have already mentioned, the uniform distribution of breaks along such a hyperbola corresponds to a uniform distribution in the rapidity of the daughter strings. Since W_{min} affects only breaks that occur close to the end of a string, where the rapidity with respect to the CM frame is the largest, most particles so produced will have large momentum (high z).

Seeing how W_{min} affects only the production of high z particles, we might be skeptical about calling it a basic parameter. Our skepticism is fostered by the observation that we can reproduce the high-z tail of fig. 5.7 with $W_{min} \approx 0$ if we use quark masses of $m_u = m_d \approx 0$, and $m_s \approx 150$ MeV in the shower formalism instead of the constituent masses $m_u = m_d = m_\pi$, and $m_s = m_\kappa$ (which are used to ensure that all strings produced in shower evolution are massive enough to evolve into multihadron systems). Since the use of constituent quark masses is simply a
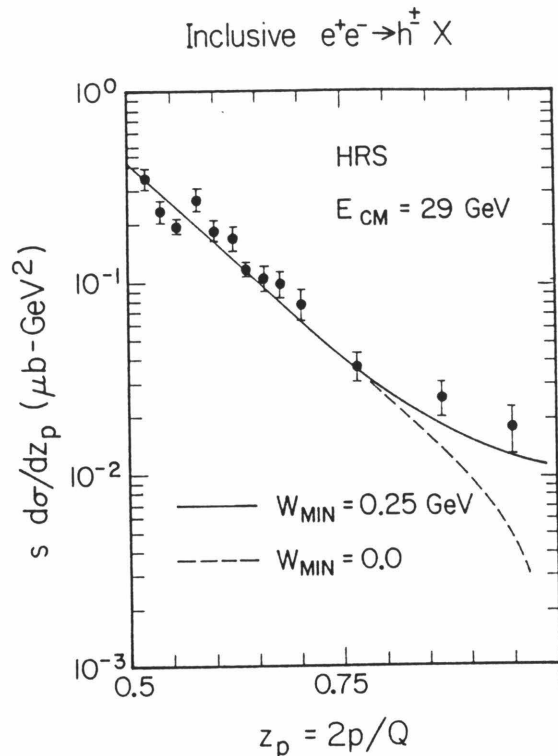
Figure 5.7 Dependence of model predictions for $sd\sigma/dz$ on the cutoff parameter W_{min}. Data are from ref. [79].

technical issue, W_{min} has only minor significance as a basic parameter.

The effect of quark masses on the tail of the z distribution can be understood by recalling how we can use a system composed of massless quarks to simulate a system of massive quarks (see sect. 4.5). Referring to fig. 4.10b we note that for massive quarks, string breaks are unconditionally forbidden in the region of the world sheet between the dashed line and world lines of the corresponding massless quarks; the forbidden region simulates the quark mass. It is easy to see that as the mass of the quark becomes smaller, the forbidden region shrinks, and breaks in regions of higher rapidity become more accessible, populating the high z tail.

5.3.5 Correlations

While the parameter-fitting procedure outlined above is relatively straightforward, there are correlations among parameters that make the task nontrivial. For

example, increasing Λ_{QCD} increases the amount of perturbative radiation and leads to more spherical or "fatter" events. But we already know that decreasing ρ_c will have the same effect. This interplay between ρ_c and Λ_{QCD} should not be surprising, since in a formal QCD-based treatment of flux tubes, we would expect ρ_c to be a function of Λ_{QCD}. With reservations concerning future improvements to Caltech-II, we adopt eqs. (5.3-5.7) as a set of parameters that give an acceptable overall description of e^+e^- annihilation data over the energy range $3\,\mathrm{GeV} \leq E_{\mathrm{CM}} \leq 45\,\mathrm{GeV}$.

5.4   Comparisons With Data

Since the string model in Caltech-II is necessarily sandwiched between the perturbative LLA QCD and the parameterized decays of low-mass clusters, it is sometimes difficult to attribute features of the model predictions to a specific stage of event evolution. In this section we demonstrate the relative harmony between the various stages of hadronization in Caltech-II by comparing results of the model to available e^+e^- annihilation data. The goal is to impress upon the reader how the choice of the fixed parameters of eqs. (5.3-5.7) reproduces observed phenomena to within 5-10% over the energy range $3\,\mathrm{GeV} \leq E_{\mathrm{CM}} \leq 45\,\mathrm{GeV}$. This point alone is of some merit since other hadronization models are tuned (perhaps to excess) to describe the details of hadronization at one particular energy.

The success of many of the comparisons in this section is not meant to draw attention to the success of the string model alone but rather is meant to point out the cooperation between all three stages of the factorized evolution of eq. (5.1). However, we also show how the incorporation of the full string equations of motion can be credited with the accurate reproduction of particle flow data and observed baryon correlations.

Figure (5.8) compares Caltech-II to sphericity, aplanarity and thrust distributions measured by TASSO at 14 GeV and 34 GeV. Aplanarity is a measure of the
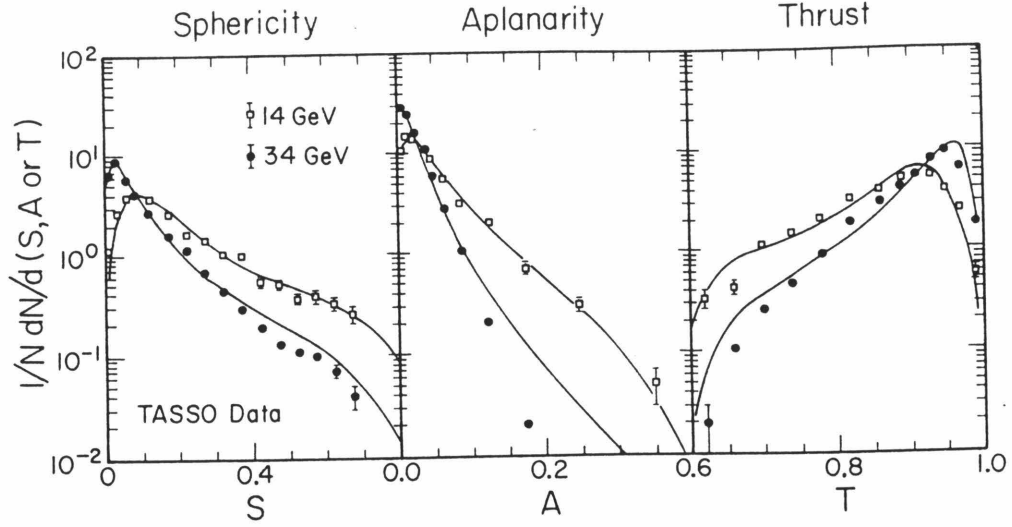
Figure 5.8 Caltech-II (solid lines) compared to various shape variables at $E_{CM} = 14$ GeV and $E_{CM} = 34$ GeV. Data are from ref. [67].

momentum out of the event plane

$$A = \frac{3}{2}Q_1, \tag{5.18}$$

where Q_1, the smallest normalized eigenvalue of the momentum tensor, is given by eq. (5.13).

An interesting deviation from the data is seen in fig. 5.8 where Caltech-II overestimates the number of high sphericity/high aplanarity/low thrust events at $E_{CM} = 34$ GeV. As discussed in ref. [3], most of these "fat" events can be traced back to the use of LLA QCD showers, which lack the quantum interference effects necessary to correlate the decay planes of highly virtual partons in four-jet events. When exact $O(\alpha_s^2)$ matrix elements are used in place of LLA QCD (with a suitable adjustment of ρ_c and W_{max}), a better agreement with the data is obtained (see fig. 5.9).

Fig. 5.10 compares the results of Caltech-II with transverse momentum distributions from TASSO at fixed energies while figs. 5.11a,b show the E_{CM} dependence of inclusive charged particle momenta. In fig. 5.11b the transverse components of momentum in and out of the event plane are measured with respect to eigenvectors
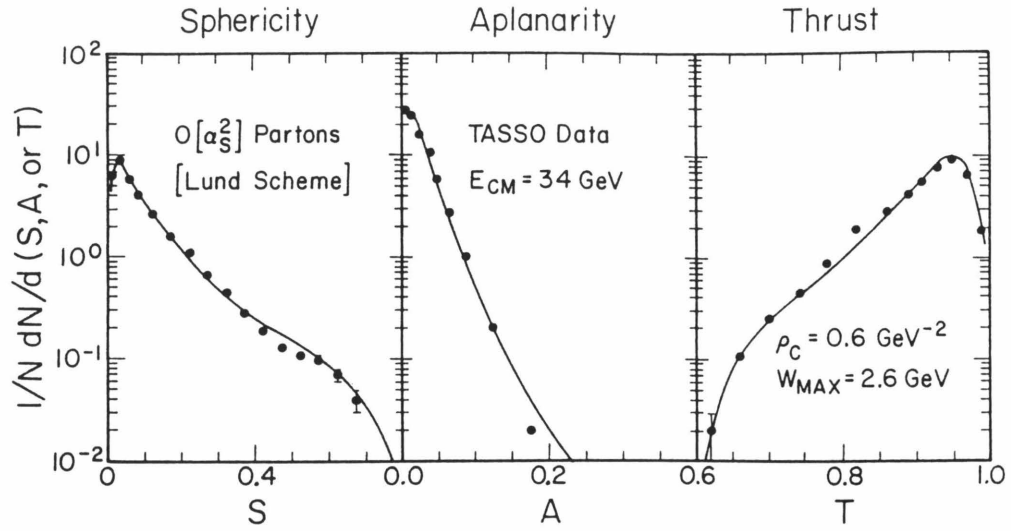
Figure 5.9 Shape distributions at $E_{CM} = 34$ GeV using Caltech-II hadronization (with parameters as indicated) and LUND exact $O(\alpha_s^2)$ matrix elements [80]. Data are from ref. [67].
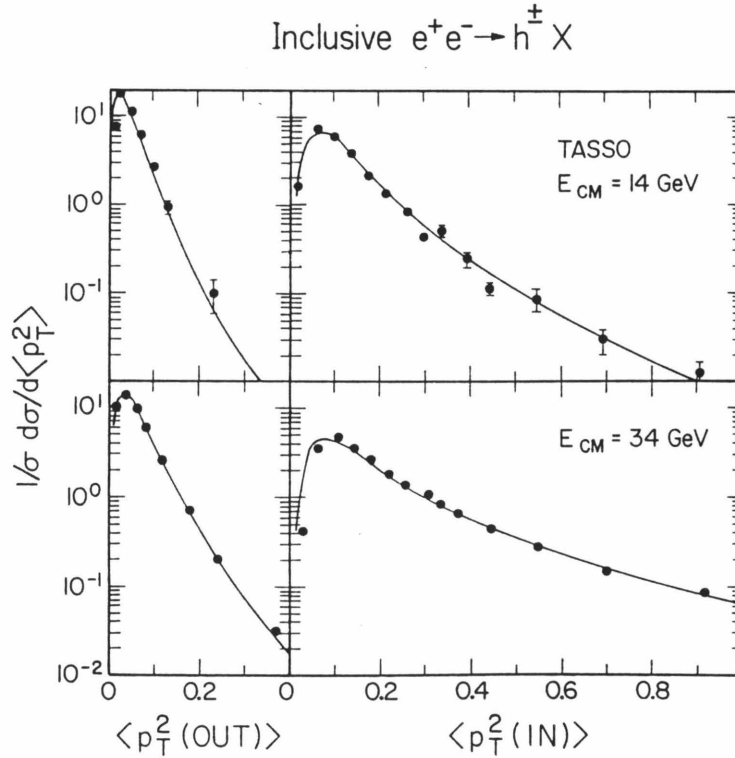
Figure 5.10 Distributions for momentum transverse to the sphericity axis for charged particles at $E_{CM} = 14$ GeV and $E_{CM} = 34$ GeV. Data are from ref. [67].

Inclusive $e^+e^- \rightarrow h^\pm X$
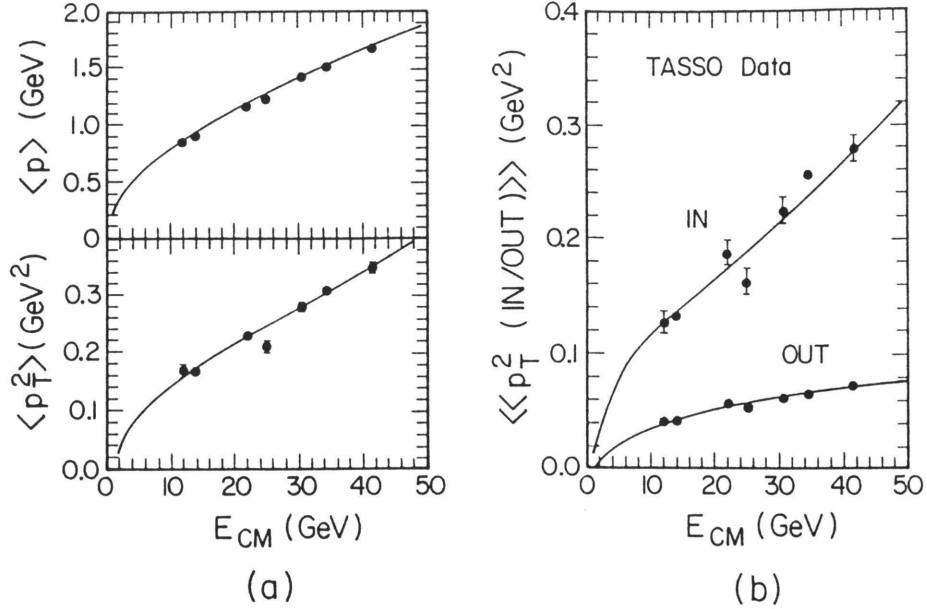
Figure 5.11 (a) Energy dependence of $\langle p \rangle$, $\langle p_T^2 \rangle$ and (b) $\langle\langle p_T^2(IN/OUT)\rangle\rangle$. Data are from ref. [67].

$\{\hat{n}_j\}$ of the momentum tensor in eq. (5.10), so that

$$\langle p_T^2(IN) \rangle = \frac{1}{N} \sum_{i=1}^{N} (\vec{p}_i \cdot \hat{n}_2)^2, \tag{5.19}$$

$$\langle p_T^2(OUT) \rangle = \frac{1}{N} \sum_{i=1}^{N} (\vec{p}_i \cdot \hat{n}_1)^2, \tag{5.20}$$

where the sums extend over all charged particles. Caltech-II is seen to faithfully reproduce the energy dependence of all the momentum distributions.

Fig. 5.12 shows how accurately Caltech-II reproduces the average charge multiplicity over the whole energy range of data. At the lowest energies ($\approx 3\,\text{GeV}$), particle production is due entirely to the parameterized decay of low-mass clusters since there is not enough energy available for string evolution. As E_{CM} increases, more and more string evolution occurs. Fig. 5.13 tracks the flavor multiplicities of kaons, protons and lambda particles. The improved string model in Caltech-II has cured a number of the pathologies observed in Caltech-I [5]. By incorporating the full string equations of motion, we have eliminated an abrupt increase in $\langle N_{\text{ch}} \rangle$ at

Inclusive Charged Particles
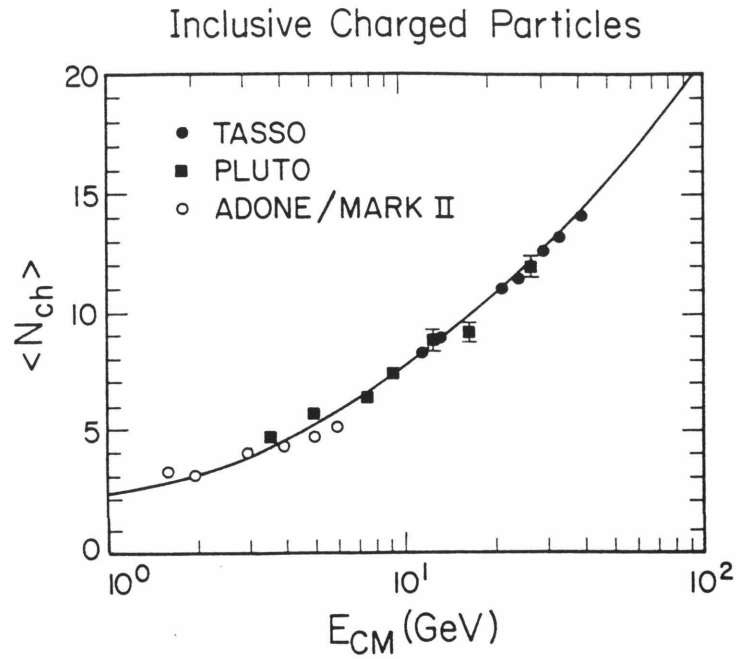
Figure 5.12 Muliplicity of inclusive charge particles as a function of E_{CM}**. Data are from refs. [67,81,82,83,84].**

Flavor Multiplicities
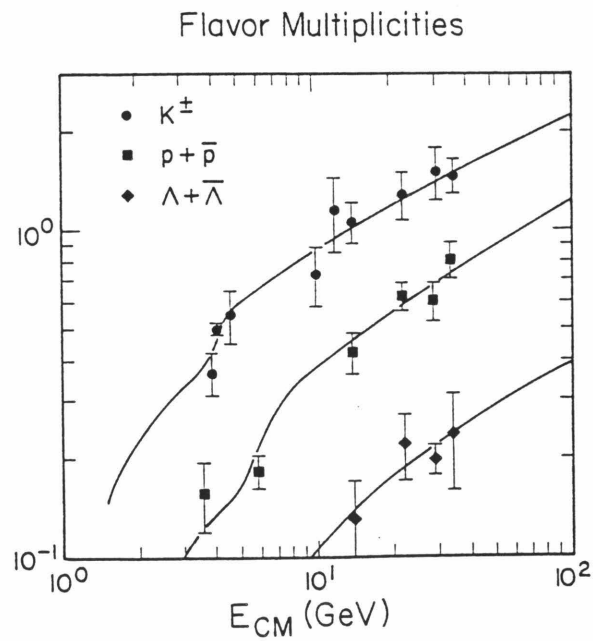
Figure 5.13 E_{CM} **dependence of kaon and baryon mulitplicities. Data are from refs. [85,86,87,88,89,90].**

Particle Flow In Three-Jet Events
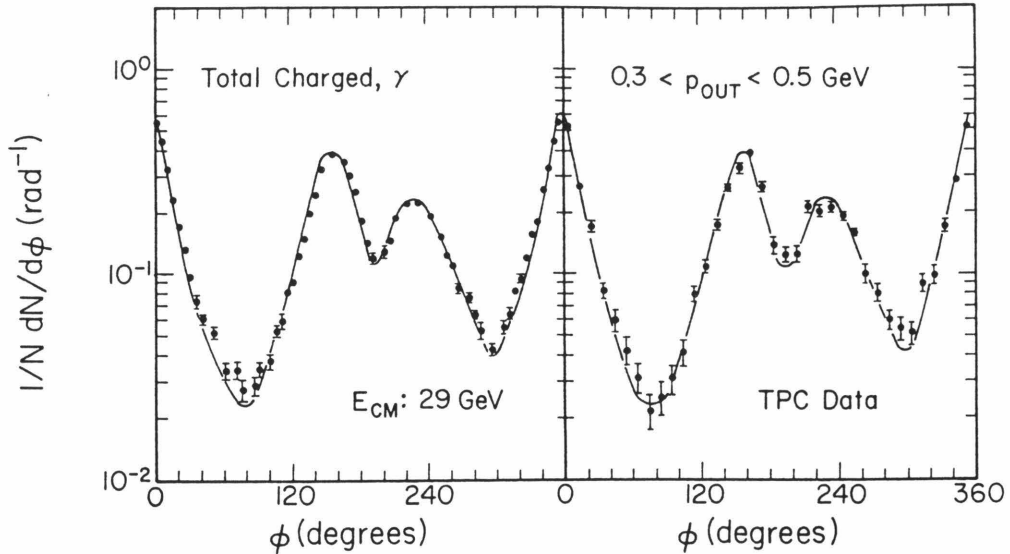
Figure 5.14 Caltech-II compared to TPC particle flow data from ref. [63].

$E_{CM} = 5$ GeV; Caltech-I's sensitivity to gluon radiation (the splitting of soft gluons) caused there to be more clusters than necessary, once gluon radiation began to appear. In addition, by allowing baryon creation during string evolution, an abrupt drop in $\langle N(p + \bar{p}) \rangle$ for $E_{CM} = 10$ GeV in Caltech-I has been avoided.

A particularly interesting observable that has surfaced in recent years is the number density of particles in the event plane for 3-jet events [59,60,61,62,63,64], suggesting asymmetries in hadronization attributable to string-like phenomena. The results of Caltech-II are compared with TPC data in fig. 5.14. The event sample in fig. 5.14 was selected according to the procedure outlined in refs. [62,63] using a jet finding algorithm based on ref. [91]. The sample consists of relatively planar events in which three jets are discernible (for TPC, a "jet" must contain at least two particles and have a total momentum of 1.5 GeV). The resulting jets are ordered in energy under the hypothesis that the two most energetic jets originate from quarks, while the least energetic jet is induced by a gluon. The particle density is a function of the angle ϕ measured in the event plane where the most energetic (quark) jet

defines $\phi = 0°$. The direction of increasing ϕ is defined so that the next most energetic (antiquark) jet occurs at $\phi \approx 150°$ and the least energetic (gluon) jet is at $\phi \approx 230°$. With this identification of jets with partons, the relative depletion of particles in the "valley" between the quark and antiquark jets corresponds to the absence of a flux tube connecting the quark and antiquark. Since the flux tube connecting the quark to the gluon and the flux tube connecting the gluon to the antiquark are boosted relative to the overall CM frame, the hadrons into which they condense will also generally travel in the direction of the respective boosts.

Caltech-II is able to reproduce the measured particle flow data in fig. 5.14, whereas Caltech-I severely overestimated the number of particles between the quark and antiquark jets [61,92]. The sample in the right panel of fig. 5.14 consists of particles with large components of momentum out of the event plane. The slightly larger depletion effect for such a sample is a consequence of the momentum out of the event plane robbing from the momentum in the event plane where momenta are measured in the CM frame of the parent cluster. When one boosts from the cluster rest frame to the overall event CM frame, there is a smaller probability that such particles will have enough momentum to overcome the boost and leak into the region between the quark and the antiquark jet.

Both the LUND and Webber models are able to reproduce the so-called string effect while, not surprisingly, independent fragmentation models cannot. Though the Webber model is in many ways similar to the original Caltech-I model, it incorporates coherence effects in its LLA QCD shower algorithms. The JADE group has claimed [61] that these coherence effects are responsible for the success of Webber's description of particle flow. Surprisingly, while Caltech-II incorporates both strings *and* coherence, it is found that switching off coherence has a negligible effect on the particle flow of fig. 5.14. This may be indicative of something more than coherence at work in the Webber model.

TPC Proton Correlations
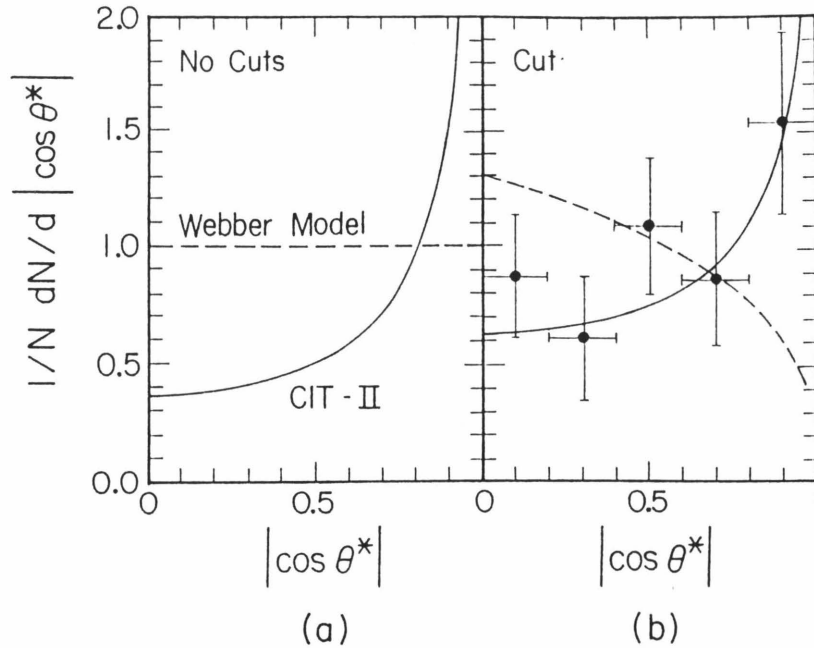
Figure 5.15 Distribution in the correlation angle of proton momentum from $p\bar{p}$ pairs with sphericity axis for Caltech-II and Webber models (a) before and (b) after experimental cuts described in the text. Data are from refs. [89,90].

Correlations in proton-antiproton production are another area in which full string motion benefits Caltech-II. The TPC collaboration has measured [89,90] the distribution of protons (in events with $p\bar{p}$ pairs) with respect to $|\cos\theta^*|$ where θ^*, measured in the $p\bar{p}$ rest frame, is the angle the proton three-momentum makes with the sphericity axis. If $p\bar{p}$ production is entirely due to isotropic cluster decay, as in the Webber model [10], a flat distribution in $|\cos\theta^*|$ is expected, as shown in fig. 5.15a. However, if one allows $p\bar{p}$ production from strings, as in Caltech-II, there is a strong correlation between the proton momentum and the sphericity axis (see fig. 5.15a). Fig. 5.15b compares Caltech-II and the Webber model with the TPC results, which include the experimental cuts of

$$0.5\,\text{GeV} \le p \le 1.5\,\text{GeV} \tag{5.21}$$

on the momenta of the proton and antiproton.

Table 5.2 Parton, cluster and hadron multiplicities for coherent and incoherent showers at various CM energies. Parameters are as in eqs. (5.3-5.7). All calculations are for $N_f = 5$.

E_{CM} (Gev)	14	14	34	34	100	100
Shower type	Coher.	Incoh.	Coher.	Incoh.	Coher.	Incoh.
$\langle N(\text{partons})\rangle$	4.45	4.56	6.29	6.75	9.20	10.46
$\langle N(\text{strings})\rangle$	1.23	1.22	1.45	1.45	1.79	1.79
$\langle N(\text{clusters})\rangle$	3.03	3.02	4.90	5.00	8.27	8.77
$\langle N(\text{Cl} = \text{H})\rangle$	0.56	0.55	1.05	1.06	2.16	2.15
$\langle N(\text{primary hadrons})\rangle$	8.90	8.91	14.00	14.34	22.46	23.87
$\langle N_{\text{tot}}\rangle$	14.85	14.88	21.84	22.30	33.13	34.96
$\langle N_{\text{ch}}\rangle$	9.18	9.19	13.48	13.76	20.59	21.67
$\langle W_{\text{Cl}} - W_{\text{th}}\rangle$ (GeV)	1.54	1.54	1.51	1.52	1.44	1.47

We end this section by noting some general features of parton and cluster final states in Caltech-II at different CM energies (see table 5.2). The entries in table 5.2 are, from top to bottom, (i) the number of final partons generated in the LLA QCD phase; (ii) the number of multiparton strings associated with the final partons; (iii) the number of final clusters from string evolution; (iv) the number of final clusters identified with single hadrons; (v) the number of primary hadrons from cluster decay; (vi) the total number of final state particles (treating π^0 as a stable hadron) (vii) the total charge multiplicity; and (viii) the average cluster mass relative to the appropriate two-particle threshold (averaged only over multihadron clusters).

One of the first things we notice in table 5.2 is that coherence effects in the shower evolution grow with E_{CM} but are generally rather small. The mean multiplicities are marginally smaller for coherent showers than for incoherent showers because the requirement of angle ordering inhibits wide-angle parton branchings. A more important feature of table 5.2 is that the average number of strings and clusters is rather small compared to the final state particle multiplicity. We should be encouraged by this aspect of the model since our original intention was to relegate the details of hadronization to the parameterized decays of low-mass clusters. We have

successfully avoided the specter of letting the semiclassical string evolution dominate the details of hadronization. Furthermore, we note that only a few percent of the primary hadrons come directly from strings (that is, through the $W_{\min}$ mechanism). This is reassuring in light of the *ad hoc* nature of $W_{\min}$.

5.5 Discussion

The success of Caltech-II as a model of hadronization over the *entire* energy range $3\,\mathrm{GeV} \leq E_{\mathrm{CM}} \leq 45\,\mathrm{GeV}$ is, to date, unparalleled. However, Caltech-II's conceptual simplicity can be viewed both to its credit and discredit. We have shown how, with very conservative assumptions about string dynamics and cluster decay, Caltech-II can reproduce most e^+e^- data to within 5-10%. Yet, in the course of comparisons with data, we have isolated areas for improvement in all three stages of the model. In this section we briefly discuss how some specific changes should improve the model as a whole.

The first area for improvement is the incorporation of $\mathrm{O}(\alpha_s^2)$ corrections in the LLA QCD shower formalism. As was mentioned in sect. 5.4, including quantum correlations between the decay planes of virtual partons leads to a suppression of high aplanarity four-jet events. There is also evidence [3] that the cluster decays currently used by Caltech-II may be too local and may give rise to particles within a narrow rapidity interval. If this is indeed the case, the solution may be as simple as reassessing the choice of parameters in the low-mass cluster decay (see appendix B) or may involve adopting a new form for the density of cluster states. However, before we consider changing the cluster decay parameterization, we should consider the possibility that we are turning on cluster decays too early in event evolution.

A potentially interesting and conceptually necessary modification to the Artru-Mennessier string in Caltech-II is the incorporation of transverse momentum at the sites of string breaks. While the transition from the perturbative stage of eq. (5.1)

to the string stage is continuous, the transition between strings and clusters has an inherent discontinuity. Consider the case of a simple $q\bar{q}$ system that has ample energy to evolve using the string model. As the original parent fragments, none of the daughter strings attain transverse momentum — the transverse momenta of final state particles are due solely to the parameterized decays of low-mass clusters.

As will be pointed out in the next chapter, when the transition from strings to clusters is made, information on the "preferred axis" of the string is lost, since low-mass clusters are forced to decay isotropically. Though the the standard value of $W_{\mathrm{max}} = 2.2\,\mathrm{GeV}$ was mandated by transverse momentum considerations, we shall show that this value results in cluster decays causing an oversoftening of the momentum spectrum of heavy quarks. These symptoms suggest that we should try to preserve the directionality of string decays by letting strings evolve to even lower mass scales before hadronizing them with the parameterized cluster decay package. Since correspondingly less transverse momentum will be introduced in the parameterized decays, we should introduce transverse momentum at each string break.

Strictly speaking, the introduction of transverse momentum at each string break is required from quantum mechanics. The small transverse dimensions of flux tubes (O(.1) fm from lattice studies) suggest, through the uncertainty principle, transverse momentum fluctuations of O(1) GeV. Toy models of 1+1 dimensional field theory [93] suggest a Gaussian distribution for locally compensated transverse momentum, as is used by both LUND and independent fragmentation models. While the introduction of transverse momentum to the Artru-Mennessier string in Caltech-II may introduce an additional parameter, the basic philosophy of the model, not to attempt to describe the intricacies of hadronization, will be preserved.

5.6 Summary

In this chapter we have demonstrated how the dynamics of Caltech-II, the dynamics of cluster formation, is controlled by only five parameters. We have selected values for these parameters and have shown how the model provides an adequate description of e^+e^- data over the entire energy range $3\,\mathrm{GeV} \leq E_{\mathrm{CM}} \leq 45\,\mathrm{GeV}$. We have pointed out that the introduction of transverse momentum in string evolution is conceptually necessary and may be required to achieve even better agreement with the data.

Chapter 6

Heavy Quark Fragmentation

6.1   Introduction

Besides the qualitatively different starting points of Caltech-II and LUND, are there measurable quantitative differences between the models? The short answer is "yes." Since LUND asks its formalism to make a direct connection between particles and strings, it cannot distinguish the "simple" physics of the string from the "complicated" physics of low-mass hadronization. LUND's "package deal" comes at the expense of predicative power at mass scales other than that at which the model is tuned.

In this chapter we demonstrate how strings in Caltech-II differ from LUND strings in their predictions for the fragmentation function of heavy quarks ($m_Q \gtrsim 5$ GeV). We look at the Artru-Mennessier strings in Caltech-II in two complementary ways. First, by artificially suppressing low-mass cluster decay in Caltech-II, we demonstrate how better agreement with measured fragmentation functions, $D(z)$, may be obtained. Next, we develop analytical results for $D(z)$ for Artru-Mennessier strings (without gluon radiation). The analytical method provides an independent check on strings in Caltech-II (without gluon radiation or cluster decay) and presents a more efficient way of predicting fragmentation functions for very heavy quarks ($m_Q \geq 20\,\text{GeV}$). Using the analytic results, we show how strings in Caltech-II,

unlike LUND, exhibit the limiting behavior expected of heavy quark fragmentation [7,8].

6.2 The Problem

Heavy hadrons are useful probes of hadronization since they contain quarks that most likely originate directly from the $\gamma^* \to q\bar{q}$ vertex in e^+e^- annihilation. Quantities that can tell us something about the hadronization process are the fractions of the available energy or momentum a heavy hadron carries off

$$x_E = \frac{E}{E_{\text{max}}}, \qquad x_p = \frac{|p|}{p_{\text{max}}}. \tag{6.1}$$

The denominators in these expressions correspond to the maximum energy and momentum a particle can carry away from an interaction while preserving global energy-momentum, flavor, etc. The variables in eq. (6.1) are the convenient experimentally measurable versions of the Lorentz invariant scaled rapidity difference

$$z = e^{y - y_{\text{max}}}, \tag{6.2}$$

where

$$y = \frac{1}{2} \ln \left[\frac{E + p}{E - p} \right] \tag{6.3}$$

is the rapidity of an object with energy E, momentum p, mass M and y_{max} is the maximum possible rapidity for such an object originating from a parent of mass $\sqrt{s}$. In the parent CM frame

$$e^{-y^*_{\text{max}}} = \frac{\dfrac{2M}{\sqrt{s}}}{1 + \dfrac{M^2}{s} - \dfrac{m^2_{\text{recoil}}}{s} + \lambda^{1/2} \left(1, \dfrac{M^2}{s}, \dfrac{m^2_{\text{recoil}}}{s} \right)}, \tag{6.4}$$

where m_{recoil} is the minimum recoil mass. The variables x_E and x_p are identical to z in the limit that they are measured in an infinite momentum frame.

The peaking of the z distribution $D(z)$ of heavy hadrons towards large z is anticipated from essentially kinematical arguments [7,8] — tacitly using the assumption
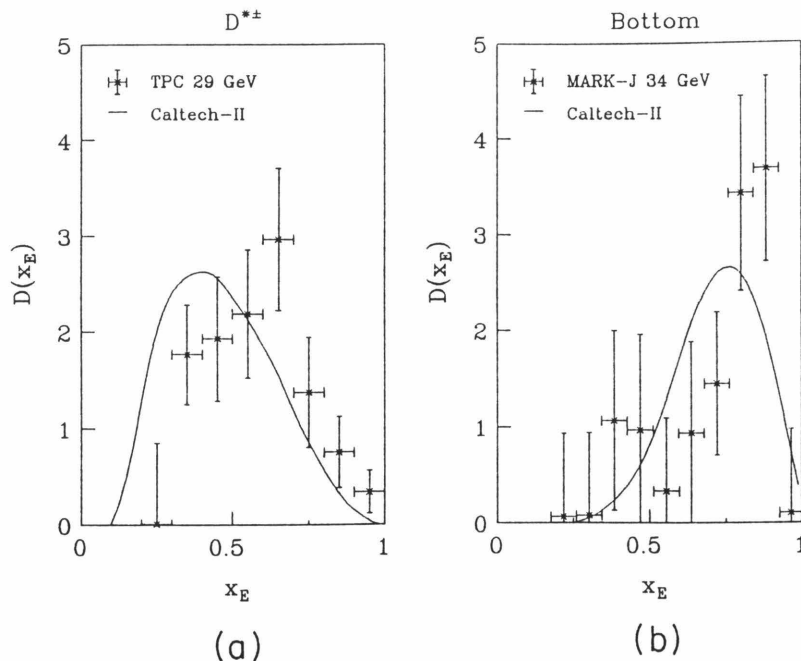
Figure 6.1 Caltech-II fragmentation functions for (a) charm (from reconstructed $D^{*\pm}$ data) and (b) bottom (from inclusive muon data). Data are from refs. [94,95].

that QCD is "flavor-blind." Available data make it plausible to investigate the detailed shape of $D(z)$. The predictions of Caltech-II are compared with 29 GeV charm data [94] in fig. 6.1a and 34 GeV bottom data [95] in fig. 6.1b. An immediate observation is that the full hadronization model predictions are consistently softer than the data. A close analysis reveals that the discrepancies in figs. 6.1a,b are due to a discontinuity in the transition from string fragmentation to cluster hadronization. As implemented in Caltech-II, string decays are always along the string axis, while the parameterized decays of low-mass clusters are isotropic. As discussed at the end of the previous chapter, incorporating transverse momentum at each string break will allow us to retain more of the directionality implied by the strings and permit us to evolve strings down to even lower mass scales before resorting to the parameterized cluster decay.

In this chapter we consider two approaches to the heavy quark fragmentation function, using the Artru-Mennessier string. After presenting the results of a modi-
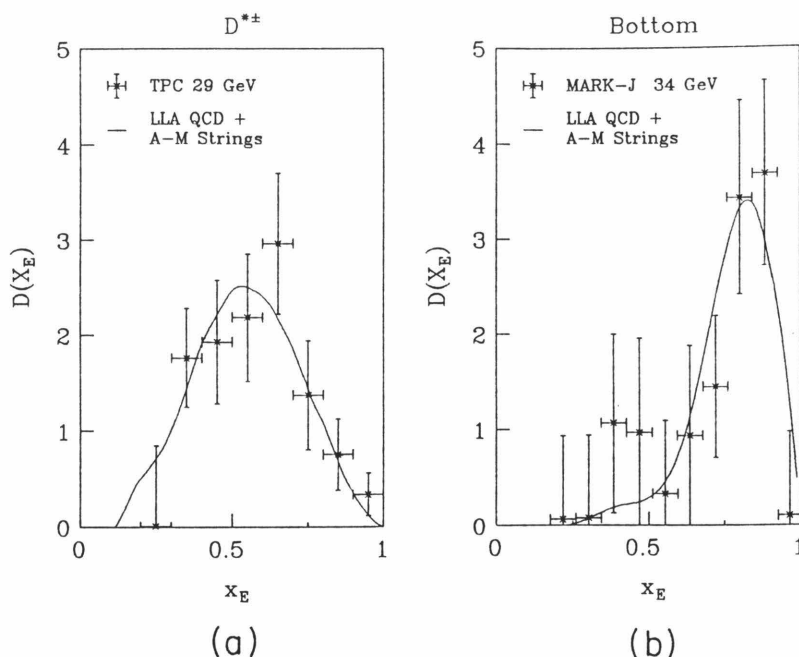
Figure 6.2 Results of Artru-Mennessier strings in Caltech-II (LLA QCD and no cluster decay) compared with (a) charm data and (b) bottom data. Data are from refs. [94,95].

fied Caltech-II model, which bypasses the need for low-mass parameterizations (and hence is applicable only for very specific observables), we develop the analytical results for heavy quark fragmentation according to the area decay law. The analytical results are valuable because they are completely separate from the full Caltech-II model and provide an independent check of iterative string decays.

Since we are interested in the inclusive z distribution of heavy hadrons, we can modify Caltech-II by evolving only the strings containing the original heavy quarks (i.e., leading strings). In doing so, we take the heavy quark mass to be the heavy meson mass and asymptotically identify the leading string with a heavy meson. Figs. 6.2a,b compare data to the results of these modifications. We have used standard parameters except that we have effectively set $W_{max} = 0$ and $m_Q = m_{meson}$ and have allowed only massless quarks to be pulled from the vacuum. The strings are allowed to fragment to within 1% of the final meson mass. It should be noted that the charm prediction (but not the data) in fig. 6.2a omits contributions from

bottom decays that would tend to populate the low x region but not otherwise alter the results. Using the successes of figs. 6.2a,b as an impetus, we will derive more clearly the Caltech-II string predictions for heavy quark fragmentation.

Aside from running the complete Monte Carlo without parameterized low-mass cluster decay and *a posteriori* isolating the leading strings, we would like to investigate the analytical form for the fragmentation function for heavy quarks. An analytical form is valuable since it lends insight to some of the mechanisms at work in string fragmentation. The remainder of this chapter outlines such a framework for the string evolution of heavy quark systems and compares the results with data and the predictions of other models.

6.3 Outline

To arrive at a final fragmentation function $D(z)$, we will have to piece together a few less ambitious components. We begin by considering a $Q\bar{Q}$ system in which the heavy quark Q initially travels along the $+x$ axis in the parent CM frame. The effects of QCD radiation are neglected as a simplifying approximation. After determining an efficient method for sampling the area used in the area decay law (sect. 6.4), we fragment the system by pulling a massless quark pair from the vacuum during the first half-cycle of string motion. Our first result (sect. 6.5) will be a form for $f_+^o(z, M^2, s)$, the probability density for producing, in the first half-cycle of string motion, a leading string with scaling variable z and mass-squared M^2. We will explain the notation as it is encountered.

The new aspect of this work is the construction of $D(z)$ from $f_+^o(z, M^2, s)$. Using $f_+^o(z, M^2, s)$, we construct $f_-^o(z, M^2, s)$ (sect. 6.6), the analogous function corresponding to the situation in which Q initially travels along the $-x$ axis. We then combine these two functions to construct $f_+(z, M^2, s)$, the first generation fragmentation function for breaks occurring anywhere on the world sheet of the $Q\bar{Q}$ system,

assuming that Q initially moves in the $+x$ direction in the parent CM frame. Setting up a framework to account for the iterative structure of the fragmentation process then allows us to derive a recursion relation for $D(z)$ (sect. 6.7), which is evaluated using elementary Monte Carlo techniques that are completely separate from the full Caltech-II model. In sect. 6.8 we discuss the implications of strings, as implemented in Caltech-II, for the fragmentation functions of very heavy quarks and we show how the predictions agree with the qualitative arguments of Bjorken [7] and Suzuki [8].

6.4   Isolation of Leading Strings

To get an analytical form for the fragmentation function, we must focus our attention on isolating the leading string from all the others produced during fragmentation. We shall often refer to stages of string fragmentation by using the concept of a "generation," which we now define. Consider the multibody decay chain of a object X

$$
\begin{array}{ccccc}
X & \to & Y_1 & Y_2 & Y_3 \\
 & & & \hookrightarrow Z_1 & Z_2
\end{array}
\quad . \tag{6.5}
$$

We refer to Y_1, Y_2 and Y_3 as first generation decay products and to Z_1 and Z_2 as second generation decay products. If we think of X as a string, as in fig. 6.3, the quality that characterizes the generation number of a string is the number of string breaks in its absolute past. First generation *leading* strings (Y_1, Y_3) have only one break in their absolute past (the one at which they were created), second generation leading strings (Z_1, Z_2) two breaks, and so on. The first generation *nonleading* string Y_2 contains two breaks in its absolute past since both its valence quarks were pulled from the vacuum separately. Since our interest here is in following the development of the leading string, it is to our advantage to concentrate on the production of the first generation string which contains the heavy quark Q. We accomplish this by going back to the basic area decay law and optimizing the way in which area
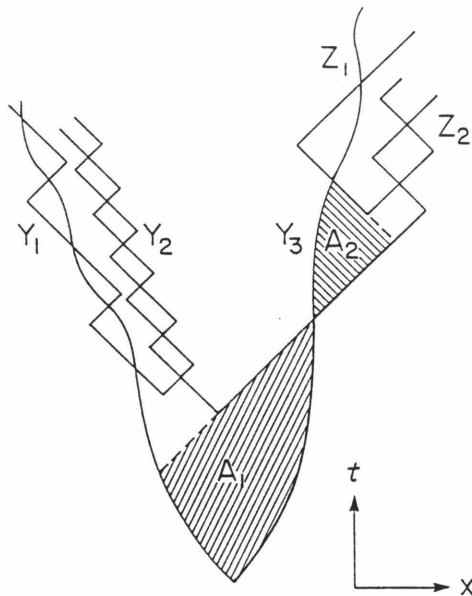
Figure 6.3 Multiple generations of leading and nonleading strings are possible with the Artru-Mennessier decay ansatz.

elements are considered as candidates for a break.

The area decay law leads to a Poisson process in which the probability of the first break occurring after invariant area A has been swept out is given by

$$dP_{\text{break}}(A) = \mathbf{P}_0 e^{-\mathbf{P}_0 A} dA. \tag{6.6}$$

The most efficient way to generate a first generation leading string is to take A in eq. (6.6) to be the invariant area bounded by the edges of the world sheet and the backwards light-cone of the heavy quark. Referring once more to fig. 6.3, we generate A_1 according to eq. (6.6), which defines a lightlike line along which a break is chosen uniformly. Iterating the process, we generate A_2 as indicated, being careful not to double count any area. During each iteration we retain only the leading string and thus accomplish our goal of isolation.

6.5 Derivation of $f_+^o(z, M^2, s)$

Having noted the iterative structure of fragmentation, we need only calculate the fragmentation function for a first generation string $f_+(z, M^2, s)$. $f_+(z, M^2, s)$ is

the probability density for producing a first generation leading string with scaling variable z and mass M from a parent string of mass $\sqrt{s}$, given that the heavy quark initially travels along the $+x$ axis in the parent CM frame (hence the subscript $+$). Before finding $f_+(z, M^2, s)$, we define the first generation fragmentation function $f_+^o(z, M^2, s)$, which is the probability density for producing a first generation leading string *in the first half-cycle* with scaling variable z and mass M from a parent string of mass $\sqrt{s}$, given that the leading quark Q initially travels in the $+x$ direction. We shall refer to the first, third, fifth, etc. half-cycles as odd half-cycles and to the remainder as even half-cycles, denoting them by the superscripts o and e, respectively. If $A_{1/2}$ is the invariant area of one half-cycle of the world sheet, we define $f_+^o(z, M^2, s)$ through the relation

$$dP_{\text{break}}(A) \equiv f_+^o(z, M^2, s)\, dz dM^2, \qquad 0 \le A \le A_{1/2}. \qquad (6.7)$$

Comparing this to eq. (6.6) and letting $|J|$ be the absolute value of the Jacobian of the transformation between A and (z, M^2) gives

$$f_+^o(z, M^2, s) \;=\; \mathbf{P}_0 |J| e^{-\mathbf{P}_0 A(z, M^2)}, \qquad 0 \le A \le A_{1/2}. \qquad (6.8)$$

It is clear that the problem is reduced to finding an expression for $A(z, M^2)$.

We shall sketch the derivation of $A(z, M^2)$ for a $Q\bar{Q}$ pair of massive quarks assuming that Q initially travels along the $+x$ axis in the parent CM frame. In $1+1$ dimensions, a linear confining potential gives the equation of motion during the first half-cycle

$$\frac{dp}{dt} = \mp \kappa, \qquad (6.9)$$

where κ is the string tension. We adopt the convention that the upper (lower) sign refers to the Q ($\bar{Q}$). Solving this relativistic equation gives the world lines

$$\kappa x = \pm \left(E_0 - \sqrt{(p_0 \mp \kappa t)^2 + m_Q^2} \right), \qquad (6.10)$$
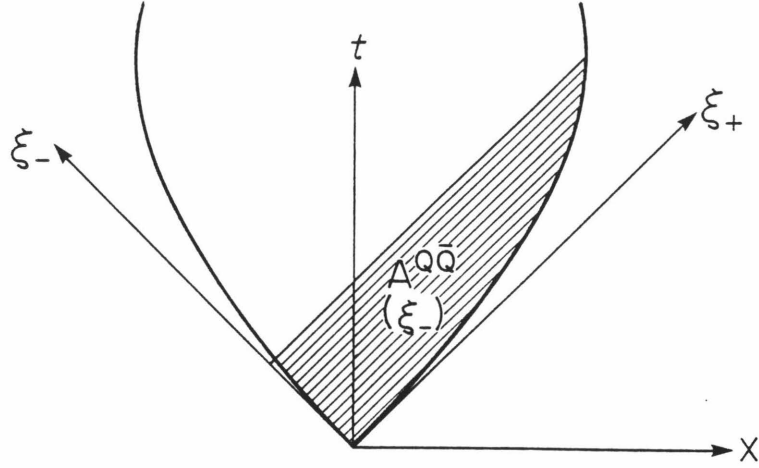
Figure 6.4 Light-cone frame (ξ_+, ξ_-) defines bounded area as a function of ξ_-.

where E_0 and $p_0 = \pm\sqrt{E_0^2 - m_Q^2}$ are the initial energy and momenta of the quarks.

Since one of the boundaries defining A is a lightlike line, it is convenient to work in a light-cone frame defined by

$$\xi_\pm = \sqrt{\frac{1}{2}}(t \pm x), \tag{6.11}$$

as depicted in fig. 6.4. In this frame, the world lines of the quarks have the representation

$$\xi_+ = \frac{m_Q^2}{2\kappa p_{0-}} \left[\frac{\kappa \xi_-/p_{0-}}{1 \pm \kappa \xi_-/p_{0-}} \right], \tag{6.12}$$

where $p_{0\pm} = \sqrt{\frac{1}{2}}(E_0 \pm p_0)$, in analogy to eq. (6.11).

The bounded invariant area is given by

$$A^{Q\bar{Q}}(\xi_-) = \int_0^{\xi_-} d\xi_- \left[\xi_{Q+} - \xi_{\bar{Q}+} \right], \qquad 0 \le A \le A_{1/2}. \tag{6.13}$$

Substituting eqs. (6.12) into eq. (6.13) gives

$$A^{Q\bar{Q}}(\xi^-) = \frac{m_Q^2}{2\kappa^2} \left[\kappa \xi_- \left(\frac{1}{p_{Q0-}} + \frac{1}{p_{\bar{Q}0-}} \right) + \ln \left(\frac{1 - \kappa \xi_-/p_{\bar{Q}0-}}{1 + \kappa \xi_-/p_{Q0-}} \right) \right]. \tag{6.14}$$

In order to express ξ_- in terms of z and M^2, we first rewrite the rapidity of eq. (6.3) in the two equivalent forms

$$E - p = M e^{-y}, \tag{6.15}$$

$$E + p = M e^{+y}, \tag{6.16}$$

where E and p are the daughter's energy and momentum. If we let (x, t) be the coordinates of a break in the string CM frame corresponding to the light-cone coordinates (ξ_+, ξ_-), the energy and momentum of the leading string are, using eq. (6.10),

$$E = E_{Q0} - \kappa x, \tag{6.17}$$

$$p = p_{Q0} - \kappa t. \tag{6.18}$$

Substituting these results into eqs. (6.15,6.16), recalling that $z = e^{y - y^*_{\max}}$, we obtain the transformation equations relating (ξ_+, ξ_-) to (z, M)

$$\kappa \xi_- = + \frac{M}{\sqrt{2}} \frac{e^{-y^*_{\max}}}{z} + p_{Q0-}, \tag{6.19}$$

$$\kappa \xi_+ = - \frac{M}{\sqrt{2}} \frac{z}{e^{-y^*_{\max}}} - p_{Q0+}. \tag{6.20}$$

In these expressions $e^{-y^*_{\max}}$ is given by eq. (6.4) with $m_{\text{recoil}} = m_Q$.

Substituting eq. (6.19) into the expression for the area, eq. (6.14), and expressing everything in terms of parent string CM quantities, we get

$$A^{Q\bar{Q}}(z, M^2) = \frac{m_Q^2}{2\kappa^2} \left[\frac{M\sqrt{s}}{m_Q^2} \frac{e^{-y^*_{\max}}}{z} + \ln\left(\frac{m_Q^2}{M\sqrt{s}} \frac{z}{e^{-y^*_{\max}}} - \frac{m_Q^2}{s} \right) \right.$$
$$\left. + 2\ln\left(\frac{\sqrt{s}}{E^* + p^*} \right) - \frac{\sqrt{s}}{E^* + p^*} \right], \tag{6.21}$$

where $p^* = \frac{1}{2}\sqrt{s - 4m_Q^2}$ and $E^* = \sqrt{s}/2$. In the limit $m_Q^2/s \to 0$ with m_Q^2 fixed, we recover Bowler's analogous result [96] for the $Q\bar{q}$ (heavy quark + massless antiquark) system

$$A^{Q\bar{q}}(z, M^2) = \frac{m_Q^2}{2\kappa^2} \left[\frac{M^2}{m_Q^2} \frac{1}{z} - 1 - \ln\left(\frac{M^2}{m_Q^2} \frac{1}{z} \right) \right]. \tag{6.22}$$

Using the transformation equations, eqs. (6.19,6.20), it is a simple matter to show that

$$dA = d\xi_+ d\xi_- = \frac{1}{2\kappa^2 z} dM^2 dz, \tag{6.23}$$

so that eq. (6.8) becomes

$$f_+^o(z, M^2, s) = \frac{\mathbf{P_0}}{2\kappa^2 z} e^{-\mathbf{P_0} A(z,M^2)}, \tag{6.24}$$

where either eq. (6.21) or eq. (6.22) is used, depending on whether the original parent system is $(Q\bar{Q})$ or $(Q\bar{q})$.

6.6 Constructing $f_+(z, M^2, s)$ From $f_+^o(z, M^2, s)$

A string system with invariant mass slightly larger than the sum of the rest masses of the endpoint quarks may go through many half-cycles before breaking since $A_{1/2}$ is small. In this section we demonstrate how one can account for breaks during *any* half-cycle by building up $f_+(z, M^2, s)$ from $f_+^o(z, M^2, s)$. We can take advantage of the periodicity of string motion by calculating the relevant probabilities for the first complete cycle of string motion and then summing over all cycles.

We begin by deriving an expression for $f_-^o(z, M^2, s)$, the probability density for getting a leading string with (z, M^2) during the first half-cycle of string motion that Q initially travels along the $-x$ axis. This is of interest because the world sheet symmetry

$$\left[\begin{array}{c} \text{First 1/2 Cycle Motion} \\ \text{For } \hat{x} \cdot \vec{p}_Q \big|_{t=0} < 0 \end{array} \right] = \left[\begin{array}{c} \text{Second 1/2 Cycle Motion} \\ \text{For } \hat{x} \cdot \vec{p}_Q \big|_{t=0} > 0 \end{array} \right], \tag{6.25}$$

where $\hat{x}$ is the unit vector in the $+x$ direction. It should be obvious that

$$f_-^o(z, M^2, s) = f_+^o(\bar{z}, M^2, s), \tag{6.26}$$

where $\bar{z}$ is the scaling variable measured with respect to the $-x$ axis. The relation connecting z (measured with respect to the $+x$ axis) and $\bar{z}$ is

$$\bar{z} = \frac{e^{-2y_{max}^*}}{z}, \tag{6.27}$$

where $e^{-y^*_{\max}}$ is given by eq. (6.4). Now, since the an area $A_{1/2}$ must be swept out before the second half-cycle begins, the probability of which is $e^{-\mathbf{P}_0 A_{1/2}}$, the probability density for getting a leading string with (z, M^2) during the second half-cycle of motion, given that Q initially travels along the $+x$ axis, is

$$e^{-\mathbf{P}_0 A_{1/2}} f_+^o(z^{-1} e^{-2y^*_{\max}}, M^2, s). \tag{6.28}$$

Adding this to the contribution for the first half-cycle gives

$$f_+^o(z, M^2, s) + e^{-\mathbf{P}_0 A_{1/2}} f_+^o(z^{-1} e^{-2y^*_{\max}}, M^2, s), \tag{6.29}$$

the probability density for getting (z, M^2) during the first complete cycle, given that Q initially travels along the $+x$ axis.

The probability density for the first string break occurring during the nth complete cycle is given by eq. (6.29) times the probability that the world sheet has no breaks in any of the previous cycles. The probability of a string surviving n complete cycles without breaking is $e^{-2n\mathbf{P}_0 A_{1/2}}$, so that summing eq. (6.29) over all cycles is equivalent to multiplying it by the factor

$$\sum_{n=0}^{\infty} e^{-2n\mathbf{P}_0 A_{1/2}} = \frac{1}{1 - e^{-2\mathbf{P}_0 A_{1/2}}}. \tag{6.30}$$

Thus, the complete first generation leading string fragmentation function is

$$f_+(z, M^2, s) = \frac{f_+^o(z, M^2, s) + e^{-\mathbf{P}_0 A_{1/2}} f_+^o(z^{-1} e^{-2y^*_{Max}}, M^2, s)}{1 - e^{-2\mathbf{P}_0 A_{1/2}}}. \tag{6.31}$$

In the limit $\mathbf{P}_0 A_{1/2} \to \infty$, $f_+(z, M^2, s)$ reduces to $f_+^o(z, M^2, s)$.

For the discussion in the next section it will be convenient to discern between breaks that occur in even and odd half-cycles. It is easy to see that we can write eq. (6.31) as a sum

$$f_+(z, M^2, s) = g_+^o(z, M^2, s) + g_+^e(z, M^2, s), \tag{6.32}$$

where

$$g_+^o(z, M^2, s) \;=\; \frac{f_+^o(z, M^2, s)}{1 - e^{-2\mathbf{P}_0 A_{1/2}}}, \tag{6.33}$$

$$g_+^e(z, M^2, s) \;=\; \frac{e^{-\mathbf{P}_0 A_{1/2}} f_+^o(z^{-1} e^{-2y_{\max}^*}, M^2, s)}{1 - e^{-2\mathbf{P}_0 A_{1/2}}}, \tag{6.34}$$

are respectively the total contributions from all odd and even half-cycles. In a similar manner we can decompose $f_-(z, M^2, s)$ as

$$f_-(z, M^2, s) = g_-^o(z, M^2, s) + g_-^e(z, M^2, s), \tag{6.35}$$

where

$$g_-^o(z, M^2, s) \;=\; \frac{f_+^o(z^{-1} e^{-2y_{\max}^*}, M^2, s)}{1 - e^{-2\mathbf{P}_0 A_{1/2}}}, \tag{6.36}$$

$$g_-^e(z, M^2, s) \;=\; \frac{e^{-\mathbf{P}_0 A_{1/2}} f_+^o(z, M^2, s)}{1 - e^{-2\mathbf{P}_0 A_{1/2}}}. \tag{6.37}$$

6.7 Iterating $f_+(z, M^2, s)$

With the first generation fragmentation function for leading strings $f_+(z, M^2, s)$ in hand, we are prepared to iterate the procedure for an infinite number of generations. Suppose the quark Q initially travels in the $+x$ direction in the parent CM frame. If the string breaks during an odd (even) half-cycle, then in the first half-cycle of the daughter's motion, Q will initially be traveling along the $-x$ $(+x)$ in the *daughter's* CM frame. Since it is important to keep track of the initial direction of Q for each generation, we will have to build this feature into an iterative framework.

We should recall that the variable z is a relation between *two* objects. The factor $e^{-y_{\max}}$ in the definition $z = e^{y - y_{\max}}$ is a function of both the daughter mass and some "reference parent" mass (see eq. (6.4)). If we define $z_i(j)$ to be the scaling variable of the ith generation leading string with respect to the jth generation leading string

(where $i \geq j$), it follows that

$$z_i(i-1) = \frac{z_i}{z_{i-1}}, \tag{6.38}$$

where $z_j \equiv z_j(0)$. As an illustration of this point, we will consider a system in the CM frame, where Q initially travels in the $+x$ direction.

Suppose we want the probability density of the first break occurring in an odd half-cycle and the second break in an even half-cycle, giving a second generation leading string with (z_2, s_2). The differential probability of the first break occurring in an odd half-cycle is

$$g_+^o(z_1, s_1, s) \, ds_1 dz_1. \tag{6.39}$$

Similarly, the differential probability that the first generation daughter breaks in an even half-cycle and yields a leading string with $(z_2(1), s_2)$ is

$$g_-^e(z_2(1), s_2, s_1) \, ds_2 dz_2(1) = g_-^e\left(\frac{z_2}{z_1}, s_2, s_1\right) ds_2 \frac{dz_2}{z_1}, \tag{6.40}$$

where we have made use of eq. (6.38). The probability density we seek is thus the product of eqs. (6.39, 6.40) integrated over all possible first generation breaks, divided by $dz_2 ds_2$

$$\int_{m_Q^2}^{s_0} ds_1 \int_{s_1/s_0}^{1} \frac{dz_1}{z_1} g_-^e\left(\frac{z_2}{z_1}, s_2, s_1\right) g_+^o(z_1, s_1, s_0) \, ds_1 dz_1. \tag{6.41}$$

As fig. 6.5 shows, there are three other classes of "histories" by which one can obtain (z_2, s_2) in the second generation. These correspond to the combinations (odd,odd), (even,odd) and (even,even) for the half-cycles in each generation in which the string breaks. In general, there are 2^n paths to the same final state after n generations. Since breaks in even half-cycles are suppressed by a factor of $e^{-P_0 A_{1/2}}$, the most favored path is the one containing breaks in odd half-cycles, exclusively.

We can summarize the possible products of fragmentation functions for two
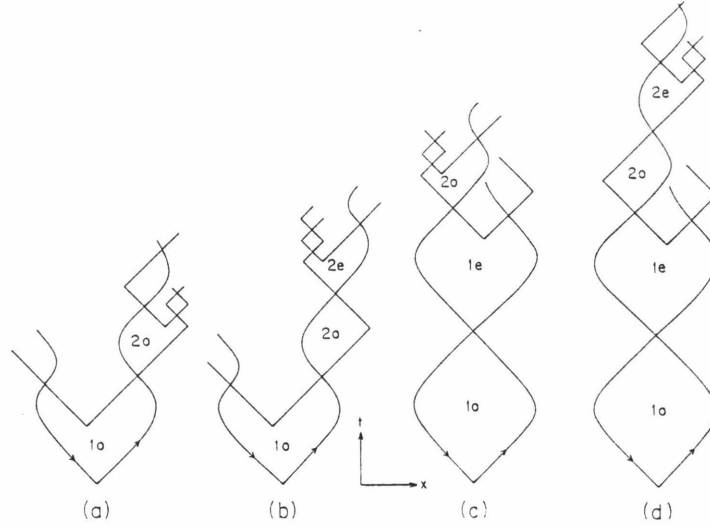
Figure 6.5 Four classes of histories leading to the same inclusive distribution for second generation leading strings

successive generations by noting that:

$$g_+^o\left(z_1, s_1, s_0\right) \quad \text{is followed only by} \quad g_-^o\left(\frac{z_2}{z_1}, s_2, s_1\right) \quad \text{or} \quad g_-^e\left(\frac{z_2}{z_1}, s_2, s_1\right),$$

$$g_+^e\left(z_1, s_1, s_0\right) \quad \text{is followed only by} \quad g_+^o\left(\frac{z_2}{z_1}, s_2, s_1\right) \quad \text{or} \quad g_+^e\left(\frac{z_2}{z_1}, s_2, s_1\right),$$

$$g_-^o\left(z_1, s_1, s_0\right) \quad \text{is followed only by} \quad g_+^o\left(\frac{z_2}{z_1}, s_2, s_1\right) \quad \text{or} \quad g_+^e\left(\frac{z_2}{z_1}, s_2, s_1\right),$$

$$g_-^e\left(z_1, s_1, s_0\right) \quad \text{is followed only by} \quad g_-^o\left(\frac{z_2}{z_1}, s_2, s_1\right) \quad \text{or} \quad g_-^e\left(\frac{z_2}{z_1}, s_2, s_1\right).$$

$$(6.42)$$

We can condense these relations by defining a Green's function

$$
G_2\left(\frac{z_2}{z_1}, s_2, s_1\right)
$$

$$
= \begin{pmatrix}
0 & g_+^o\left(\frac{z_2}{z_1}, s_2, s_1\right) & g_+^o\left(\frac{z_2}{z_1}, s_2, s_1\right) & 0 \\
0 & g_+^e\left(\frac{z_2}{z_1}, s_2, s_1\right) & g_+^e\left(\frac{z_2}{z_1}, s_2, s_1\right) & 0 \\
g_-^o\left(\frac{z_2}{z_1}, s_2, s_1\right) & 0 & 0 & g_-^o\left(\frac{z_2}{z_1}, s_2, s_1\right) \\
g_-^e\left(\frac{z_2}{z_1}, s_2, s_1\right) & 0 & 0 & g_-^e\left(\frac{z_2}{z_1}, s_2, s_1\right)
\end{pmatrix},
$$

$$(6.43)$$

which acts on vector

$$
\Psi_1(z_1, s_1) = \begin{pmatrix}
g_+^o\left(z_1, s_1, s_0\right) \\
g_+^e\left(z_1, s_1, s_0\right) \\
0 \\
0
\end{pmatrix}
$$

$$(6.44)$$

to produce

$$\Psi_2(z_2, s_2) = \int\limits_{m_Q^2}^{s_0} ds_1 \int\limits_{s_1/s_0}^{1} \frac{dz_1}{z_1} G_2\left(\frac{z_2}{z_1}, s_2, s_1\right) \Psi_1(z_1, s_1). \qquad (6.45)$$

The first two components of $\Psi_1(z_1, s_1)$ are, respectively, the probability densities for getting a first generation leading string with (z_1, s_1) in odd and even cycles, given that Q initially travels in the $+x$ direction. The third and fourth components are the corresponding densities when Q initially travels in the $-x$ direction (explicitly zero for the case under consideration). The multiplication $G_2(z_2/z_1, s_2, s_1)\Psi_1(z_1, s_1)$ in eq. (6.45) picks out only the histories allowed by eq. (6.42) and the double integral sums over all possible intermediate states. The components of $\Psi_2(z_2, s_2)$ have an interpretation analogous to those of $\Psi_1(z_1, s_1)$.

It is clear that we can iterate this procedure indefinitely. For example, we have

$$\Psi_3(z_3, s_3) = \int\limits_{m_Q^2}^{s_0} ds_2 \int\limits_{s_2/s_0}^{1} \frac{dz_2}{z_2} G_2\left(\frac{z_3}{z_2}, s_3, s_2\right) \Psi_2(z_2, s_2). \qquad (6.46)$$

By inserting eq. (6.45) into eq. (6.46) we see that we can alternatively define a Green's function, which takes us directly from $\Psi_1(z_1, s_1)$ to $\Psi_3(z_3, s_3)$

$$G_3\left(\frac{z_3}{z_1}, s_3, s_1\right) = \int\limits_{m_Q^2}^{s_0} ds_2 \int\limits_{s_2/s_0}^{1} \frac{dz_2}{z_2} G_2\left(\frac{z_3}{z_2}, s_3, s_2\right) G_2\left(\frac{z_2}{z_1}, s_2, s_1\right), \qquad (6.47)$$

so that

$$\Psi_3(z_3, s_3) = \int\limits_{m_Q^2}^{s_0} ds_1 \int\limits_{s_1/s_0}^{1} \frac{dz_1}{z_1} G_3\left(\frac{z_3}{z_1}, s_3, s_1\right) \Psi_1(z_1, s_1). \qquad (6.48)$$

More generally, we have

$$\Psi_n(z_n, s_n) = \int\limits_{m_Q^2}^{s_0} ds_1 \int\limits_{s_1/s_0}^{1} \frac{dz_1}{z_1} G_n\left(\frac{z_n}{z_{n-1}}, s_n, s_1\right) \Psi_1(z_1, s_1), \qquad (6.49)$$

where

$$G_n\left(\frac{z_n}{z_1}, s_n, s_1\right) = \int\limits_{m_Q^2}^{s_0} ds_{n-1} \int\limits_{s_{n-1}/s_0}^{1} \frac{dz_{n-1}}{z_{n-1}} G_2\left(\frac{z_n}{z_{n-1}}, s_n, s_{n-1}\right) G_{n-1}\left(\frac{z_{n-1}}{z_1}, s_{n-1}, s_1\right).$$

$$(6.50)$$
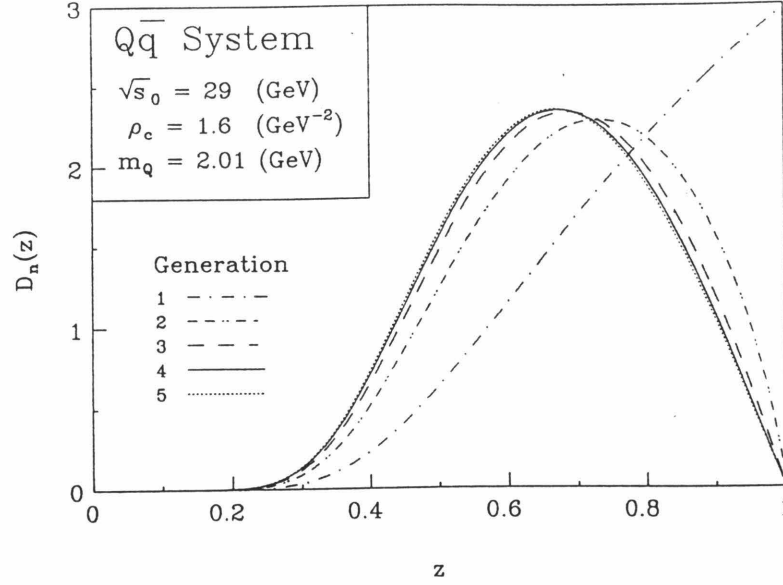
Figure 6.6 Fragmentation function convergence for fixed parameters.

In the limit $n \to \infty$, eq. (6.50) becomes an integral equation for the Green's function between the first generation and "final" generation. In this limit the fragmentation function $D(z)$ is the sum over the four components of $\Psi_n(z_n, s_n)$ integrated over s_n

$$D(z) = \lim_{n \to \infty} \int_{m_Q^2}^{s_0} ds_n \sum_{i=1}^{4} \Psi_n^i(z_n, s_n). \qquad (6.51)$$

In practice, only a few generations need be considered for $D(z)$ to converge. Fig. 6.6 shows the nth generation fragmentation function $D_n(z)$ for $n \leq 5$ for the indicated parameters. Note how the fragmentation function has already converged after five generations. Fig. 6.7 shows the corresponding mass distribution for the leading string after n generations. As expected, the mass distribution tends to a delta function as the number of generations increases.

Fig. 6.8 shows how the final fragmentation function varies with $\rho_c = \mathbf{P}_0/\kappa^2$ for fixed m_Q and s_o. As expected, larger ρ_c gives a harder fragmentation function.
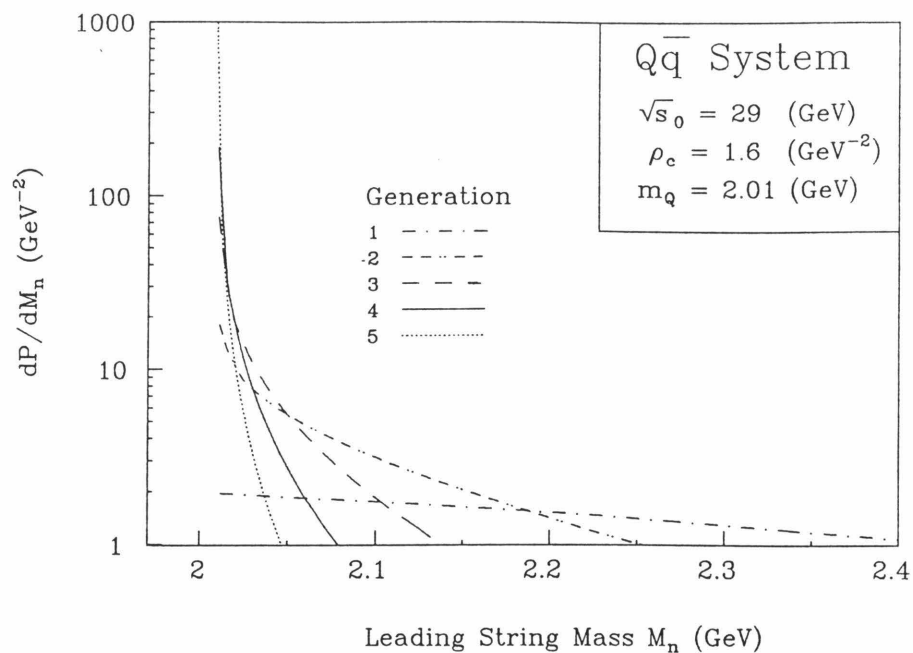
Figure 6.7 Mass distribution of leading string after n generations for the indicated parameters.
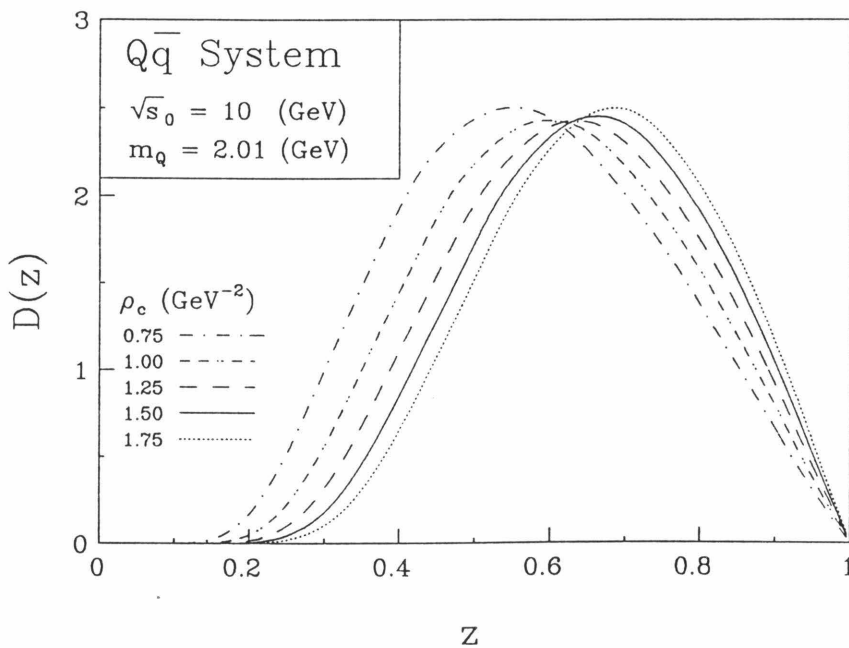
Figure 6.8 Variation of analytic fragmentation function with ρ_c.
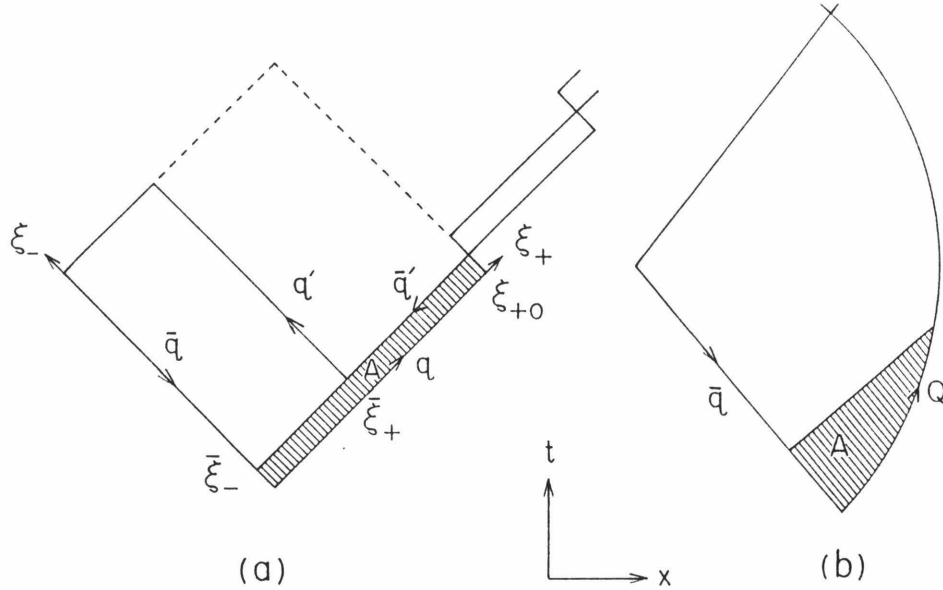
Figure 6.9 Comparison of area decay law for (a) massless and (b) massive quark systems.

6.8   Discussion

It is easy to get an intuitive feel for the fragmentation function in the model described above. For purposes of comparison, consider the fragmentation of a massless $q\bar{q}$ system viewed from its CM frame, as depicted in fig. 6.9a. Suppose the area law dictates that an invariant area A, defined by the lightlike line $\xi_- = \bar{\xi}_-$, is swept out before the first break. Choosing the break uniformly along this boundary, say at $(\bar{\xi}_+, \bar{\xi}_-)$, gives rise to a leading string S($q\bar{q}'$). The momentum of the leading daughter is equal to the momentum of q at the time of the break. Thus, the momentum of S($q\bar{q}'$) decreases linearly as the break point moves along the boundary from $\xi_+ = 0$ until the leading daughter actually moves *backwards* in the CM frame if the break occurs at ξ_{0+}. However, if we replace q with a massive quark Q as in fig. 6.9b, the lightlike boundary defining A intersects the world line of Q before Q changes direction in the CM frame. Since *all* the points along the boundary now correspond to leading daughters with large positive momentum, a hard fragmentation function results.
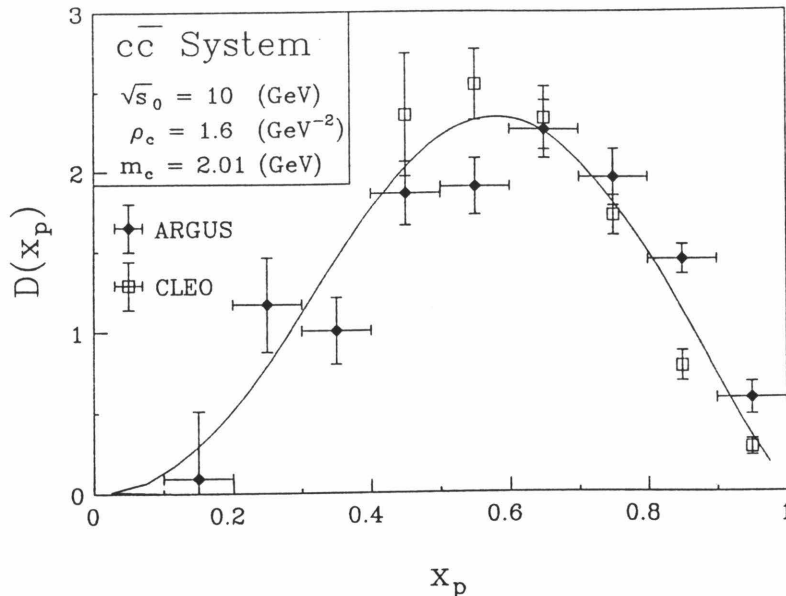
Figure 6.10 String model with Caltech-II LLA QCD compared $D^{*\pm}$ fragmentation functions. Data and model are normalized to 1 for $x_p \geq$ .4. Data are from [97,98].

Now that we have an analytical means of generating fragmentation functions for simple systems, we may ask if we can sensibly compare any results to data — remember, we have neglected gluon radiation. It turns out that we must be wary of comparing our analytical results directly to data. For example, fig. 6.10 compares the "bare" string model in Caltech-II (with LLA QCD but no cluster decay) with charm data from ARGUS and CLEO. The point we wish to make is that the value of $\rho_c = 1.6 \, \text{GeV}^{-2}$ in fig. 6.10 is higher than the value $\rho_c \approx 1 \, \text{GeV}^{-2}$ one would guess from fig. 6.8, which does not include perturbative QCD. The observation is that we must compensate for the softening effects of perturbative QCD by increasing ρ_c [79]. We mention this point because it puts the results of this section in perspective — our analytic results provide a convenient check of the "bare" strings in Caltech-II but must still be tacked on the end of perturbative QCD before quantitative results should be believed. Nevertheless, our analytic results are helpful in exploring the qualitative behavior of fragmentation functions for very heavy quarks. Because Caltech-II simulates heavy quarks by using the veto technique described in sect. 4.5,

the calculation of heavy quark fragmentation functions is prohibitively slow (though precise). The analytic technique developed in this chapter is four to six orders of magnitude faster. In the next section we use the analytic technique to demonstrate the behavior of the Caltech-II string fragmentation function for very heavy quarks.

6.9 Alternative Models; Top Fragmentation (and Beyond)

The availability of data for charm (and now increasingly so for bottom) has inspired many forms for the associated fragmentation functions. Nevertheless, no individual model yet has conspicuously risen above the others in its ability to fit the data. It may require looking towards even heavier quarks to determine the best description. In this section we briefly discuss three alternate pictures: the fragmentation functions of the LUND group [11], Peterson *et al.* [99] and Amiri and Ji [100]. We will show how, compared to other models, the fragmentation function predicted by the Artru-Mennesser string in Caltech-II readily exhibits the limiting behavior for large quark masses outlined by Bjorken [7] and Suzuki [8].

The Peterson fragmentation function is derived from elementary nonrelativistic perturbation theory. In the transition $Q \to H(Q\bar{q})\,q$, where Q is a heavy quark, $q\bar{q}$ are a light quark pair pulled from the vacuum, and $H(Q\bar{q})$ is a heavy meson, the probability of producing H with a fraction z of the Q momentum $p = |\vec{p}|$ is taken to be proportional to $z^{-1}(\Delta E)^{-2}$ where

$$\Delta E = E_Q - E_H - E_q = \sqrt{m_Q^2 + p^2} - \sqrt{m_H + z^2 p^2} - \sqrt{m_q^2 + (1 - z)p^2}. \quad (6.52)$$

Expanding the energies about the particle masses yields

$$f(z) = \frac{N}{z\left[1 - 1/z - \epsilon/(1 - z)\right]^2}, \quad (6.53)$$

where nominally $\epsilon = m_q^2/m_Q^2$ and N is a normalization factor.
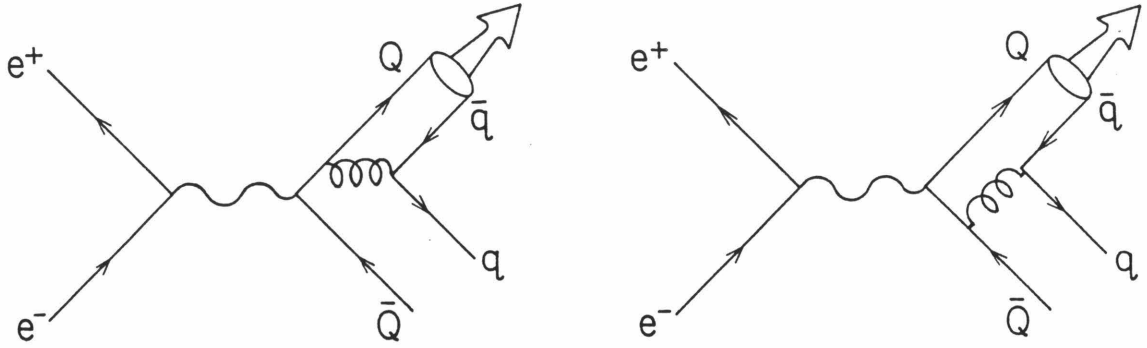
Figure 6.11 Typical diagrams used in ref. [100] to calculate $D(z)$ perturbatively.

The LUND fragmentation function is of the form

$$f(z) = N\frac{(1-z)^a}{z}e^{-bm_T^2/z}, \tag{6.54}$$

where N is a normalization constant, a and b are (possibly flavor-dependent) parameters, and $m_T = \sqrt{m^2 + p_T^2}$ is the transverse mass of the produced hadron. In practice, the possible flavor dependence is neglected and the standard parameters are empirically determined to be $a = 1$ and $b = .7\,\mathrm{GeV}^{-2}$. The form of the LUND fragmentation function is fixed uniquely by the symmetry requirement that in the iterative process,

$$\text{String} \rightarrow \text{String} + \text{Hadron}, \tag{6.55}$$

it should make no difference if particles are peeled off one end of the string or the other.

To obtain predictions that may be compared directly with experiments, the analytic results of this chapter and the LUND and Peterson fragmentation functions should all be imbedded in a framework, which accounts for perturbative QCD. In contrast, Amiri and Ji [100] have perturbatively calculated the z distribution for the inclusive process $e^+e^- \rightarrow \gamma^* \rightarrow H(Q\bar{q})$X, which includes the diagrams shown in fig. 6.11. Assuming a simple nonrelavitistic form for the amplitude of identifying a collinear $Q\bar{q}$ pair with a pseudoscalar meson $H(Q\bar{q})$, the z distribution for the heavy
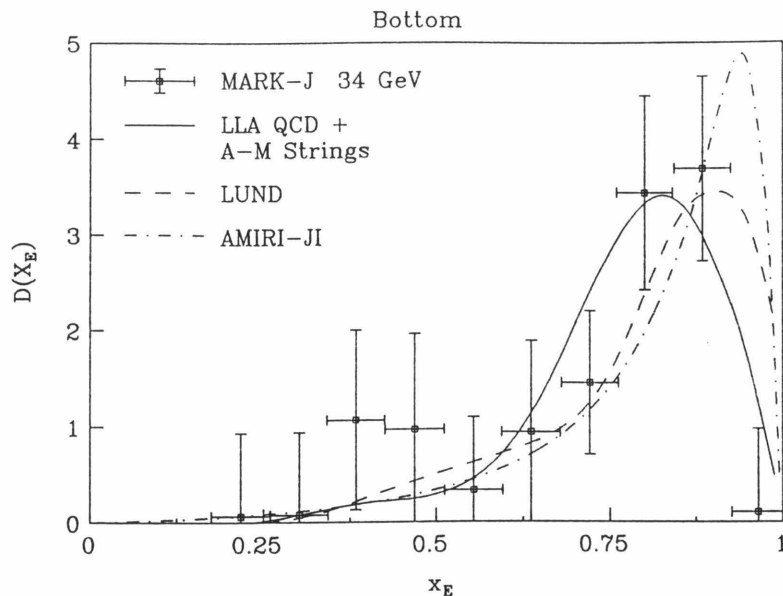
Bottom

Figure 6.12 Different models compared with bottom data from ref. [95].

meson, well above threshold, is

$$D_Q^H(z) = Nz(1-z)\left[\frac{e_Q^2}{(1-r)^2}\frac{[1+(1-r)z]^2}{(1-rz)^4} + \frac{e_q^2}{r^2}\frac{(1+rz)^2}{[1-(1-r)z]^4}\right], \qquad (6.56)$$

where N is a normalization constant, e_Q and e_q are the quark charges and $r = m_Q/(m_Q + m_q)$.

Fig. 6.12 compares the four models with bottom data at 34 GeV. The LUND curve in fig. 6.12 was calculated, using the LUND fragmentation function inside the full LUND Monte Carlo [80]. The Caltech-II curve is the same as that in fig. 6.2 and so includes LLA QCD but no cluster decays. The Amiri-Ji curve is from ref. [100]. A curve using the Peterson function of eq. (6.53) is not shown because it does not include perturbative QCD effects. As we can see, uncertainties in the data prohibit us from making strong statements regarding the most successful model.

Fig. 6.13 compares all four models for top assuming a top quark of mass 40 GeV in e^+e^- annihilation at $E_{\rm CM} = 200\,{\rm GeV}$. The LUND, Peterson and Caltech-II curves are all shown without perturbative QCD (strictly speaking, this isn't valid but we only want qualitative results). The most striking feature of fig. 6.13 is that the LUND function is essentially a delta function compared to the other models.
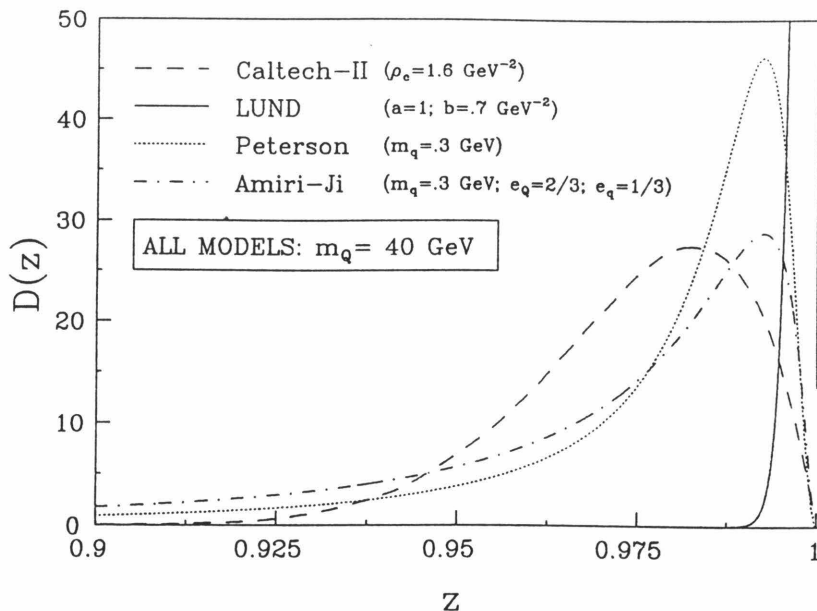
Figure 6.13 Fragmentation functions for top assuming $m_t = 40\,\text{GeV}$ in e^+e^- annihilation at $E_{\text{CM}} = 200\,\text{GeV}$. All curves are normalized to unity. LUND curve reaches a maximum (not shown) of ~ 413 for $z \sim .9991$.

This is not an artifact of leaving out perturbative QCD. This point can be clarified if we look at the behavior of the mean value of z as a function of quark mass.

The various models may be compared with Bjorken's [7] and Suzuki's [8] expectations of average z behaving as $\langle z \rangle = 1 - c/m_Q$, where c is a constant O(1 GeV). Fig. 6.14 plots $(1 - \langle z \rangle)m_Q$ against the heavy quark mass m_Q for the *bare* LUND, Peterson, and Caltech-II functions (i.e., not embedded in QCD), and the Amiri-Ji calculation. The curve corresponding to the Caltech-II string approaches Bjorken's asymptotic form rather quickly, followed later by the Peterson and Amiri-Ji curves. The significant feature is that the LUND curve behaves as $(1 + a)/(bm_Q)$ for large m_Q. Though there is only a hint of the LUND function's being too hard for bottom in fig. 6.12 (the data are not yet compelling), the anomalous LUND effect should be obvious for heavier quarks. The apparent resolution for the LUND model would be the introduction of flavor-dependent parameters a and b in eq. (6.54).
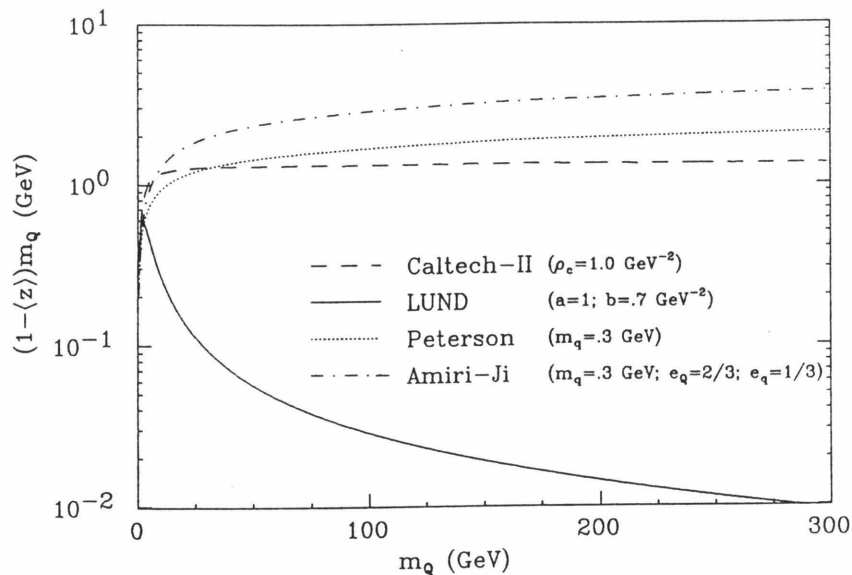
Figure 6.14 Average z behavior as a function of quark mass.

6.10   Summary

In this chapter we have developed analytic results for the Artru-Mennessier string in the Caltech-II model, which gives the fragmentation function for heavy quarks in the limit of no gluon radiation. We have shown that the oversoftening of the momentum spectrum of heavy hadrons in Caltech-II can be alleviated by letting the string phase of the model evolve strings down to smaller mass scales than suggested in earlier chapters. We have also shown how the string model in Caltech-II exhibits the behavior proposed by Bjorken [7] and Suzuki [8], whereas the LUND model does not.

Chapter 7
Conclusions

7.1 Synopsis

In this thesis we have presented the motivation, formalism and results for the full equations of motion of the relativistic string in the Caltech-II model of e^+e^- annihilation and hadronization. We have shown how the full hadronization model, with *fixed* parameters, provides a good description of e^+e^- annihilation data over the entire energy range $3\,\mathrm{GeV} \leq E_{\mathrm{CM}} \leq 45\,\mathrm{GeV}$. We have pointed out the difference between our use of strings and those used in the LUND model. We have shown how the simple string decay ansatz of Caltech-II, unlike LUND, leads to heavy quark fragmentation functions that are in agreement with model-independent expectations.

7.2 Review and Outlook

Caltech-II is a phenomenological model of hadronization which, in attempting to untangle the complexities of hadron formation, factorizes event evolution into three stages:

1. The generation of final state partons using the leading logarithmic approximation to QCD.

2. The mapping of final state partons onto color singlet strings that are evolved according to a simple, covariant ansatz.

3. The decay of low-mass color singlets (clusters) using a parameterization of low-mass data.

This factorization is appealing since it relegates many of the intricacies of hadron production to the parameterized decay of clusters. This permits the rest of the model to focus on the simpler problem of *cluster* formation, not hadron formation. With the low-mass parameterization fixed by low energy data, there are only five adjustable (and correlated) parameters to describe the perturbative QCD and string evolution phases of the model.

The relativistic string is used as a phenomenologically motivated model of color confinement. Using only the gross properties of the semiclassical relativistic string, we map perturbatively generated partons onto color singlet strings, which are subsequently decayed using a generalization of the radioactive decay law for point relativistic particles. The string evolution phase continues until the masses of the daughter strings fall below a cutoff, beyond which we use the parameterized decay of low-mass clusters.

Acknowledging the semiclassical nature of the relativistic string used in this thesis, we have not pressed the string formalism to yield details of hadron formation; we have used only the most generic string-like features. In regard to this point, we have noted that the string phase in Caltech-II should be elaborated to allow transverse momentum at the sites of string breaks. This modification is conceptually necessary since actual QCD flux tubes, which strings are meant to approximate, have transverse dimensions and so, by the uncertainty principle, have transverse fluctuations.

In our comparisons with data we have noted how the string parameter ρ_c and the cutoff W_{max} roughly govern the longitudinal and transverse momentum in an event. By introducing transverse momentum at string breaks, we will be able to let the string phase of the model run longer and hence achieve more continuity between the string and cluster phases.

We have also shown how the Artru-Mennessier string in Caltech-II exhibits the behavior expected of heavy quark fragmentation functions. This development underscores the simplicity of the strings in Caltech-II and contrasts LUND strings, which do not exhibit the expected asymptotic behavior. These points are relevant to the next generation of e^+e^- experiments (TRISTAN, SLC, LEP) and hadronic colliders (TEVATRON, SSC) in which the top quark (or even new generations) may be observed. A firm understanding of hadronization in these energy regimes will allow us to untangle signatures of new physics as well as determine what role hadronic strings play in the hadronization of heavy quarks.

Appendix A

The Leading Logarithm Approximation

In this appendix we briefly discuss the way perturbative QCD is modeled in Caltech-II. In summary, Caltech-II generates multiparton final states by using the leading log approximation (LLA) to QCD supplemented with the constraints of gluon coherence and with the first gluon branching weighted by the exact $O(\alpha_s)$ $e^+e^- \to q\bar{q}g$ matrix element.

In sect. A.1 we introduce the concept of factorization and show how it leads to a classical probabilistic interpretation of perturbative QCD suitable for use in a Monte Carlo format. Sect. A.2 discusses the property of local color screening inherent to the LLA and points out how the independent evolution of partons in the LLA leads to an absence of correlations that are present in fixed order matrix elements. We finish in sect. A.3 by reviewing the incorporation of gluon coherence effects into LLA showers. We point out that coherence effects at $E_{\mathrm{CM}} \leq 40$ are generally masked by other effects in Caltech-II.

A.1 Factorization of Mass Singularities

There are two common approaches to perturbative QCD: fixed order matrix elements and the leading log approximation. While fixed order matrix elements

are "exact" up to a given order of the strong coupling constant α_s, they are prohibitively complicated to calculate beyond the first few orders for multiparton final states because of the of the proliferation of Feynman graphs. There is already evidence suggesting that the state of the art fixed $\mathrm{O}(\alpha_s^2)$ matrix elements for e^+e^- annihilation cannot account for certain features of available data. The MARK-II collaboration has published results [101] which suggest that multiparton final states generated according to the leading logarithm approximation are needed to reproduce the observed softness of gluon jets at $E_{\mathrm{CM}} = 29\,\mathrm{GeV}$.

The leading log approximation to perturbative QCD is capable of generating final states with an arbitrarily large number of partons by summing a perturbative expansion to *all* orders in α_s but keeping only the dominant, so-called leading logarithm, contributions at each order. A bonus is that the LLA approximation is easily expressed in the language of classical probability — ideal for an implementation on a computer.

The approximation hinges on a factorization property [102] of QCD, which exploits the equivalence between, say, a massless quark and collinear quark-gluon pair with the same overall quantum numbers. This factorization property relates an $N + 1$ parton cross section σ_{N+1} to an N parton cross section σ_N

$$d\sigma_{N+1} \rightarrow d\sigma_N \times \left[\frac{\alpha_s(t)}{2\pi} \frac{dt}{t} P_{A \rightarrow BC}(z)\, dz \right], \tag{A.1}$$

in which one of the N partons, labelled A, splits into two partons B and C, where B carries a fraction z of A's energy. In eq. (A.1), t is the square of A's off-shell mass and $P_{A \rightarrow BC}(z)$ is a universal function, known as an Altarelli-Parisi splitting kernel [9], which depends only on the flavor of the partons. In their most basic forms

$$P_{q \rightarrow q\,g}(z) = \frac{4}{3} \left[\frac{1 + z^2}{1 - z} \right], \tag{A.2}$$

$$P_{g \to g\,g}(z) \;=\; 6\left[\frac{(1-z+z^2)^2}{z(1-z)}\right], \tag{A.3}$$

$$P_{g \to q\,\bar{q}}(z) \;=\; N_f\left[\frac{z^2+(1-z)^2}{2}\right], \tag{A.4}$$

where N_f is the number of quark flavors.

The property of factorization may seem fine on the surface, but one may feel uncomfortable about imposing classical probability arguments on quantum phenomena. In the LLA, this is not a problem. The argument goes as follows. Suppose we have to sum and square n Feynman amplitudes $\{A_i,\ i=1,n\}$ in order to calculate a *fixed order* matrix element for $e^+e^- \to$ [partons]. As usual, interference between the various diagrams can be traced to cross terms in the sum

$$\sum_{i,j=1}^{n} A_i^* A_j. \tag{A.5}$$

However, if one works in an axial gauge, it can be shown [102] that the *leading* collinear singularities in eq. (A.5) are contained in the *incoherent* sum

$$\sum_{i=1}^{n} A_i^* A_i. \tag{A.6}$$

Each term $A_i^* A_i$ may then be factorized in manner similar to eq. (A.1).

Strictly speaking, the LLA is exact only in the collinear limit $t \to 0$. The generation of transverse momentum in parton splittings requires $t \neq 0$ and forces a consideration of nonleading terms in perturbative expansions. One way to account partially for this is in the definition of the splitting variable z or the argument of the running coupling constant in eq. (A.1). In Caltech-II, a generic branching of the form

$$q^*(p_1) \to q(p_3) + g(p_4), \tag{A.7}$$

as shown in fig. A.1a, is accomplished with the splitting variable z defined as

$$z \equiv \frac{1}{2}\left[1 - \frac{t}{t_p}\right](1 + \cos\theta^*). \tag{A.8}$$

Parton Branching

CM(I) Frame
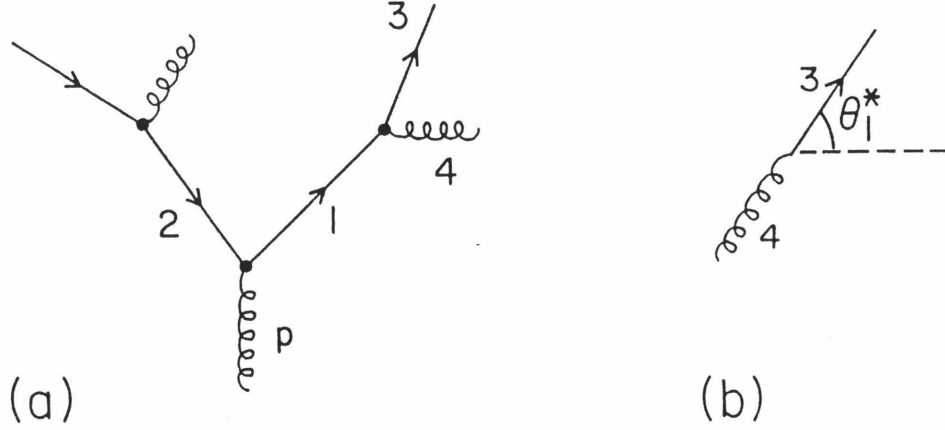
Figure A.1 Kinematics of timelike showers.

In this equation, t and t_p are the squared masses of p_1 and p_1's parent. In the rest frame of p_1, θ^* is the angle between $\vec{p}_3^*$ and a unit vector $\hat{n}$ (the dashed line in fig. A.1b), where a single boost by

$$\gamma = \frac{E_{\text{lab}}(p_1)}{\sqrt{t}} \tag{A.9}$$

along $\hat{n}$ transforms the rest frame of p_1 to the overall lab frame. For the initial $\gamma^* \to q\bar{q}$ vertex, $t_p(q) = t_p(\bar{q}) = Q^2$. Our definition of z differs from that of Odorico [49] and Webber [10] who use, respectively, $\alpha_s[tz(1-z)]$ and $\alpha_s[tz^2(1-z)^2]$ to partially account for the summing of nonleading terms.

In practice, a collection of final state partons is generated as follows. Starting with an off-shell q and $\bar{q}$ generated according to the cross section for $e^+e^- \to q\bar{q}$, we take

$$dP_{\text{radiation}} = \frac{\alpha_s(t)}{2\pi} \frac{dt}{t} P_{q \to qg}(z) \, dz \tag{A.10}$$

to be the probability of a virtual quark with squared mass t emitting a gluon, which carries away a fraction $(1-z)$ of the energy. Blindly generating branchings according to this distribution would result in an infinite number of soft gluons that habitually
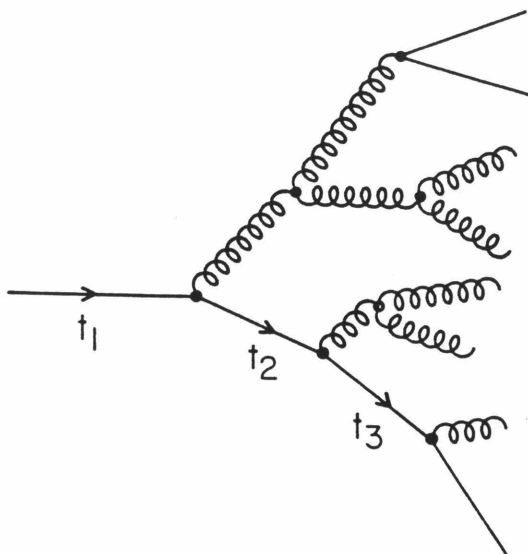
Figure A.2 Treelike structure of a parton shower in LLA QCD.

accompany a quark. We are more interested in those branchings that stick out above the background of soft radiations. By defining a criterion for resolvable radiation, it is possible [69] to sum up the irresolvable splittings and define a function $\Pi(t_i, t_f)$, which gives the probability that a quark of initial virtualness t_i evolves to virtualness t_f before emitting a resolvable gluon.

The basic procedure is to recursively generate *resolvable* splittings according to the distribution $\Pi(t_i, t_f)$ and hence generate a treelike structure or shower as shown in fig. A.2. The virtual masses of partons decrease monotonically as one follows a branch starting from the initial e^+e^- vertex. Perturbative evolution is terminated when a parton's virtuality falls below some cutoff t_0 ($\approx 1-2\,\mathrm{GeV}^2$), at which point it is put on-mass-shell. Below t_0, shower evolution would be expected to generate only irresolvable radiation (irrespective of our wariness concerning the use of perturbative methods at such small mass scales).
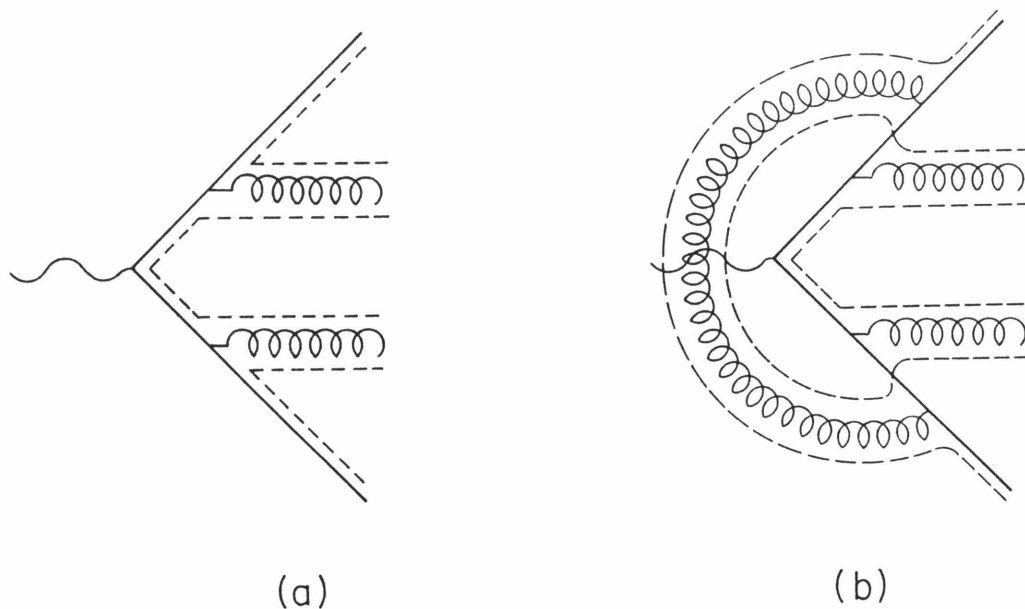
Figure A.3 (a) LLA showers lead to local color compensation whereas (b) nontreelike structure may not.

A.2   Local Color Screening

The treelike structure of LLA showers in fig. A.2 results in what is called planar color flow and preconfinement [9]. This can naively be understood as follows. Because shower development includes only the *splitting* of partons, local color conservation implies that the color charge on a parton is neutralized, or compensated for, by its nearest neighbor in the shower tree, as illustrated in fig. A.3a. This contrasts the nontreelike situation in fig. A.3b, where the added gluon permits color communication between partons, which were color-independent in fig. A.3a.

The implication of planar color flow is the formation of localized colorless objects, which can then be hadronized independently. The Caltech-I [5] and Webber [10] models take an extreme view of localized color screening by insisting that final state gluons split into $q\bar{q}$ pairs, so that there are $N/2$ independent low-mass colorless objects in an N parton (before forced gluon splittings) final state. Alternatively, Caltech-II retains the full color connection information and maps partons onto relativistic strings. In Caltech-II the number of colorless objects is equal to the number

of $q\bar{q}$ pairs that arise naturally in LLA QCD shower evolution.

The independent evolution of partons in a LLA shower can not be completely correct. Total independence implies that there are only kinematic correlations between partons. As is discussed in chapter 5, this can lead to, for example, an overabundance of high aplanarity four-jet events because of a lack of correlation between the decay planes of $q^* \rightarrow q + g$ and $\bar{q}^* \rightarrow \bar{q} + g$. Such correlations are automatically included in fixed-order matrix elements but have to be "put in by hand" in LLA showers. While the shower model in Caltech-II incorporates $O(\alpha_s)$ corrections to ensure the correct distribution of hard gluons in $e^+e^- \rightarrow q\bar{q}g$, it overestimates the number of high aplanarity four-jet events for the above reasons. As discussed in sect. 5.4, the incorporation of $O(\alpha_s^2)$ corrections into the LLA shower formalism for e^+e^- annihilation is a high priority.

A.3 Color Coherence

The inadequacies of the LLA approximation can be traced back, not unexpectedly, to the omission of nonleading contributions. Including an important class of the next-to-leading-logarithm contributions [103] forces us to consider cross terms in eq. (A.5), which lead to interference effects. The net result is destructive interference, which suppresses the emission of wide angle gluon radiation. It has been shown [104,105,106] that this color or gluon coherence effect can be incorporated into LLA showers simply by requiring that the gluon emission angles decrease along any given branch of the shower tree. This angle ordering is illustrated in fig. A.4, where

$$\theta_1 > \theta_2 > \theta_3 \ldots \qquad . \tag{A.11}$$

Though not manifestly covariant, the angle ordering ansatz leads to frame independent results.

Further details of gluon coherence, as incorporated in Caltech-II, may be found
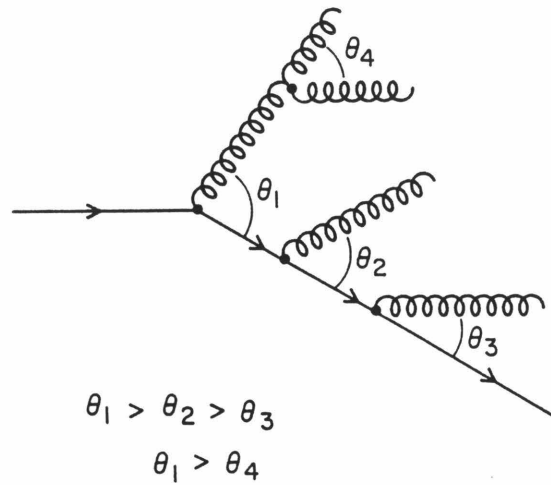
Figure A.4 Angle ordering of successive gluon emissions imposed by color coherence.

in ref. [107]. Refs. [107,108] show how the inclusion of coherence effects correctly reproduces the expected energy dependence of the average hadronic multiplicity of jets, albeit at energies far above those generally considered in this thesis (i.e., for which there are experimental data). The simple incoherent LLA overestimates hadronic multiplicities by a factor of ≈ 2 for $1\,\mathrm{TeV}$ quark jets, whereas for e^+e^- annihilation at $E_{CM} \leq 45\,\mathrm{GeV}$, the effect on multiplicity is generally negligible and can be easily masked by other uncertainties.

Appendix B

Low-Mass Cluster Decay

B.1   Introduction

The decay of low-mass clusters is the final stage in the process of hadronization in Caltech-II. It is the stage in which primary hadrons are produced from objects with mass a few GeV above particle production threshold. Rather than speculate on the nature of the dynamical mechanisms at work in this nonperturbative regime, we instead choose to parameterize the decays of low-mass clusters with a simple model motivated by phase space. In this appendix we discuss the general form of the parameterization used in Caltech-II. Except for a few minor changes, the formalism is identical to that used in Caltech-I, so the following description will closely follow that given in ref. [4].

B.2   Outline Of The Model

A cluster in Caltech-II is completely characterized by its mass W and its flavor. As a matter of convention, we refer to a cluster composed of a quark and an antiquark as a meson cluster and a cluster composed of a quark and a diquark as a baryon cluster. In general, a cluster will decay into two or more primary hadrons. We simulate such decays by a sequence of two-body decays

$$Cl \rightarrow X_1 + H_2, \tag{B.1}$$

MESON PRODUCTION   BARYON PRODUCTION
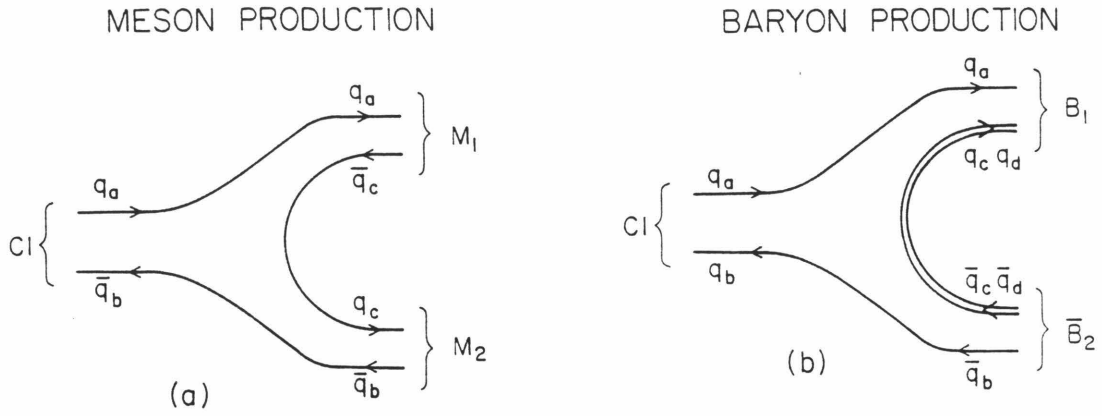
Figure B.1 Meson cluster decays via the creation of (a) quark pair or (b) diquark pair. M_2 and B_2 are on-mass-shell particles, whereas M_1 and B_1 can be either subclusters or on-mass-shell particles.

where X_1 can be either a hadron H_1 or a subcluster Cl_1. The last decay in the sequence is always into two hadrons. We visualize the two-body decay in eq. (B.1) as proceeding through the creation of a quark-antiquark pair or an effective diquark-antidiquark pair as depicted in fig. B.1. In general, the mass spectrum of X_1 consists of both discrete levels, corresponding to hadrons, and a continuum corresponding to subcluster production.

To decay a cluster of mass W and particular valence flavor, we compile a list of relative decay probabilities corresponding to each of the available decay channels and then pick a mode at random. The relative probability of a particular decay mode is taken to be the product of a flavor factor, a spin factor and a kinematic factor

$$P_F \times P_S \times P_K, \tag{B.2}$$

which we now describe.

B.2.1 Flavor Factors

P_F is a flavor factor that accounts for the relative abundances of pair flavors pulled from the vacuum. In the decay of a meson cluster, the quark or diquark content of the pulled pair is chosen from the set

$$\{u, d, s, uu, ud, us, dd, ds, ss\}. \tag{B.3}$$

In the decay of baryon clusters, no diquark pairs are allowed to be pulled from the vacuum. For each flavor pulled from the vacuum, we compile a list of all the exclusive decay modes consistent with the daughters' valence flavors. Each mode is given the appropriate flavor factor according to eq. (B.3). To avoid overcounting, modes in which H_2 has the same spin and valence flavor (eg. $H_2 = \{\pi^0, \eta, \eta'\}$) receive additional weightings (in this case $\{1/2, 1/4, 1/4\}$), which sum to unity. This additional factor is included in P_F where necessary.

B.2.2 Spin Factors

Each of the exclusive decay modes is weighted by a spin multiplicity factor

$$P_S = (2J_1 + 1)(2J_2 + 1), \tag{B.4}$$

determined from the spin of each of the decay products. For modes that have $X_1 = Cl_1$, a meson subcluster is defined to have spin 0 and a baryon subcluster spin $1/2$.

B.2.3 Kinematic Factors

The remaining factor, P_K, is a kinematic factor proportional to the Lorentz invariant phase space [109] available for each mode. The kinematic factor for a cluster decay into two hadrons is given by

$$P_K = \frac{1}{W} \lambda^{1/2}(W^2, M_1^2, M_2^2) \tag{B.5}$$

where, as usual,

$$\lambda(a, b, c) = a^2 + b^2 + c^2 - 2ab - 2ac - 2bc. \tag{B.6}$$

The case where $X_1 = Cl_1$ is a generalization of the above formalism. For a fixed flavor pulled from the vacuum and fixed H_2, of mass M_2, it is convenient to consider all decays to a subcluster as one decay mode — we can generate the exact mass of the subcluster afterwards, if this collective mode is chosen. The kinematic factor for this collective mode is

$$P_K = \frac{1}{W} \int\limits_{M_0}^{W-M_2} dM \, \rho(M) \lambda^{1/2}(W^2, M^2, M_2^2), \tag{B.7}$$

where $\rho(M)$ is the phase space density associated with a subcluster of mass M, and M_0 is the minimum subcluster mass. In principle, $\rho(M)$ can be calculated by summing the phase space densities of *all* possible exclusive multibody decay modes consistent with the flavor of the subcluster Cl_1. In lieu of this, we propose the parameterization

$$\rho(M) = A(M - M_0)^N \theta(M - M_0), \tag{B.8}$$

where A, N, and M_0 are, in general, flavor-dependent parameters. In practice, $A = 20$ and $N = 1/2$ are found to provide a good description of data, *independent* of the cluster flavor. If the collective mode where $X_1 = Cl_1$ is chosen, then the mass of the subcluster is generated according to the mass distribution $\rho(M)$.

B.3   Discussion

The parameters governing low-mass cluster decay may be determined almost exclusively by fits to low energy data such as $p\bar{p}$ annihilation at rest, $\bar{p}n \to \kappa\bar{\kappa}X$ at rest and charm production at $E_{CM} = 5.2\,\text{GeV}$. The details of the parameter determination may be found in ref. [4]. The place where one must resort to high energy data is where low energy data provides only weak constraints on a parameter.

Such is the case for the flavor selection factor for ss diquarks. As discussed in ref. [3], the availability of new data for strange baryons has permitted a more accurate determination of $P_F[ss]$. Thus, the only change to the parameterization of ref. [4] is that now

$$P_F[u\bar{u}] : P_F[us] : P_F[ss] = 1 : .10 : .08. \tag{B.9}$$

As mentioned in sect. 2.4, the parameterization discussed in this appendix was motivated by a deficiency in the cluster decay ansatz used in the Field-Wolfram model [27]. The Field-Wolfram model allowed only cluster decays of the form

$$Cl \rightarrow H_1 + H_2, \tag{B.10}$$

which was found to be adequate only for rather light clusters ($W \lesssim 1.5$ GeV). It is interesting to note that since cluster decays in the Webber model [10] are also exclusively of the form in eq. (B.10), they are limited in their applicability. For instance, for a $u\bar{u}$ cluster with $W \approx 1.9\,\text{GeV}$,

$$\langle N_{\text{ch}}[u\bar{u}] \rangle \sim 2.6 \qquad (\text{Webber Model}), \tag{B.11}$$

$$\langle N_{\text{ch}}[u\bar{u}] \rangle \sim 3.2 \qquad (\text{Caltech} - \text{II}). \tag{B.12}$$

The data in this energy range [110,111] are consistent with eq. (B.12). The fact that the Webber model generates cluster masses in a regime where the ansatz of eq. (B.10) is known to be deficient underscores the importance of having an accurate parameterization of cluster decays, as in Caltech-II.

Appendix C

Fragmentation of Closed Strings

The treatment of closed strings is similar to that of open strings in sect. 3.2 with only a few changes. The continuity of the closed string is expressed by the periodic boundary conditions of eq. (3.15). The functions $f^\mu(\sigma)$ and $g^\mu(\sigma)$ in eq. (3.23) are extended by defining them on the compact domain $\sigma \in [0, \pi)$. In contrast to the open string, the whole σ domain is physical. All the other equations of sect. 3.2 are valid except for eqs. (3.34,3.35,3.36) because in general, $P_+^\mu(\sigma, \tau = 0)$ and $P_-^\mu(\sigma, \tau = 0)$ are independent for closed strings, so that both are needed for a complete specification of the string.

Fig. C.1 demonstrates how cutting a closed string produces an open string. If a string breaks at $(\sigma = \bar{\sigma}, \tau = \bar{\tau})$, we rotate the contours of $P_+(\sigma, \tau = 0)$ by $\tau = \bar{\tau}$ and the contours of $P_-(\sigma, \tau = 0)$ by $-\bar{\tau}$. Introducing a cut reroutes the momentum from one domain to the other so that we fuse the topologies of the two domains to form one large domain. The cut defines the physical endpoints of an open string but does not distinguish the physical and unphysical regions of the new σ domain. This is not a problem, since the two identifications correspond physically to momentum currents along the different branches of the local light cones. Since we know that for an open string these currents are related by eq. (3.34), we are assured that both choices correspond to the same physical situation. With initial conditions for the open string in hand, we can apply all the formalism of chapter 3, should we decide
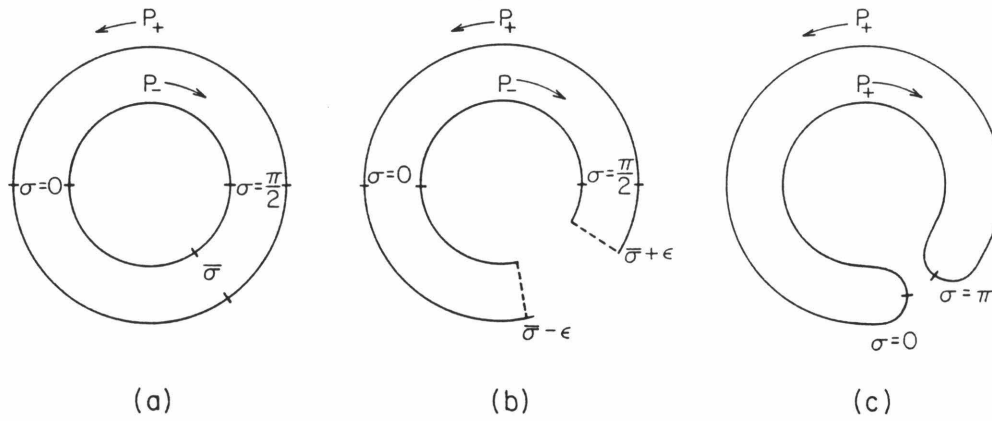
Figure C.1 (a) Momentum currents for closed strings flow on closed domain. (b) A string break associates points on different domains. (c) Domains are pasted together to create the domain of an open string.

to fragment the string further.

References

[1] A. Zee, Study of the renormalization group for small coupling constants, *Phys. Rev.* **D7** (1973) 3630.

[2] S. Coleman and D.J. Gross, Price of asymptotic freedom, *Phys. Rev. Lett.* **31** (1973) 851.

[3] T.D. Gottschalk and D.A. Morris, *A New Model for Hadronization and e^+e^- Annihilation*, Caltech preprint CALT-68-1365 (1986).

[4] T.D. Gottschalk, A simple phenomenological model for hadron production from low mass clusters, *Nucl. Phys.* **B239** (1984) 325.

[5] T.D. Gottschalk, An improved description of hadronization in the QCD cluster model for e^+e^- annihilation, *Nucl. Phys.* **B239** (1984) 349.

[6] D.A. Morris, *A Framework for the Fragmentation of the Massless Relativistic String*, Caltech preprint CALT-68-1392 (1986).

[7] J.D. Bjorken, Properties of hadron distributions in reactions containing very heavy quarks, *Phys. Rev.* **D17** (1978) 171.

[8] M. Suzuki, Fragmentation of hadrons from heavy quark partons, *Phys. Lett.* **71B** (1977) 139.

[9] D. Amati, R. Petronzio, and G. Veneziano, Relating hard QCD processes through universality of mass singularities, *Nucl. Phys.* **B140** (1978) 54.

[10] B.R. Webber, A QCD model for jet fragmentation including soft gluon interference, *Nucl. Phys.* **B238** (1984) 492.

[11] B. Andersson, G. Gustafson, B. Soderberg, and T. Sjöstrand, Parton fragmentation and string dynamics, *Phys. Rep.* **97** (1983) 33.

[12] R.D. Field and R.P. Feynman, A parameterization of the properties of quark jets, *Nucl. Phys.* **B136** (1978) 1.

[13] R. Brandelik *et al.* (TASSO), Comparison of e^+e^- annihilation with QCD and determination of the strong coupling constant, *Phys. Lett.* **94B** (1980) 437.

[14] T. Meyer, A Monte Carlo model to produce baryons in e^+e^- annihilation, *Z. Phys.* **C12** (1982) 77.

[15] G. Altarelli and G. Parisi, Asymptotic freedom in parton language, *Nucl. Phys.* **B126** (1977) 298.

[16] A. Ali, E. Pietarinen, G. Kramer, and J. Willrodt, A QCD analysis of the high energy e^+e^- data from PETRA, *Phys. Lett.* **93B** (1980) 155.

[17] P. Hoyer, P. Osland, H.G. Sander, T.F. Walsh, and P.M. Zerwas, Quantum chromodynamics and jets in e^+e^- annihilation, *Nucl. Phys.* **B161** (1979) 349.

[18] T. Sjöstrand, Some comments on jet fragmentation models and α_s determinations, *Z. Phys.* **C26** (1984) 93.

[19] M.D. Corcoran, Monte Carlo studies of high transverse energy hadronic reactions, *Phys. Rev.* **D32** (1985) 984.

[20] T.D. Gottschalk, *Pictures of Hadronization*, Caltech preprint CALT-68-1413 (1986).

[21] F.E. Paige and S. D. Protopopescu, Brookhaven Preprint BNL-38774 (1986).

[22] R. Odorico (COJETS), Simulation of QCD in hard hadronic processes including gluon radiation effects, *Nucl. Phys.* **B228** (1983) 381.

[23] R. Odorico, COJETS: a Monte Carlo program simulating QCD in hadronic production of jets and heavy flavors with inclusion of initial QCD bremsstrahlung, *Comp. Phys. Comm.* **B32** (1984) 139.

[24] R.D. Field, Jets and event topologies at the SSC, In R. Donaldson and J.G. Morfin, editors, *Proceedings of the 1984 Summer Study on the Design and Utilization of the Superconducting Super Collider,* Snowmass, Colorado (1984) p.713.

[25] B. van Eijk (EUROJET), *Proceedings of the Fifth Topical Workshop on $p\bar{p}$ Collider Physics* (1985).

[26] D. Amati and G. Veneziano, Preconfinement as a property of perturbative QCD, *Phys. Lett.* **83B** (1979) 87.

[27] R.D. Field and S. Wolfram, A QCD model for e^+e^- annihilation, *Nucl. Phys.* **B213** (1983) 65.

[28] G. Gustafson, Topological properties of the colour field in hard processes, *Z. Phys.* **C15** (1982) 155.

[29] T. Sjöstrand, Jet fragmentation of multiparton configurations in a string framework, *Nucl. Phys.* **B248** (1984) 469.

[30] M. Derrick and T.D. Gottschalk, Report of the snowmass hadronization group, In R. Donaldson and J.G. Morfin, editors, *Proceedings of the 1984 Summer Study on the Design and Utilization of the Superconducting Super Collider,* Snowmass, Colorado (1984) p.49.

[31] Y. Nambu, Quark model and the factorization of the Veneziano amplitude, In R. Chand, editor, *Symmetries and Quark Models,* Gordon and Breach: New York (1970) p. 269.

[32] H.B. Nielson, An almost physical interpretation of the integrand of the n-point Veneziano model, In *15th Conference on High Energy Physics, Kiev* 1970.

[33] L. Susskind, Dual symmetric theory of hadrons - I, *Nuovo Cim.* **69** (1970) 457.

[34] J. Scherk and J.H. Schwarz, Dual field theory of quarks and gluons, *Phys. Lett.* **57B** (1975) 463.

[35] H.B. Nielson and P. Olesen, Vortex-line models for dual strings, *Nucl. Phys.* **B61** (1973) 45.

[36] V.P. Nair and C. Rosenzweig, Bags versus strings: hadrons in the type I and type II superconducting vacua, *Nucl. Phys.* **B250** (1985) 729.

[37] J.M. Drouffe and J.B. Zuber, Strong coupling and mean field theories, *Phys. Rep.* **102** (1983) 1.

[38] J.W. Flower and S.W. Otto, The field distribution in SU(3) lattice gauge theory, *Phys. Lett.* **160B** (1985) 128.

[39] M. Baker, J.S. Ball, and F. Zachariason, The static quark potential according to the dual superconductor picture of QCD, *Phys. Rev.* **D34** (1986) 384.

[40] X. Artru and G. Mennessier, String model and multiproduction, *Nucl. Phys.* **B70** (1974) 93.

[41] X. Artru, Classical string phenomenology. How strings work, *Phys. Rep.* **97** (1983) 147.

[42] B. Andersson, The LUND string model, 1986, U.C.L.A. Spring Seminar Series.

[43] I. Montvay, Where are the jets?, *Phys. Lett.* **84B** (1979) 331.

[44] C. Rebbi, Dual models and relativistic quantum strings, *Phys. Rep.* **C12** (1974) 3.

[45] S. Mandlelstam, Dual resonance models, *Phys. Rep.* **C13** (1974) 260.

[46] B.M. Barbashov and V.V. Nesterenko, Dynamics of a relativistic string, *Sov. J. Part. Nucl.* **9** (1978) 391.

[47] G.P. Pron'ko, A.V. Razumov, and L.D. Solov'ev, Classical dynamics of a relativistic string, *Sov J. Part. Nucl.* **14** (1983) 229.

[48] G.C. Fox and S. Wolfram, A model for parton showers in QCD, *Nucl. Phys.* **B168** (1980) 285.

[49] R. Odorico, Exclusive calculations for QCD jets in a Monte Carlo approach, *Nucl. Phys.* **B172** (1980) 157.

[50] B. Andersson, G. Gustafson, and B. Söderberg, A probability measure on parton and string states, *Nucl. Phys.* **B264** (1986) 29.

[51] E. Eichten, K. Gottfried, T. Kiroshita, K.D. Lane, and T.M. Yan, Charmonium: 1. The Model, *Phys. Rev.* **D17** (1978) 313.

[52] G. Karl and W. Roberts, Sequential fragmentation and rate oscillations in exclusive decays, *Phys. Lett.* 144B (1984) 263.

[53] X. Artru, Correspondences between the symmetric LUND model and the dual resonance model, *Z. Phys.* **26** 83.

[54] B. Andersson and W. Hofmann, Bose-Einstein correlations and color strings, *Phys. Lett.* **169B** (1986) 364.

[55] X. Artru and M.G. Bowler, *Quantisation of the String Fragmentation Model*, Oxford preprint 79/86 (1986).

[56] A. Chodos and C.B. Thorn, Making the massless string massive, *Nucl. Phys.* **B72** (1974) 509.

[57] W.A. Bardeen, I. Bars, A.J. Hanson, and R.D. Peccei, Study of the longitudinal kink modes of the string, *Phys. Rev. D* **13** (1976) 2364.

[58] J. von Neumann, Various techniques used in connection with random digits, *U.S. Nat. Bur. Stand. Appl. Math. Ser.* **12** (1951) 36.

[59] W. Bartel *et al.* (JADE), Particle distribution in 3-jet events produced by e^+e^- annihilation, *Z. Phys.* **C21** (1983) 37.

[60] W. Bartel *et al.* (JADE), Test of fragmentation models by comparison with three-jet events produced in e^+e^- annihilation, *Phys. Lett.* **134B** (1984) 275.

[61] W. Bartel *et al.* (JADE), Comparison of three-jet events with QCD shower models, *Phys. Lett.* **157B** (1985) 340.

[62] J.W. Gary, *Tests of Models for Parton Fragmentation in e^+e^- Annihilation*, Ph.D. thesis Berkeley 1985, LBL-20638.

[63] H. Aihara *et al.* (TPC), Tests of models for parton fragmentation by means of three-jet events in e^+e^- annihilation at $\sqrt{s} = 29$ GeV, *Phys. Rev. Lett.* **54** (1985) 270.

[64] H. Aihara *et al.* (TPC), Tests of models for quark and gluon fragmentation in e^+e^- annihilation at $\sqrt{s} = 29$ GeV, *Z. Phys.* **C28** (1985) 31.

[65] H. Aihara *et al.* (TPC), Characteristics of proton production in jets from e^+e^- annihilation at 29 GeV, *Phys. Rev. Lett.* **53** (1984) 130.

[66] H. Aihara *et al.* (TPC), Baryon production in e^+e^- annihilation at $\sqrt{s} = 29$ GeV : clusters, diquarks, popcorn?, *Phys. Rev. Lett.* **55** (1985) 1047.

[67] M. Althoff *et al.* (TASSO), Jet production and fragmentation in e^+e^- annihilation at 12-43 GeV, *Z. Phys.* **C22** (1984) 307.

[68] J.D. Bjorken and S.J. Brodsky, Statistical model for electron-positron annihilation into hadrons, *Phys. Rev.* **D1** (1970) 1416.

[69] T.D. Gottschalk, Energy distributions for charmed hadrons in the QCD cluster model for e^+e^- annihilations, *Nucl. Phys.* **B227** (1983) 413.

[70] C.L. Basham, L.S. Brown, S.D. Ellis, and S.T. Love, Electron-positron annihilation energy pattern in quantum chromodynamics: aymptotically free peturbation theory, *Phys. Rev.* **D17** (1978) 2298.

[71] C.L. Basham, L.S. Brown, S.D. Ellis, and S.T. Love, Energy correlation in electron-positron annihilation in quantum chromodynamics, *Phys. Rev.* **D19** (1979) 2018.

[72] W. Bartel *et al.* (JADE), Measurements of energy correlations in $e^+e^- \rightarrow$ hadrons, *Z. Phys.* **C25** (1985) 231.

[73] E. Farhi, Quantum chromodynamic tests for jets, *Phys. Rev. Lett.* **39** (1977).

[74] D.G. Richards, W.J. Stirling, and S.D. Ellis, Second-order corrections to the energy-energy correlation function in quantum chromodynamics, *Phys. Lett.*

119B (1982) 193.

[75] D.G. Richards, W.J. Stirling, and S.D. Ellis, Energy-energy correlations to second order in quantum chromodynamics, *Nucl. Phys.* **B229** (1983) 317.

[76] A. Ali and F. Barreiro, An $O(\alpha_s^2)$ calculation of energy-energy correlation in e^+e^- annihilation and comparison with data, *Phys. Lett.* **118B** (1982) 155.

[77] H.N. Schneider, G. Kramer, and G. Schierholz, Higher order QCD corrections to the energy-energy correlation function, *Z. Phys.* **C22** (1984) 201.

[78] R.Y. Zhu, *Determination of the Strong Coupling Constant up to Complete Second Order in QCD*, Ph.D. thesis Massachusetts Institute of Technology 1983.

[79] S. Bethke, Experimental studies on the heavy quark fragmentation function, *Z. Phys.* **29** (1985) 175.

[80] T. Sjöstrand, The LUND Monte Carlo for jet fragmentation and e^+e^- physics — JETSET version 6.2, *Comput. Phys. Commun.* **39** (1986) 347.

[81] J.L. Siegrist *et al.* (MARK I), Hadron production by e^+e^- annihilation at center-of-mass energies between 2.6 and 7.8 GeV. I. total cross section, multiplicities and inclusive momentum distributions, *Phys. Rev.* **D26** (1982) 969.

[82] Ch. Berger *et al.* (PLUTO), Multiplicty distributions in e^+e^- annihilations at PETRA energies, *Phys. Lett.* **95B** (1980) 313.

[83] L. Criegee and G. Knies, e^+e^- physics with the PLUTO detector, *Phys. Rep.* **83** (1982) 151.

[84] C. Bacci *et al.* ($\gamma\gamma2$), Total cross section for hadronic production by e^+e^- annihilation in the total cm energy 1.2-3.09 GeV, *Phys. Lett.* **86B** (1979) 234.

[85] A. Brody *et al.* (CLEO), Decay of B mesons into charged and neutral kaons, *Phys. Rev. Lett.* **48** (1982) 1070.

[86] V. Lüth *et al.* (MARK I), K^0 production in e^+e^- annihilation, *Phys. Lett.* **70B** (1977) 120.

[87] M. Althoff *et al.* (TASSO), A detailed study of strange particle production in e^+e^- annihilation at high energy, *Z. Phys.* **C27** (1985) 27.

[88] G.S. Abrams *et al.* (MARK II), Observation of charmed-baryon production in e^+e^- annihilation, *Phys. Rev. Lett.* **44** (1980) 10.

[89] H. Aihara *et al.* (TPC), Charged hadron production in e^+e^- annihilation at 29 GeV, *Phys. Rev. Lett.* **52** (1984) 577.

[90] H. Aihara *et al.* (TPC), Λ production in e^+e^- annihilation at 29 GeV, *Phys. Rev. Lett.* **54** (1985) 274.

[91] A. Bäcker, Normicity, a general jet measure, *Z. Phys.* **C12** (1982) 161.

[92] G. Flügge, Jet fragmentation, In *The Quark Structure of Matter* World Scientific (1986) p.79.

[93] A. Casher, H. Neuberger, and S. Nussinov, Chromoelectric-flux-tube model of particle production, *Phys. Rev.* **D20** (1979) 179.

[94] H. Aihara *et al.* (TPC), Charged-D^*-meson production in e^+e^- annihilation at $\sqrt{s} = 29$ GeV, *Phys. Rev.* **D34** (1986) 1945.

[95] B. Adeva *et al.* (MARK-J), A summary of experimental results from Mark-J: high energy e^+e^- collisions at PETRA, *Phys. Rep.* **109** (1984) 131.

[96] M.G. Bowler, e^+e^- production of heavy quarks in the string model, *Z. Phys.* **11** (1981) 169.

[97] R. Galik (CLEO), Charm production and fragmentation at CLEO, In L. Nitti and G. Preparata, editors, *Prodeedings of the International Europhysics Conference on High-Energy Physics,* Bari, Italy (1985) p.513.

[98] R.S. Orr (ARGUS), Charm production and fragmentation in e^+e^- annihilation at 10 GeV centre of mass energy, In L. Nitti and G. Preparata, editors, *Proceedings of the International Eurohysics Conference On High-Energy Physics,* Bari, Italy (1985) p.517.

[99] C. Peterson, D. Schlatter, I. Schmitt, and P.M. Zerwas, Scaling violations in inclusive e^+e^- annihilation spectra, *Phys. Rev. D* **27** (1983) 105.

[100] F. Amiri and C.R. Ji, *Perturbative Quantum Chromodynamic Prediction for the Heavy Quark Fragmentation Function,* SLAC preprint SLAC-PUB-4023 (1986).

[101] A. Peterson *et al.* (MARK II), Inclusive charged-particle distribution in nearly threefold-symmetric three-jet events at $E_{CM} = 29$ GeV, *Phys. Rev. Lett.* **55** (1985) 1954.

[102] R.K. Ellis, H. Georgi, M. Machacek, H.D. Politzer, and G. Ross, Perturbation theory and the parton model in QCD, *Nucl. Phys.* **B152** (1979) 285.

[103] Yu.L. Dokshitzer, V.S. Fadin, and V.A. Khoze, Coherent effects in the perturbative QCD parton jets, *Phys. Lett.* **115B** (1984) 242.

[104] A. H. Mueller, Multiplicity and hadron distributions in QCD jets: non-leading terms, *Nucl. Phys.* **B213** (1983) 85.

[105] A. H. Mueller, Multiplicity and hadron distributions in QCD jets (II). a general procedure for all non-leading terms, *Nucl. Phys.* **B228** (1983) 351.

[106] A. H. Mueller, $\sqrt{\alpha(Q^2)}$ corrections to particle multiplicity ratios in gluon and quark jets, *Nucl. Phys.* **B241** (1984) 141.

[107] T.D. Gottschalk, A new model for coherent final state parton showers, In H-U Bengtsonn, C. Buchanan, T.D. Gottschalk, and A. Soni, editors, *Observable Standard Model Physics at the SSC: Monte Carlo Simulation and Detector Capabilities,* Los Angeles, California (1986) p.122.

[108] R.K. Ellis, Topics in perturbative QCD at collider energies, In H-U Bengtsonn, C. Buchanan, T.D. Gottschalk, and A. Soni, editors, *Observable Standard Model Physics at the SSC: Monte Carlo Simulation and Detector Capabilities,* Los Angeles, California (1986) p.167.

[109] E. Byckling and K. Kajantie, *Particle Kinematics,* John Wiley and Sons: London (1973).

[110] C. Baltay *et al.*, Annihilation of antiprotons at rest in hydrogen. V. multipion annihilations, *Phys. Rev.* **145** (1966) 1103.

[111] C. Baltay *et al.*, Observation of the B meson in the reaction $\bar{p}p \rightarrow \omega^0 + \pi^+ + \pi^-$, *Phys. Rev. Lett.* **18** (1967) 93.